34287

National Library of Canada
Bibliothèque nationale du Canada

CANADIAN THESES ON MICROFICHE

THÈSES CANADIENNES SUR MICROFICHE

NAME OF AUTHOR/*NOM DE L'AUTEUR* JOHN RICHARD BANNISTER

TITLE OF THESIS/*TITRE DE LA THÈSE* A MAGNETOMETER ARRAY STUDY OF POLAR MAGNETIC SUBSTORMS

UNIVERSITY/*UNIVERSITÉ* THE UNIVERSITY OF ALBERTA

DEGREE FOR WHICH THESIS WAS PRESENTED/ *GRADE POUR LEQUEL CETTE THÈSE FUT PRÉSENTÉE* Ph. D.

YEAR THIS DEGREE CONFERRED/*ANNÉE D'OBTENTION DE CE GRADE* 1977

NAME OF SUPERVISOR/*NOM DU DIRECTEUR DE THÈSE* D. I. GOUGH

Permission is hereby granted to the NATIONAL LIBRARY OF CANADA to microfilm this thesis and to lend or sell copies of the film.

The author reserves other publication rights, and neither the thesis nor extensive extracts from it may be printed or otherwise reproduced without the author's written permission.

L'autorisation est, par la présente, accordée à la BIBLIOTHÈQUE NATIONALE DU CANADA de microfilmer cette thèse et de prêter ou de vendre des exemplaires du film.

L'auteur se réserve les autres droits de publication; ni la thèse ni de longs extraits de celle-ci ne doivent être imprimés ou autrement reproduits sans l'autorisation écrite de l'auteur.

DATED/*DATÉ* JUNE 6 1977 SIGNED/*SIGNÉ*

PERMANENT ADDRESS/*RÉSIDENCE FIXÉ*
UNIVERSIDAD DE CHILE
DEPARTAMENTO DE GEOFISICA
CASILLA [redacted] 2777 SANTIAGO CHILE

NL-91 (3-74)

National Library of Canada

Cataloguing Branch
Canadian Theses Division

Ottawa, Canada
K1A 0N4

Bibliothèque nationale du Canada

Direction du catalogage
Division des thèses canadiennes

NOTICE

The quality of this microfiche is heavily dependent upon the quality of the original thesis submitted for microfilming. Every effort has been made to ensure the highest quality of reproduction possible.

If pages are missing, contact the university which granted the degree.

Some pages may have indistinct print especially if the original pages were typed with a poor typewriter ribbon or if the university sent us a poor photocopy.

Previously copyrighted materials (journal articles, published tests, etc.) are not filmed.

Reproduction in full or in part of this film is governed by the Canadian Copyright Act, R.S.C. 1970, c. C-30. Please read the authorization forms which accompany this thesis.

THIS DISSERTATION
HAS BEEN MICROFILMED
EXACTLY AS RECEIVED

AVIS

La qualité de cette microfiche dépend grandement de la qualité de la thèse soumise au microfilmage. Nous avons tout fait pour assurer une qualité supérieure de reproduction.

S'il manque des pages, veuillez communiquer avec l'université qui a conféré le grade.

La qualité d'impression de certaines pages peut laisser à désirer, surtout si les pages originales ont été dactylographiées à l'aide d'un ruban usé ou si l'université nous a fait parvenir une photocopie de mauvaise qualité.

Les documents qui font déjà l'objet d'un droit d'auteur (articles de revue, examens publiés, etc.) ne sont pas microfilmés.

La reproduction, même partielle, de ce microfilm est soumise à la Loi canadienne sur le droit d'auteur, SRC 1970, c. C-30. Veuillez prendre connaissance des formules d'autorisation qui accompagnent cette thèse.

LA THÈSE A ÉTÉ
MICROFILMÉE TELLE QUE
NOUS L'AVONS REÇUE

NL-339 (3/77)

THE UNIVERSITY OF ALBERTA

A MAGNETOMETER ARRAY STUDY OF POLAR MAGNETIC SUBSTORMS

by

© J. R. BANNISTER

A THESIS

SUBMITTED TO THE FACULTY OF GRADUATE STUDIES AND RESEARCH
IN PARTIAL FULFILMENT OF THE REQUIREMENTS FOR THE DEGREE
OF DOCTOR OF PHILOSOPHY
IN
GEOPHYSICS

DEPARTMENT OF PHYSICS

EDMONTON, ALBERTA
FALL, 1977

THE UNIVERSITY OF ALBERTA

FACULTY OF GRADUATE STUDIES AND RESEARCH

The undersigned certify that they have read, and recommend to the Faculty of Graduate Studies and Research, for acceptance, a thesis entitled A MAGNETOMETER ARRAY STUDY OF POLAR MAGNETIC SUBSTORMS

submitted by JOHN RICHARD BANNISTER

in partial fulfilment of the requirements for the degree of DOCTOR OF PHILOSOPHY in GEOPHYSICS

D. I. Gough
Supervisor

Gordon Rostoker

Peter R. Smy

W. K. Dawson

M. E. Evans

J. R. Burrows
External Examiner

DATE... May 10, 1977

ABSTRACT

Four polar magnetic substorms were recorded in the late summer of 1974 by most stations of a two-dimensional array of 29 three-component magnetometers located in western Canada beneath the auroral oval. The mean perturbation fields over five minute intervals at representative epochs of each substorm are presented, the first just before the main perturbations and the last in the coda of the event. At 4 epochs of the substorm of September 11, and at 6 epochs of the other substorms, the perturbation fields have been fitted, on a least-squares criterion, by calculated fields of three-dimensional magnetospheric-ionospheric current loops (Boström type 1) with field aligned currents at east and west ends of the ionospheric segment. Several parameters of the ionospheric current segment position were varied in each case, to obtain best fit by iteration. The first substorm presented (1974 September 11) was modelled with uniform current density across the width. All other substorms (1974, September 7, September 18 and August 14) could not be modelled with uniform current density. An inverse method due to Oldenburg was therefore used to estimate current density distributions, and satisfactory fits of calculated to observed fields resulted. Tests and brief description of this inverse method are presented. In all model calculations, induction in a superconducting

sphere was included, at depths in the range 250-600 km.

At four epochs of the September 7 substorm and throughout the September 18 substorm, significant eastward ionospheric current (or its equivalent in terms of the fields produced) was found present north of the main westward electrojet. At five of the six epochs modelled for the August 14 substorm, significant westward ionospheric current was found present north of the main eastward electrojet.

Northwestward bends in the ionospheric current segments were found at three epochs on September 11, at four epochs on September 7 and at three epochs on September 18. These bends were either west of or close to magnetic midnight. In some cases the bends may follow the auroral oval, but in others they are sharper and may be associated with the Harang discontinuity. East of geomagnetic midnight the ionospheric currents tend to run in a constant geomagnetic latitude range. At three epochs on August 14 northwestward bends in the ionospheric currents were present in the evening sector. In all four substorms the bends disappeared when the ionospheric current segment lay entirely in the morning sector.

Developments of the four substorms show a variety of shifts in longitude of the ionospheric segment, though all moved eastward relative to magnetic midnight.

The new contributions to the knowledge of polar magnetic substorms recorded in this thesis are the following:

1. Birkeland field aligned currents at the east and west end of the ionospheric current that give rise to the perturbation fields have been firmly established.

2. During substorms there is a general tendency of the current system to drift eastward with respect to geomagnetic midnight.

3. The ionospheric current segment exhibits a bend to the north-west near or just west of geomagnetic midnight.

4. Eastward electrojet associated with a substorm studied corotates with the earth maintaining the upward field aligned current at the east end near the edge of the array for four hours or more.

5. Eastward ionospheric current (or equivalent current) north of the westward electrojet was observed.

6. Westward ionospheric current north of the eastward electrojet was observed.

ACKNOWLEDGEMENTS

I wish to express my sincere thanks to Dr. D. I. Gough, for supervising and suggesting this research. I am also grateful for his initiative in arranging my enrollment in a Ph.D. programme, for his continuous encouragement and invaluable advice during this project. I greatly value the friendship he has given me.

I am very grateful to Dr. L. T. Aldrich of the Department of Terrestrial Magnetism, Carnegie Institution of Washington who introduced me to magnetometer array studies and who made the necessary arrangements for my attendance at The University of Alberta. I wish to thank the Carnegie Institution of Washington for granting me a Predoctoral Fellowship and for their support during my attendance at this University.

I offer my sincere thanks to Dr. G. Rostoker for the use of data acquired through four of his stations and for very helpful discussion at all stages of the work. I wish to thank Drs. D. D. Wallis and J. V. Olson who operated and provided the fully edited data for those four stations. I thank Drs. P. A. Camfield and P. H. Serson for providing data from the temporary magnetometer at Yellowknife Magnetic Observatory.

I greatly appreciate the help from and informative discussion with my friends and colleagues Dr. J. H. Debeer,

Dr. J. L. Kisabeth, Mr. T. J. Hughes, Dr. D. W. Oldenburg and Dr. R. J. Withers, all of whom have made it very enjoyable for my family and I during our stay in Edmonton. I also wish to thank them for making their computer programs available for my use.

I owe my thanks to Dr. Edgar Kausel, Director of the Department of Geophysics, of the Universidad de Chile for his willingness to grant me leave of absence from the Department of Geophysics to complete my studies in Edmonton. I also appreciate the support obtained from the Universidad de Chile.

This study was supported by the National Research Council of Canada. Thanks are due to the University of Alberta for supporting me through a Graduate Teaching assistantship. I wish to acknowledge the assistance received from the Organization of American States through a scholarship during the last two years.

I would like to thank Mrs. Ella Ritz and her staff, in particular Mrs. Heather Bishop, at the Data Entry Services for the typing of the text. I wish to acknowledge the assistance received by Mr. C. Sackiw in the field work, and by Mrs. D. Sample in the editing of the magnetic records.

I admire the patience and understanding that my wife Liliana has shown during the period of this study. I am very grateful for that, and for her assistance in drafting. I apologize to my sons Daniel and Edgar for the many evenings

I have been absent from home while working on this study.

TABLE OF CONTENTS

CHAPTER PAGE

1. MAGNETOSPHERE-IONOSPHERE CURRENT SYSTEMS: A REVIEW 1
    - 1.1 The Magnetosphere 1
    - 1.2 Magnetospheric substorms 9
    - 1.3 Magnetosphere - ionosphere interactions 15
    - 1.4 Polar magnetic substorms 20

2. FIELD OBSERVATIONS AND DATA PROCESSING 30
    - 2.1 The magnetometer array 30
    - 2.2 Data processing 40

3. DEVELOPMENT OF A POLAR MAGNETIC SUBSTORM ON SEPTEMBER 11, 1974 43
    - 3.1 Introduction 43
    - 3.2 Induced currents in the earth 46
        - 3.2.1 Electrical conductivity distribution in the earth 46
        - 3.2.2 Maps of Fourier spectral components 47
    - 3.3 Perturbation Fields 55
    - 3.4 Model Calculations 59
    - 3.5 Model currents for four epochs of

Substorm 1 63
3.6 Discussion 77

4. DEVELOPMENT OF TWO POLAR MAGNETIC SUBSTORMS ON SEPTEMBER 7 AND SEPTEMBER 18, 1974 85
4.1 Introduction 85
4.2 Observations 85
4.3 Substorm 2: 1974 September 7 86
4.3.1 Perturbation Fields 86
4.3.2 Inversion of magnetic perturbation fields 96
4.3.3 Model calculations 108
4.3.4 Model currents for six epochs of Substorm 2 112
4.4 Substorm 3: 1974 September 18 129
4.4.1 Perturbation Fields 129
4.4.2 Model calculations 135
4.4.3 Model currents at six epochs of Substorm 3 136
4.5 A comparison of polar magnetic Substorms 2 and 3 153

5. DEVELOPMENT OF A POLAR MAGNETIC SUBSTORM ON AUGUST 14, 1974 169
5.1 Introduction 169
5.2 Observations 170

5.3 Perturbation Fields 173
5.4 Model calculations 178
5.5 Model currents for six epochs of Substorm 4 183
5.6 Discussion 200

6. CONCLUDING REMARKS 210

REFERENCES 217

APPENDIX A: THE MAGNETIC FIELD FROM A THREE-DIMENSIONAL LINE CURRENT 223

APPENDIX B: Kp AND AURORAL ELECTROJET MAGNETIC ACTIVITY INDICES 229

LIST OF TABLES

Table	Description	Page
2.1	Location of magnetometer stations.	34
2.2	Location of Canadian and U.S. observatories.	40
3.1	Statistical parameters for Substorm 1.	73
4.1	Parameters of the ionospheric segment varied for Substorm 2	111
4.2	Statistical parameters for Substorm 2.	125
4.3	Parameters of the ionospheric segment varied for Substorm 3	136
4.4	Statistical parameters for Substorm 3.	149
5.1	Parameters of the ionospheric segment varied for Substorm 4	182
5.2	Statistical parameters for Substorm 4.	196
B.1	Observatories used for the derivation of AE indices.	230
B.2	AE and Kp indices for Substorm 1, 1974 September 11.	232
B.3	AE and Kp indices for Substorm 2, 1974 September 7.	233
B.4	AE and Kp indices for Substorm 3, 1974 September 18.	234
B.5	AE and Kp indices for Substorm 4, 1974 August 14.	235

LIST OF FIGURES

Figure		Page
1.1	A three dimensional representation of the magnetosphere.	5
1.2	Earth's magnetosphere in a noon-midnight meridian plane.	7
1.3a	Equatorial cross section of a closed model magnetosphere.	11
1.3b	A model of the open magnetosphere.	13
1.4	Schematic diagram showing the collapse of the tail current.	17
1.5	Electric fields and current flow in the polar ionosphere.	19
1.6a	The Boström Type 1 three-dimensional current model.	22
1.6b	The Boström Type 2 three-dimensional current model.	24
1.7	Boström Type 1 current loop used in modelling the observed fields.	28
2.1	Map of the magnetometer array in geographic coordinates.	33
2.2	The auroral oval and array outline in	

geomagnetic coordinates. 37

2.3 Location of Canadian and U.S. permanent magnetic observatories. 39

3.1 Magnetograms of Substorm 1 from 14 stations. 45

3.2 Fourier contour maps at period 120.5 minutes from Substorm 3. 50

3.3 Fourier contour maps at period 60.2 minutes from Substorm 1. 52

3.4 Fourier contour maps at period 21.1 minutes from Substorm 3. 54

3.5a Mean perturbation fields at three epochs before and during Substorm 1. 57

3.5b Mean perturbation fields at three epochs during Substorm 1. 58

3.6 Outline of the ionospheric segment used to model Substorm 1. 61

3.7 Observed, calculated and residual fields for epoch 07.48 U.T. of Substorm 1. 65

3.8 Observed, calculated and residual fields for epoch 08.13 U.T. of Substorm 1. 67

3.9 Observed, calculated and residual fields for epoch 08.38 U.T. of Substorm 1. 69

3.10 Observed, calculated and residual fields for epoch 08.58 U.T. of Substorm 1. 71

3.11 Ionospheric segments of current loops for Substorm 1, in a Mercator projection. 76

3.12 Ionospheric segments of current loops for Substorm 1, in azimuthal equidistant projection. 80

3.13 Horizontal perturbation fields recorded by Canadian and U.S. observatories at epoch 08.38 U.T. of Substorm 1. 82

3.14 Horizontal perturbation fields recorded by Canadian and U.S. observatories at epoch 08.58 U.T. of Substorm 1. 84

4.1 Magnetograms of Substorm 2 from 13 stations. 88

4.2 Magnetograms of Substorm 3 from 14 stations. 90

4.3a Mean perturbation fields at four epochs before and during Substorm 2. 93

4.3b Mean perturbation fields at four epochs during Substorm 2. 95

4.4 A test of resolution of the Oldenburg inversion method. 102

4.5 An inversion by Oldenburg's method from observed fields of Substorm 3. 105

4.6 Outline of the ionospheric segment of the current loop used to model Substorm 2 and 3. 110

4.7 Observed, calculated and residual fields for epoch 08.28 U.T. of Substorm 2. 114

4.8 Observed, calculated and residual fields for epoch 08.58 U.T. of Substorm 2. 116

4.9 Observed, calculated and residual fields for epoch 09.43 U.T. of Substorm 2. 118

4.10 Observed, calculated and residual fields for epoch 10.13 U.T. of Substorm 2. 120

4.11 Observed, calculated and residual fields for epoch 10.48 U.T. of Substorm 2. 122

4.12 Observed, calculated and residual fields for epoch 11.23 U.T. of Substorm 2. 124

4.13 Ionospheric segments of current loops at six epochs of Substorm 2, in Mercator projection. 128

4.14a Mean perturbation fields at four epochs before and during Substorm 3. 131

4.14b Mean perturbation fields at four epochs during Substorm 3. 133

4.15 Observed, calculated and residual fields for epoch 07.53 U.T. of Substorm 3. 138

4.16 Observed, calculated and residual fields for epoch 08.03 U.T. of Substorm 3. 140

4.17 Observed, calculated and residual fields for epoch 08.18 U.T. of Substorm 3. 142

4.18 Observed, calculated and residual fields for epoch 08.33 U.T. of Substorm 3. 144

4.19 Observed, calculated and residual fields for epoch 08.48 U.T. of Substorm 3. 146

4.20 Observed, calculated and residual fields for epoch 09.03 U.T. of Substorm 3. 148

4.21 Ionospheric segments of current loops, at six epochs of Substorm 3, in a Mercator projection. 152

4.22 Ionospheric segments of current loops at six epochs of Substorm 2, in azimuthal equidistant projection. 155

4.23 Ionospheric segments of current loops at six epochs of Substorm 3, in azimuthal equidistant projection. 157

4.24 Horizontal perturbation fields recorded by Canadian and U.S. observatories at epoch 08.58 U.T. of Substorm 2. 159

4.25 Horizontal perturbation fields recorded by Canadian and U.S. observatories at epoch 11.23 U.T. of Substorm 2. 161

4.26 Horizontal perturbation fields recorded by Canadian and U.S. observatories at epoch 08.03 U.T. of Substorm 3. 163

4.27 Horizontal perturbation fields recorded by Canadian and U.S. observatories at epoch 08.48 U.T. of Substorm 3. 165

5.1 Magnetograms of Substorm 4 from 10 stations. 172

5.2a Mean perturbation fields at four epochs before and during Substorm 4. 175

5.2b Mean perturbation fields at four epochs during the polar magnetic Substorm 4. 177

5.3 Outline of the ionospheric segment of the current loop used to model Substorm 4. 180

5.4 Observed, calculated and residual fields for epoch 04.13 U.T. of Substorm 4. 185

5.5 Observed, calculated and residual fields for epoch 04.53 U.T. of Substorm 4. 187

5.6 Observed, calculated and residual fields for epoch 05.53 U.T. of Substorm 4. 189

5.7 Observed, calculated and residual fields for epoch 06.53 U.T. of Substorm 4. 191

5.8 Observed, calculated and residual fields for epoch 07.38 U.T. of Substorm 4. 193

5.9 Observed, calculated and residual fields for epoch 08.53 U.T. of Substorm 4. 195

5.10 Ionospheric segments of current loops at four epochs of Substorm 4 in a Mercator projection. 199

5.11 Ionospheric segments of current loops at six epochs of Substorm 4, in azimuthal equidistant projection. 202

5.12 Horizontal perturbation fields recorded by Canadian and U.S. observatories at epoch 04.53 U.T. of Substorm 4. 205

5.13 Horizontal perturbation fields recorded by Canadian and U.S. observatories at epoch 07.38 U.T. of Substorm 4. 207

A.1 Diagram defining vectors for magnetic field calculations. 225

B.1 Map of observatories used in calculating AE indices. 231

CHAPTER 1

MAGNETOSPHERE-IONOSPHERE CURRENT SYSTEMS: A REVIEW.

1.1 The Magnetosphere

Information obtained from artificial satellites and space probes launched in these last two decades has enormously improved our knowledge of interplanetary space. It is now recognized that there is a fully ionized solar plasma flow (solar wind) composed primarily of protons (hydrogen) and electrons streaming continually from the sun, that fills the interplanetary medium. It has long been suspected that some relation might exist between auroral phenomena and the flow of charged particles from the sun. Chapman and Ferraro (1931) suggested that the interplanetary space was virtually a vacuum exept for discrete clouds of solar particles emitted from the sun during solar flares. This misconception was corrected by Biermann (1951) who suggested that the direction of the comet tails which always point away from the sun, could be explained by a continuous flow of plasma away from the sun. Parker (1958,1963) developed a general theory of continuous expansive motion of coronal gas from the sun. Parker showed that for the solar wind to overcome gravity, temperature must decrease less rapidly than 1/r.

Weak magnetic fields of the sun are carried radially outward (in a fixed frame of reference) by the outward streaming of highly conductive coronal supersonic gas, forming Archimedes spirals in the frame of reference rotating with the sun's angular velocity. This magnetic field carried away by the solar wind, known as the Interplanetary Magnetic Field (IMF), has been found to have a sector structure (Wilcox and Ness, 1965). At earth orbit the inclination of the lines of force to the sun-earth line (garden hose angle) is determined by the solar wind speed, and is of the order of 56°. Spacecraft observations indicate that solar wind velocity and particle density increase sharply on entering a sector boundary. Near the trailing edge of the sector the velocity and density fall in magnitude. Magnetospheric activity appears to be modulated by the interplanetary magnetic field sector structure.

Typical values of the IMF at earth orbit are 5-10 nT with approximately 80% of the field lying parallel to the ecliptic plane. Substorms tend to occur in periods when the component normal to the ecliptic plane is directed southward (Dungey, 1961; Fairfield and Cahill, 1966; Rostoker and Fälthammer, 1967), and activity dies down when the field turns northward. Arnoldy (1971) found that substorm activity tends to lag the southward change of the IMF by about one hour.

By the time the solar wind reaches the earth it has a bulk velocity of 300-500 km/sec, its number density is 5-10/cm^3 and its temperature is typically 25x10^4 ^{o}K but varies from 10^4 ^{o}K to 10^6 ^{o}K with increase of solar activity. The corresponding Alfvén velocity of 50-100 km/sec and sound velocity of 100-200 km/sec make the solar plasma flow at earth orbit supersonic and super-Alfvénic.

The presence in the path of the solar wind of the earth, with its mainly dipolar magnetic field, produces a standing magnetohydrodynamic shock wave at approximately 14 earth radii (R_E) upstream from the earth (Fig. 1.2). Axford (1962) and Kellog (1962) treated the problem of the impact of the solar wind on a dipole field using standard magnetohydrodynamic (MHD) equations. As solar wind plasma enters the shock wave (bow shock) it becomes thermalized, the flow becomes subsonic , so that the plasma can flow around the obstacle represented by the earth's magnetic field. The cavity to which the magnetic field is confined by the solar wind is called the magnetosphere and its boundary is referred to as the magnetopause (Figs 1.1, 1.2). In the region of thermalized plasma (magnetosheath) that surrounds the magnetosphere the solar wind is deflected from its original direction. It is most strongly thermalized at the apex of the magnetopause where the flow is subsonic (Mach number = 0.2), and recovers its speed as it passes the obstacle to become supersonic again as it leaves the magnetotail region.

Figure 1.1 A three dimensional representation of the magnetosphere (after Heikkila, 1973) with the plasma mantle added by Rostoker (1976).

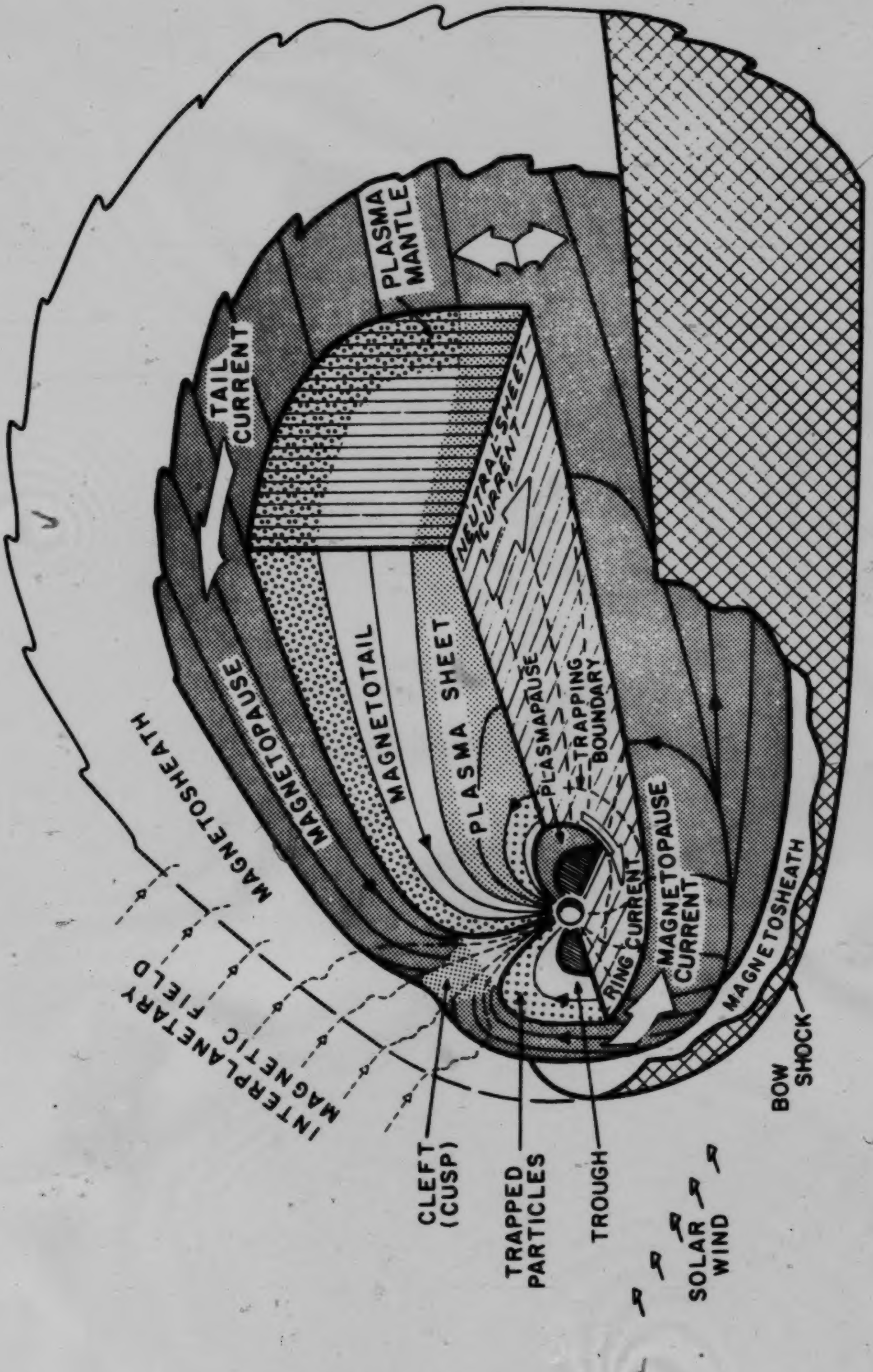
TAIL CURRENT
PLASMA MANTLE
NEUTRAL SHEET CURRENT
MAGNETOSHEATH
MAGNETOPAUSE
MAGNETOTAIL
PLASMA SHEET
PLASMAPAUSE
TRAPPING BOUNDARY
INTERPLANETARY MAGNETIC FIELD
RING CURRENT
MAGNETOPAUSE CURRENT
MAGNETOSHEATH
CLEFT (CUSP)
TRAPPED PARTICLES
TROUGH
SOLAR WIND
BOW SHOCK

Figure 1.2 Earth's magnetosphere in a noon-midnight meridian plane illustrating the magnetotail and the plasma sheet field lines that map to the night side auroral oval (after Ness, 1969).

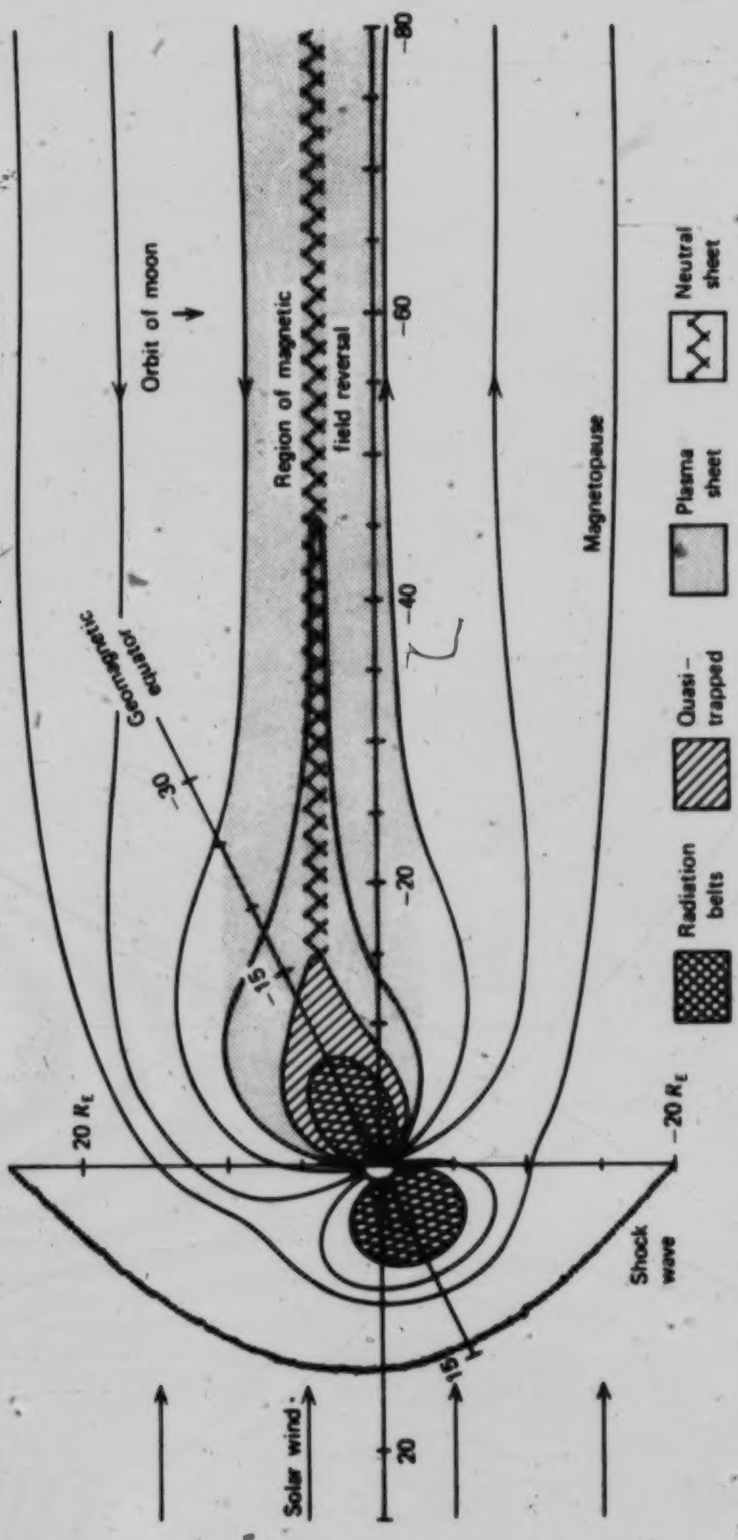
Solar wind
20
Shock wave
15
20 R_E
−20 R_E
−15
−30
Geomagnetic equator
Orbit of moon
Region of magnetic field reversal
Magnetopause
−20
−40
−60
−80
Radiation belts
Quasi-trapped
Plasma sheet
Neutral sheet

The solar wind greatly distorts the magnetosphere, compressing it on the sunward side and stretching it on the night side (down stream) forming the magnetotail which has been detected beyond the orbit of the moon (60 R_E) (Ness et al., 1967). The radius of the magnetic tail is approximately 22 R_E and varies only slightly for at least 100 R_E away from the earth. Beyond the plasmapause (Fig. 1.1) there is an extensive layer of plasma which extends to the magnetotail along an equatorial plane. This layer of plasma called the plasma sheet has a thickness of about 5 R_E at the centre of the tail and gets thicker towards the flanks, to reach a thickness of about 10 R_E near the magnetopause.

The central plane of the plasma sheet is a region where the magnetic field is very weak and normal to the central plane. This region is referred to as the neutral sheet and has a thickness of about 0.1 R_E (Ness, 1969). Above and below the plasma sheet, within the magnetotail, are the tail lobes which are regions of low density plasma (lower than $0.01/cm^3$) and enhanced magnetic field.

Close to the earth (3 to 5 R_E) the particles in the magnetosphere are trapped in the earth's magnetic field. This region of stably trapped particles is referred to as the plasmasphere and its boundary as the plasmapause (Figs. 1.1 and 1.2). Outside this region there is another of quasi-trapped particles which are stably trapped on the dayside of the earth but which, because of the distortion of the magnetic field lines in the night side, may escape down the field lines into the earth's ionosphere or out to the magnetic tail.

1.2 Magnetospheric Substorms

It has long been known that solar activity and auroral activity were related but the mechanism of transfer of energetic particles to the polar regions of the ionosphere is still not completely solved. Birkeland (1913) suggested that auroral activity was generated by particles streaming from the sun. Chapman and Ferraro (1931) indicated that direct entry of solar plasma into the night side auroral zone was impossible but did not describe the solar wind as a continuous flow. As mentioned earlier, it was Biermann (1951) who envisioned the solar wind as a continuous flow creating a continuous pressure on the magnetosphere. Two schools of thought have developed concerning energy transfer into the magnetosphere. Axford and Hines (1961) presented a "closed model" of the magnetosphere (Fig. 1.3a) in which energy is transferred by a sort of viscous interaction across the magnetopause. On the other hand, Dungey (1961) suggested an "open model" (Fig. 1.3b) for the magnetosphere in which field lines of the magnetosphere merge or connect to the IMF on the dayside and a process of reconnection occurs in the night side at the magnetotail. Here the magnetic field behind the bow shock is taken to have a general southward direction (below the ecliptic plane).

Figure 1.3a Equatorial cross section of a closed model magnetosphere illustrating the motion impressed on the magnetospheric plasma by a viscous-like interaction with the solar wind (after Axford and Hines 1961). When corotational effects are superimposed on this model, the two convective cells become asymmetric.

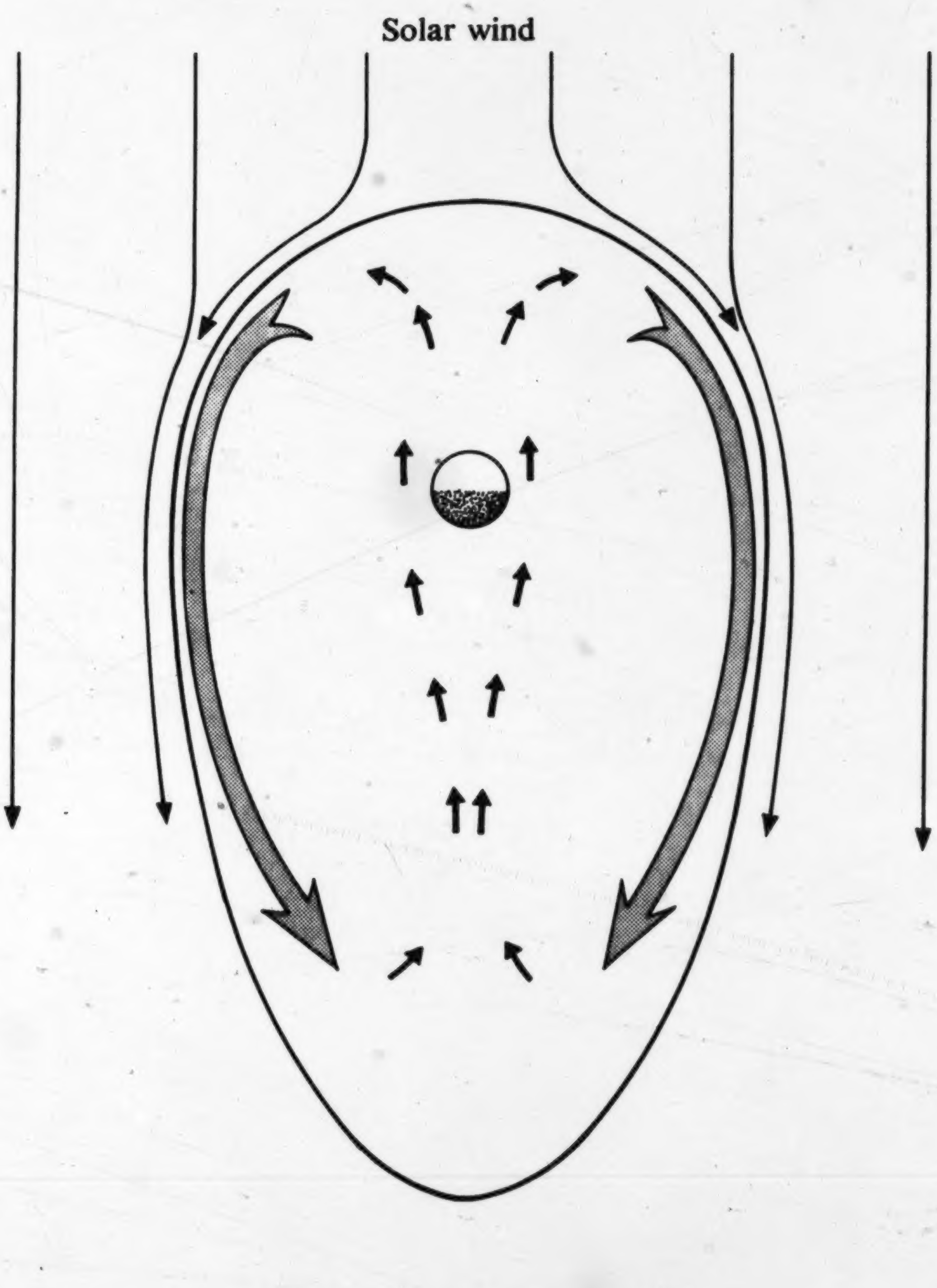
Solar wind

Figure 1.3b A model of the open magnetosphere with the interplanetary magnetic field connecting to the geomagnetic field. In this noon-midnight meridian plane the magnetic field is shown by heavy arrows and plasma flow by open arrows. For simplicity the bow shock is not shown. The numbers indicate the motion of individual field lines, with the motion progressing towards higher numbers. The shaded area in the tail represents the neutral sheet where the B field is very low. (after Hess, 1968).

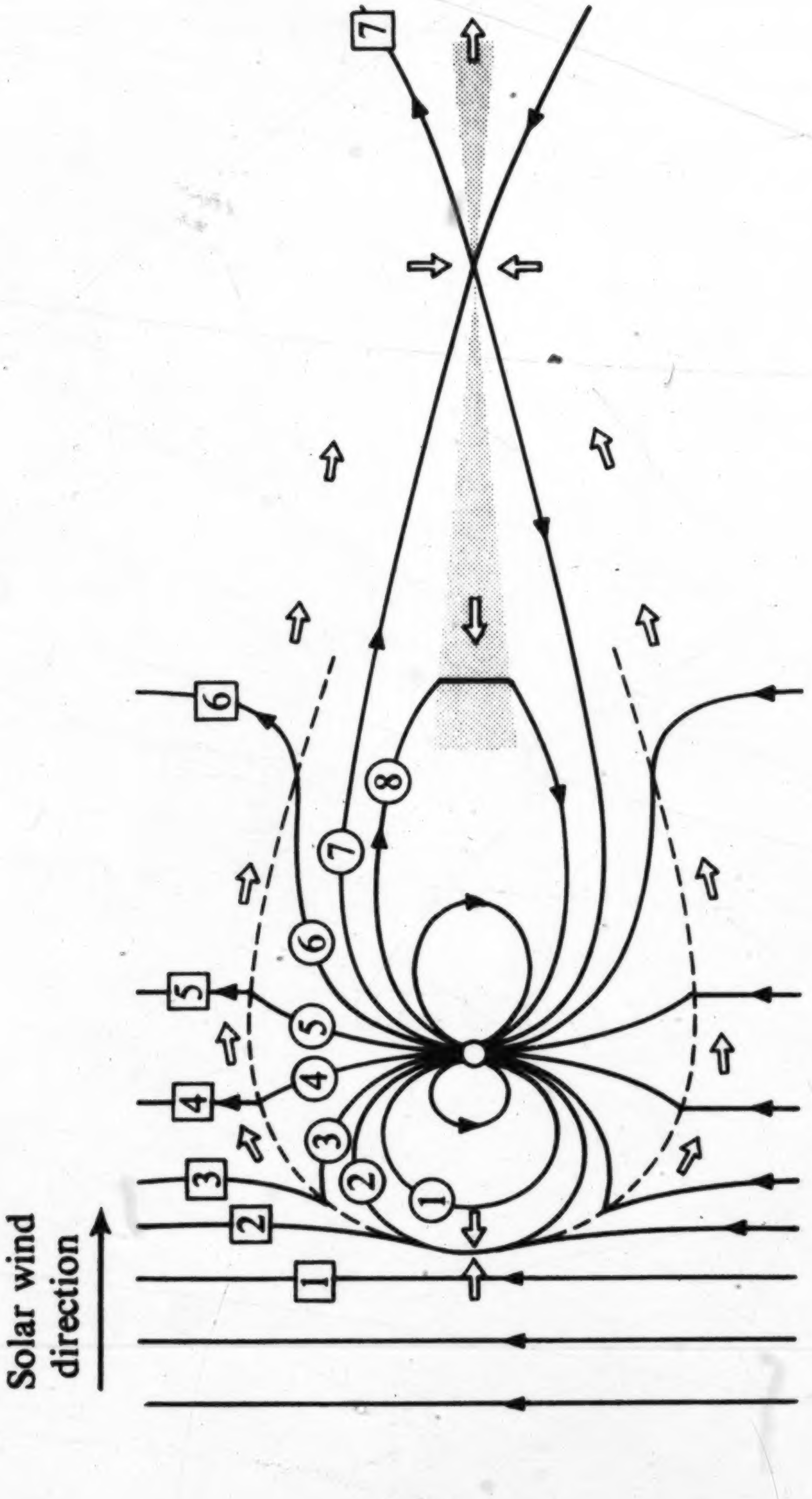
Solar wind direction

Connected field lines are dragged past the earth by the solar wind, leaving field lines that map to the polar caps directly connected to the IMF. The solar wind outside the magnetosphere continues to drag these field lines downstream for several hundred earth radii, where reconnection takes place. It is possible that reconnection in the magnetotail is responsible for the feeding of energy from the solar wind into the night side of the magnetosphere (Rostoker 1972).

Recently Rosenbauer et al. (1975) suggested that solar wind plasma enters the magnetosphere through the polar cleft (Fig 1.1) region to form a stream of particles flowing away from the earth forming the plasma mantle (Fig. 1.1). These particles may eventually form part of the plasma sheet where they acquire a drift velocity toward the earth (Rostoker 1976). It has been found by Schopke et al (1976) that the thickness of plasma mantle increases with increasing southward component of the IMF suggesting a regulatory effect of the IMF.

It is possible to consider the conductivity along magnetic field lines to be nearly infinite, since the plasma in the magnetotail can be considered collisionless. The magnetic field lines may therefore be considered as electric equipotentials. This allows us to map electric fields from the magnetotail onto the ionosphere.

The existence of an electric field in the plasma sheet has been established, its main component being in the dawn to dusk direction. Axford and Hines (1961) and Rostoker (1976) regard this electric field as a polarization field associated with plasma convecting along the plasma sheet towards the earth across the magnetic field lines.

1.3 Magnetosphere - ionosphere interactions.

Siscoe (1966) describes the development of electric current systems in the tail region as produced by pressure gradients in the tail. These currents reproduce the configuration of the magnetotail with a dawn to dusk tail current in the neutral sheet (Figs. 1.1 and 1.2). Akasofu (1972) suggested that during a substorm, there is a sudden increase of the cross-tail electric field leading to an increase of the earthward motion of plasma in the plasma sheet. The increased motion of the plasma can lead to disruption of the cross-tail current (Fig. 1.4), forcing the current to flow along field lines toward the night side part of the ionosphere where these field lines map. The current in the ionosphere would be westward, with an equivalent eastward flow in the magnetotail to close the current loop.

Drifting particles of the plasma sheet precipitate into the upper atmosphere causing ionization and excitation of neutral atoms in the atmosphere. The result is a region of enhanced electric conductivity and luminosity known as the auroral oval. The plasma-sheet field lines map to the auroral oval. As the lifetime of excited states of

Figure 1.4 Schematic diagram showing the collapse of the tail current and its divergence along field lines to the ionosphere (After McPherron et al., 1973).

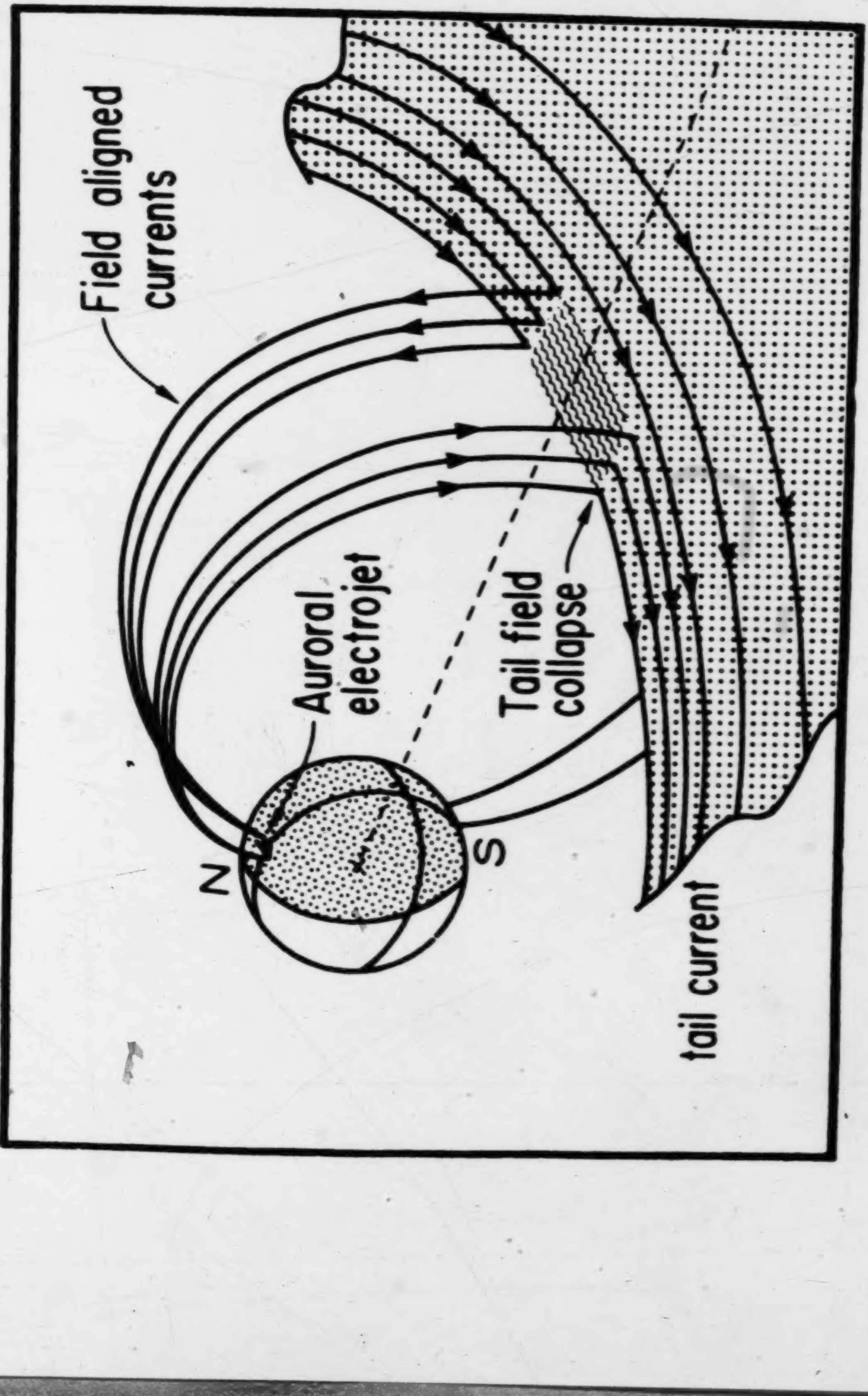
Field aligned currents
Auroral electrojet
Tail field collapse
N
S
tail current

atmospheric atoms is very short, the luminous regions must coincide with the regions where the auroral ionization is produced. The conductivity along magnetic field lines is so high compared to the Hall and Pederson conductivities in the ionosphere that one can disregard any potential drop along the field lines. Assuming that the magnetic field $\vec{B}$ is vertical, the relation between the height-integrated current $\vec{J}$ and the horizontal electric field $\vec{E}_\perp$ is given by:

$$\vec{J} = \sigma_P \vec{E}_\perp + \sigma_H \frac{\vec{B} \times \vec{E}}{B} = \vec{J}_P + \vec{J}_H$$

where σ_P, σ_H are the Pedersen and Hall conductivities respectively and $\vec{J}_P$, and $\vec{J}_H$ are the Pedersen and Hall currents. The Hall conductivity is very large in the E region of the ionosphere (about 100 Km above the surface of the earth). This Hall current, which flows perpendicular to both $\vec{E}_\perp$ and $\vec{B}$, is mainly carried by the electrons. The Pedersen current flows in the direction of $\vec{E}_\perp$. Rostoker and Boström (1976) indicate a mechanism by which currents originate in the plasma sheet within the magnetosphere, and flow along field lines to drive the currents in the ionosphere. Fig 1.5 shows the directions of field aligned (Birkeland) currents and of ionospheric electric fields and currents in the polar ionosphere. The ionospheric electric fields are mapped from the plasma sheet electric fields, along magnetic field lines which are considered as electric equipotentials.

In the strongly anisotropic, highly conductive auroral

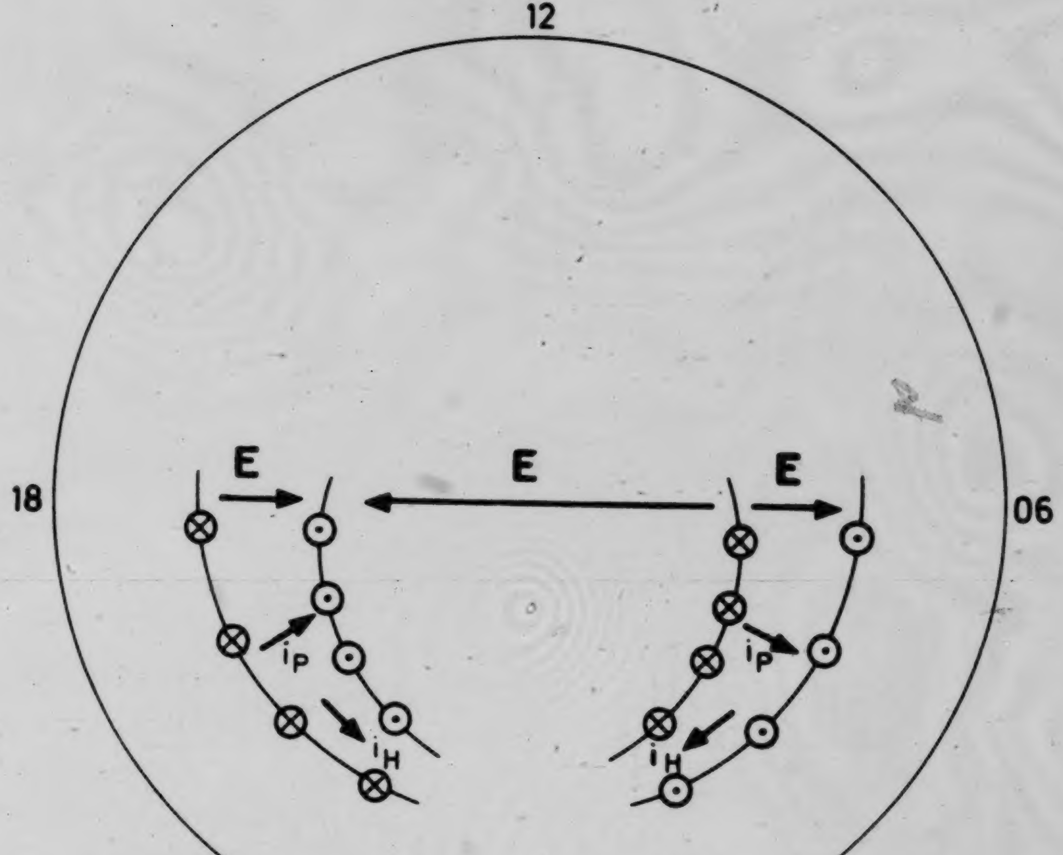

Figure 1.5 Direction of Birkeland current flow and ionospheric electric fields and current flow in the polar ionosphere associated with steady state processes in the magnetosphere (after Rostoker and Boström, 1976).

ionosphere, the electric fields give rise to both Hall and Pedersen currents (Fig 1.5). In the auroral oval the Hall currents produce a westward electrojet in the morning sector, and an eastward electrojet in the evening sector. The Pedersen currents, northward in the evening sector and southward in the morning sector, flow across the highly-conductive auroral zone but are diverted to the field-aligned Birkeland current sheets where they encounter the less conductive ionosphere outside the auroral zone (Fig. 1.5).

1.4 Polar magnetic substorms.

The concept of field aligned currents was first introduced in connection with polar magnetic substorms by Birkeland (1908, 1913). For some decades his model of substorm currents was disregarded in favour of a model whose currents were confined to the ionosphere (Vestine and Chapman 1938). The concept of ionospheric currents diverging to flow along the geomagnetic field was re-introduced by Fejer (1961) and Kern (1962), and was developed extensively by Boström (1964), who proposed two types of magnetosphere-ionosphere current systems. In Type 1 (Fig 1.6a) current flowed down along the field lines into the ionosphere, then westward in the ionosphere and up field lines at the west end of the ionospheric electrojet, into the magnetosphere. Current systems of Type 2 (Fig 1.6b) included antiparallel field-aligned sheet currents joining the ionosphere, at the

Figure 1.6a The Boström Type 1 three-dimensional current model where current flows down along magnetic field lines into the ionosphere, then westward along the electrojet and up field lines into the magnetosphere, with the closure of the loop in the magnetotail (after Boström, 1964).

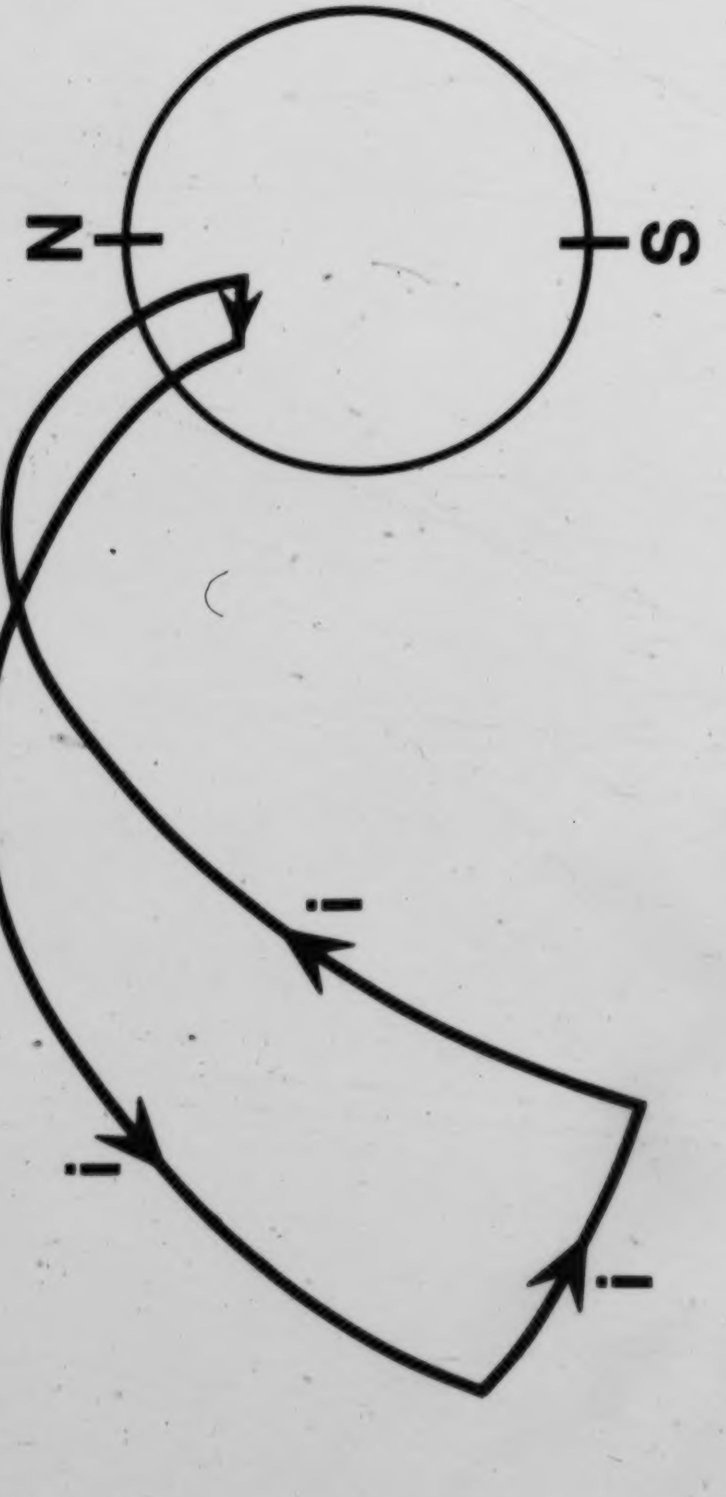
N
S
i
i
i
i

Figure 1.6b The Boström Type 2 three-dimensional current model with Birkeland sheet currents at the north and south with closure in the ionosphere by a north-south current (after Boström, 1964).

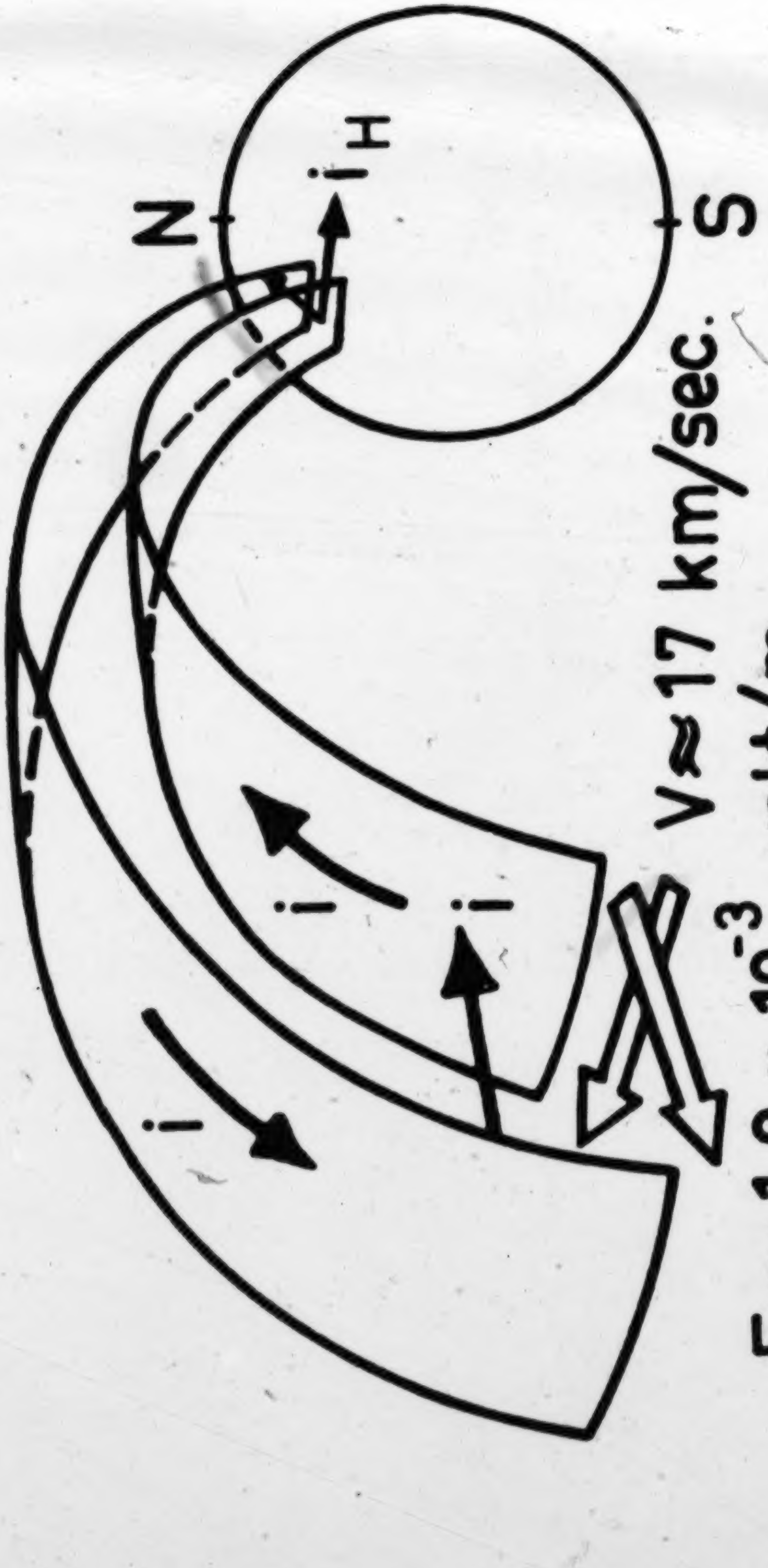
N
S
i_H
i
i
i
V ≈ 17 km/sec.
E ≈ 1.8 × 10^{-3} volt/m

northern and southern boundaries of the auroral zone, to the magnetosphere; in these models northward or southward current in the ionosphere linked the field-aligned current sheets.

In studies of substorm perturbation magnetic fields Akasofu and Meng (1969) and Bonnevier et al . (1970) showed that Boström's Type 1 current system best represented the observations. Satellites at high altitudes in polar orbits have recorded magnetic perturbation fields, in auroral latitudes, consistent with Boström's Type 2 current system (Zmuda et al ., 1967; Zmuda and Armstrong, 1974). On present information it appears probable that both Type 1 and Type 2 current configurations exist near auroral latitudes.

Recent years have seen further rapid advances in the understanding of the magnetosphere-ionosphere current systems associated with polar magnetic substorms. Rostoker and others have contributed to these advances using data from a linear array of magnetometers across the auroral zone, between Newport, Washington, U.S.A. and Cambridge Bay, Victoria Island, Canada, together with the permanent magnetic observatories of Canada and the United States. Knowledge of substorm phenomena up to June, 1971 has been reviewed by Rostoker (1972). The Canadian linear array showed that the fields observed during substorms could be attributed to an equivalent current system similar to Boström's Type 1 current system, linking each end of a westward or eastward current in the auroral-zone ionosphere by field-aligned currents to an equivalent closure in the neutral sheet of the magnetotail (Kisabeth 1972; Kisabeth and Rostoker 1971, 1974; Rostoker and Kisabeth, 1973). A modified version of the Kisabeth-Rostoker equivalent current loop is illustrated in Fig. 1.7. As Rostoker (1974) has emphasized, this is an equivalent current system corresponding to transient disturbance of quasi-steady currents by the substorm. For example, the closure in the magnetotail may represent transient removal, during the substorm, of current in the opposite direction (Fig. 1.4), and satellite data suggest that this is indeed the case (McPherron et al., 1973). More recently Wiens and Rostoker (1975) have used magnetograms from the linear array to show that the ionospheric segment of a substorm current may develop in a number of discrete steps toward the northwest. At present the development of understanding of substorms phenomena relates them to ground-based and satellite data concerning the steady-state current systems in the magnetosphere and ionosphere (Rostoker et al ., 1975).

In the two alternative three-dimensional current systems illustrated in Fig. 1.6, the closure in the magnetosphere is least well understood at this time. This problem is fundamental for understanding the substorm mechanism, but is of little concern for the modelling of the magnetic fields produced by magnetic substorms from ground based magnetometers, as the magnetic perturbations at the

Figure 1.7 The three dimensional current loop used in modelling the observed fields. This is the Boström Type 1 current model of finite width, with a bend in the ionospheric segment.

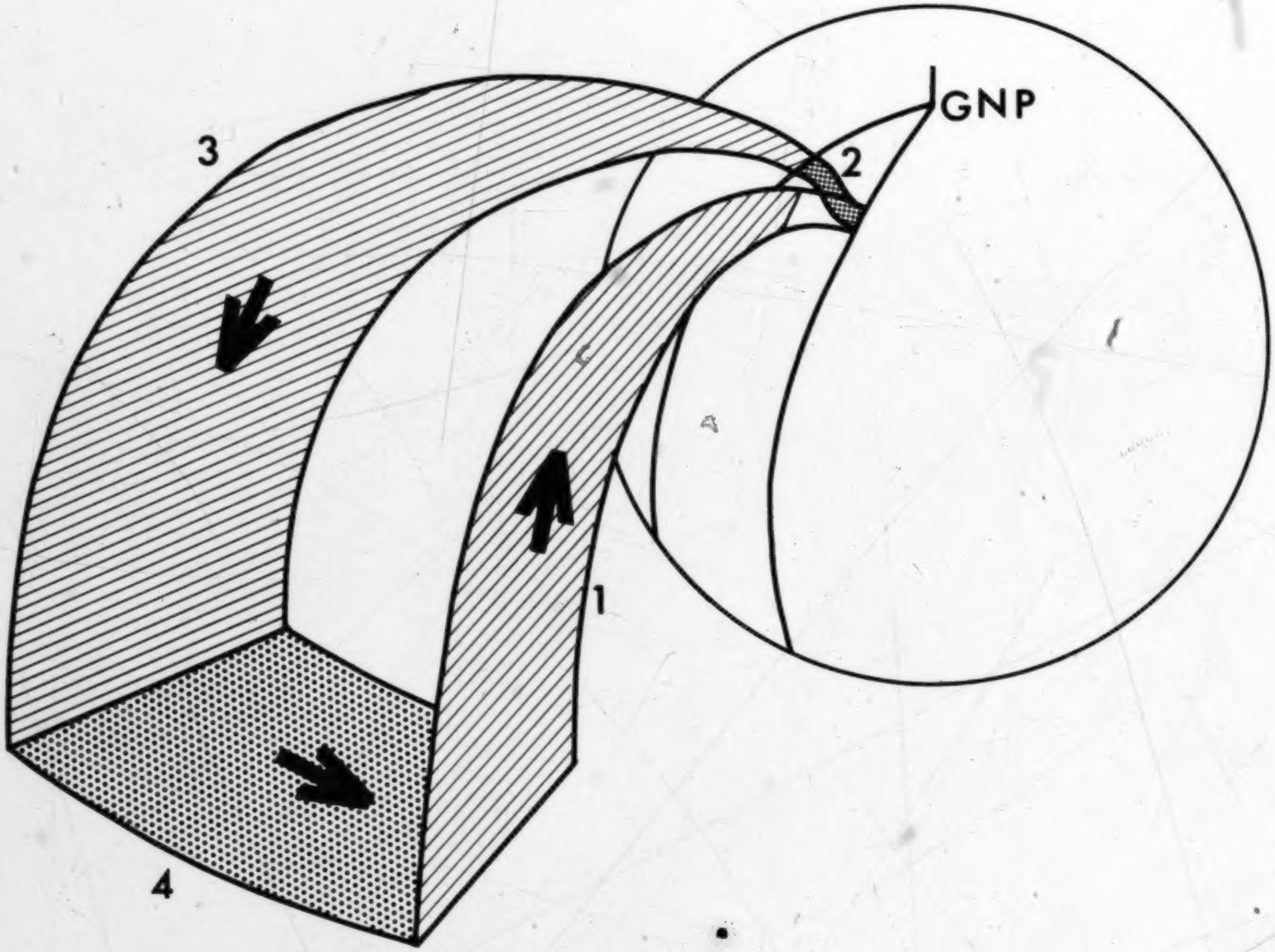
GNP

earth's surface are related mainly to the ionospheric current segment and the nearer sections of the field aligned currents.

In 1974 a two-dimensional array of three-component magnetometers was operated in a range of geomagnetic latitudes such that the ionospheric electrojet currents of some substorms would cross the array. It was expected that observation of the magnetic field perturbations in two dimensions would extend the results from the Rostoker group's linear array, for two reasons. The first is that simultaneous observation over a range of longitude enables time-dependent effects to be distinguished from east-west position-dependent effects. Secondly, while current models remain non-unique, they are more strongly constrained when they must match observed fields in three components over an area of the earth's surface, than when fields need be matched only along one magnetic meridian.

CHAPTER 2

FIELD OBSERVATIONS AND DATA PROCESSING

2.1 The magnetometer array.

The aim of the array study was to study polar magnetic substorms. Therefore its location was selected such that it would cover the latitudinal range in which the ionospheric current systems are expected to flow. The final location of the stations was subject to the availability of ground access to the sites. For northern Canada this proved to be a serious limitation, as it was necessary to install and service five stations (RUT, MEY, BUL, MIK and MAL) with the use of an aircraft. Sites were found, by examination of the ground from the air, where sand banks known as eskers lay close to lakes. The aircraft could then use the lake and the magnetometer could be buried in the sand.

Spacing of the stations within the array was kept to approximately 115 km (one ionospheric height) whenever possible. Oldenburg (1976) has subsequently shown that this value is a good compromise between maximizing the resolution and simultaneously minimizing the number of stations.

The array consisted of 29 three-component magnetometers, operated for 10 weeks from mid-July, 1974 to the end of September, at the positions mapped in Fig. 2.1;

coordinates of these stations are listed in Table 2.1. Four were fluxgate-type digitally recording systems made available by Dr. G. Rostoker and operated at SMI, URA, MCM and HAY (Fig. 2.1) by Dr. D.D. Wallis. The sampling rate for these five magnetometers was 1.91992 seconds. A full description of these instruments is given by Kisabeth (1972). One was a fluxgate-chart recorder temporary system run for our study by the Earth Physics Branch, Energy, Mines and Resources Canada, at the Yellowknife magnetic observatory (YEL) where the permanent instruments had not yet been installed. Data of the YEL station were provided by Dr. P.A. Camfield, and digitized on a trace-following type digitizing table.

The remaining 24 magnetometers were of the Gough-Reitzel (GR) type (Gough and Reitzel, 1967). The sensitivity of these magnetometers was reduced to about one quarter of the values used in previous arrays, (Alabi et al., 1975) in order to extend the range for the large magnetic field variations expected in the polar regions. The reduced sensitivity was obtained by reducing the magnetic moment of each sensing magnet. This reduction in sensitivity later proved insufficient, particularly for the northern stations, where only events with perturbation fields not larger than 500 nT were available for study with good coverage by the array. The sample interval for these magnetometers was 20 seconds controlled by an electronic clock. Field procedures used for the GR type magnetometers have been excellently

Figure 2.1 Map of the magnetometer array in Lambert conical projection of geographic coordinates. The broken-line curve indicates the south-western boundary of the Canadian shield.

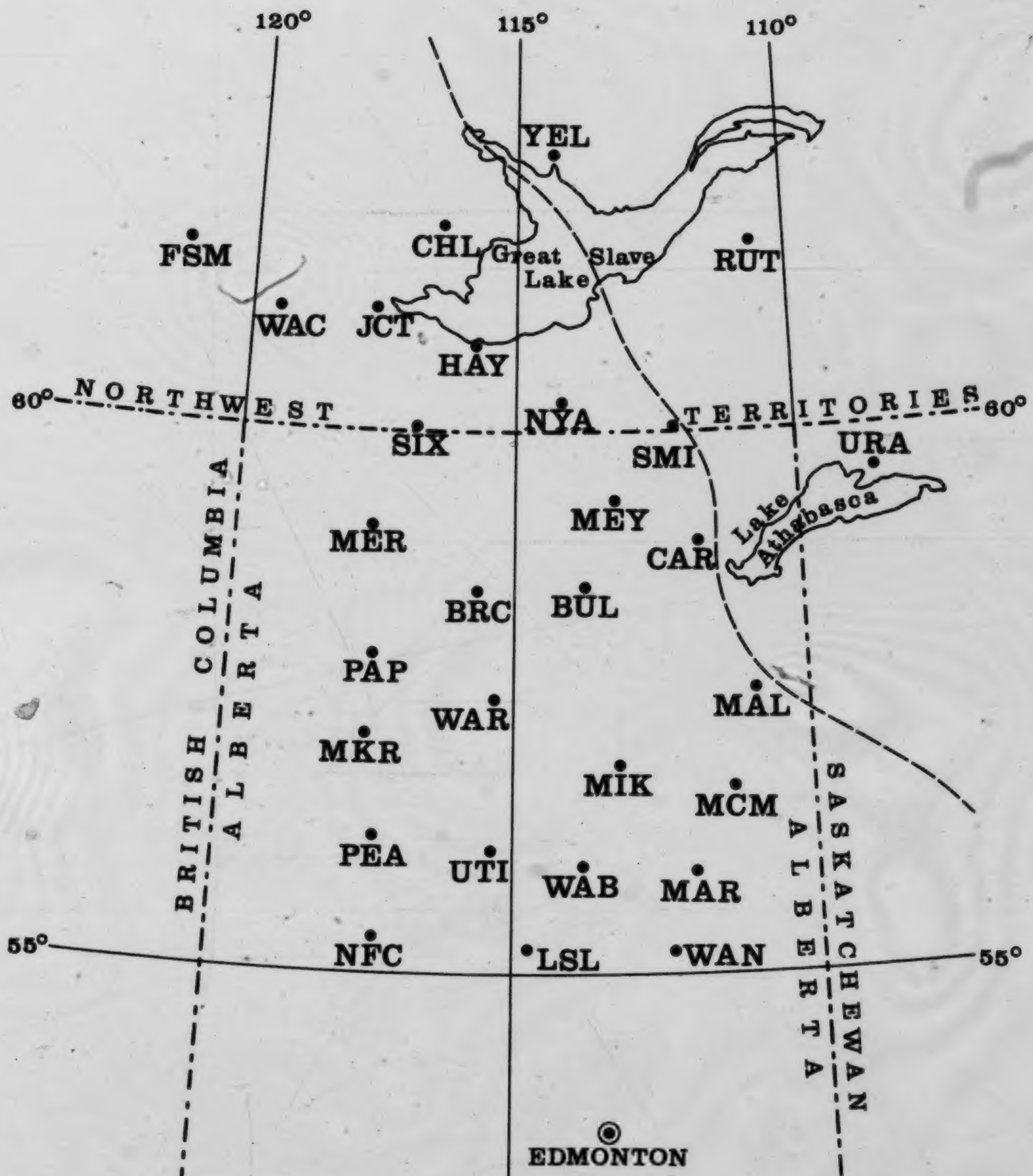
120°
115°
110°
YEL
FSM
CHL
Great Slave Lake
RUT
WAC
JCT
HAY
60°
NORTHWEST TERRITORIES
60°
SIX
NYA
SMI
URA
Lake Athabasca
MEY
MER
CAR
BRC
BUL
PAP
WAR
MAL
MKR
MIK
MCM
BRITISH COLUMBIA
ALBERTA
SASKATCHEWAN
ALBERTA
PEA
UTI
WAB
MAR
55°
NFC
LSL
WAN
55°
EDMONTON
120°
115°
110°

described by Camfield (1973) and will not be given here.

TABLE 2.1

LOCATIONS OF MAGNETOMETER STATIONS

Station Code Name	Geographic Coordinates		Centred Dipole Geomagnetic Coordinates	
	LAT.N.	LONG.E.	LAT.N.	LONG.E.
FSM	61.67	238.71	67.13	287.18
CHL	61.90	243.48	68.23	292.40
RUT	61.74	249.35	69.13	299.62
YEL	62.50	245.60	69.17	294.25
WAC	61.14	240.61	67.00	289.86
JCT	61.07	242.44	67.28	292.02
HAY	60.79	244.19	67.34	294.33
NYA	60.24	246.10	67.16	297.12
SIX	60.04	243.14	66.45	293.82
SMI	60.02	248.03	67.29	299.65
URA	59.56	251.51	67.45	304.33
MEY	59.34	246.65	66.42	298.58
MER	59.07	242.30	65.39	293.69
CAR	58.98	248.20	66.34	300.74
BUL	58.56	246.18	65.60	298.66
BRC	58.53	244.28	65.24	296.44
PAP	57.99	242.59	64.43	294.90
MAL	57.64	249.07	65.22	302.84
WAR	57.61	244.64	64.44	297.59
MKR	57.21	242.46	63.67	295.36
MIK	56.91	246.74	64.14	300.58
MCM	56.65	248.77	64.23	303.19
UTI	56.38	244.65	63.28	298.49
PEA	56.30	242.60	62.84	296.17
WAB	55.98	246.11	63.15	300.48
MAR	55.97	248.00	63.45	302.73
NFC	55.27	242.78	61.89	297.07
LSL	55.24	245.25	62.29	299.96
WAN	55.22	247.54	62.66	302.67

The array location is shown in Fig. 2.2 in relation to the auroral oval with local midnight at the array (305°

longitude). The oval shown in Fig 2.2 corresponds to low activity conditions (Q=2, Feldstein and Starkov, 1967; Whalen 1970) plotted in centred dipole geomagnetic coordinates with the magnetic north pole at geographic coordinates 78°.565 N and 69°.761 W (Russell, 1971). It can be seen that the array was placed in the only position, under the auroral oval, which lies on a continent in the northern hemisphere well away from induced currents in oceans. The array covers a latitudinal range from 70°N to 62°N geomagnetic. Magnetic records from Canadian and American observatories located outside the array limits were examined at the times of the substorms studied. The locations of these observatories are shown in Fig. 2.3, and their coordinates are listed in Table 2.2.

Figure 2.2 The auroral oval (Q = 2) and array outline in azimuthal equidistant projection of centred dipole geomagnetic coordinates, at 08.00 U.T.

U. OF ALBERTA ARRAY 1974

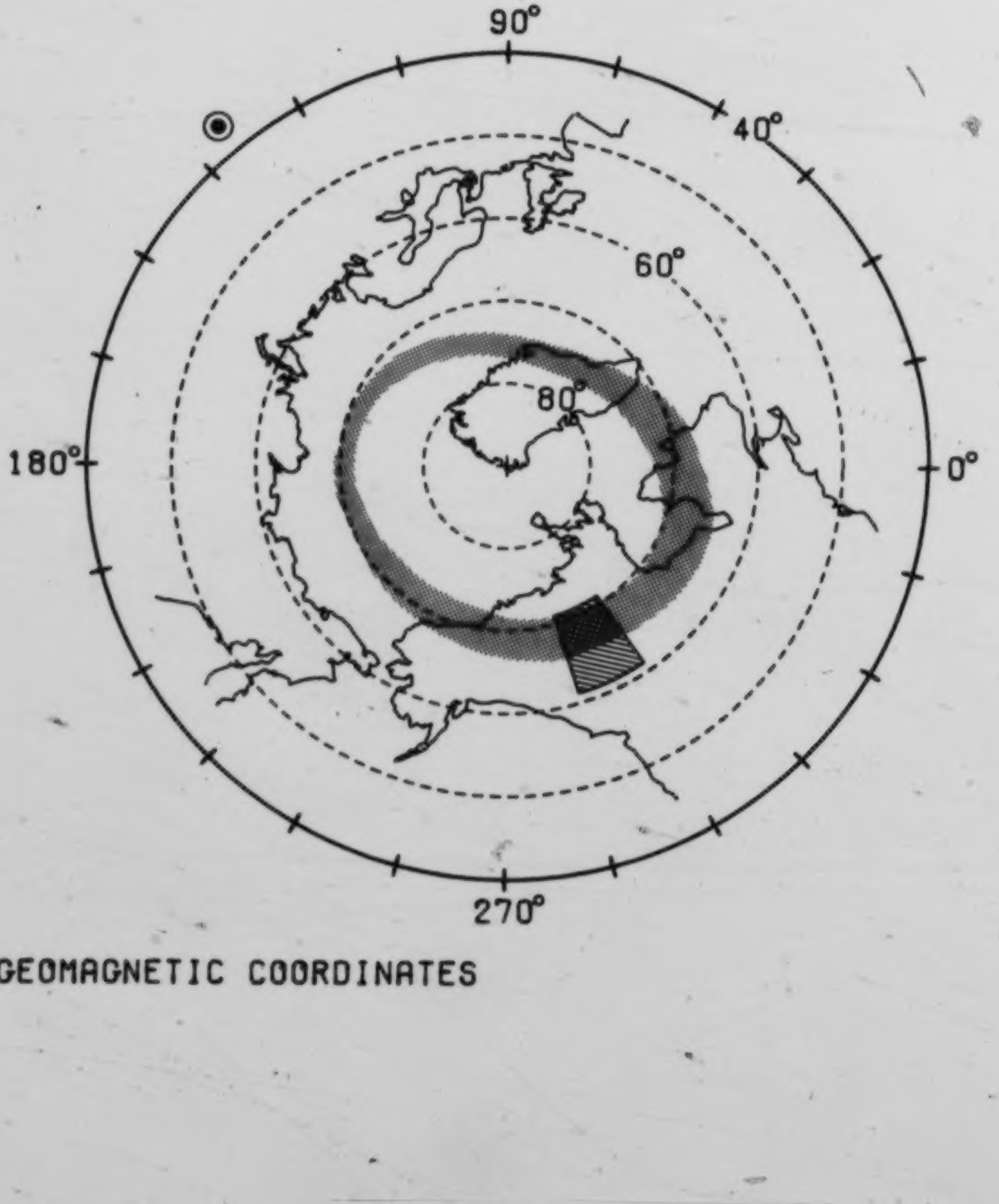
90°
40°
60°
80°
180°
0°
270°

GEOMAGNETIC COORDINATES

Figure 2.3 Location of Canadian and U.S. permanent magnetic observatories in the same polar azimuthal equidistant projection of centred dipole geomagnetic coordinates as in Fig. 2.2.

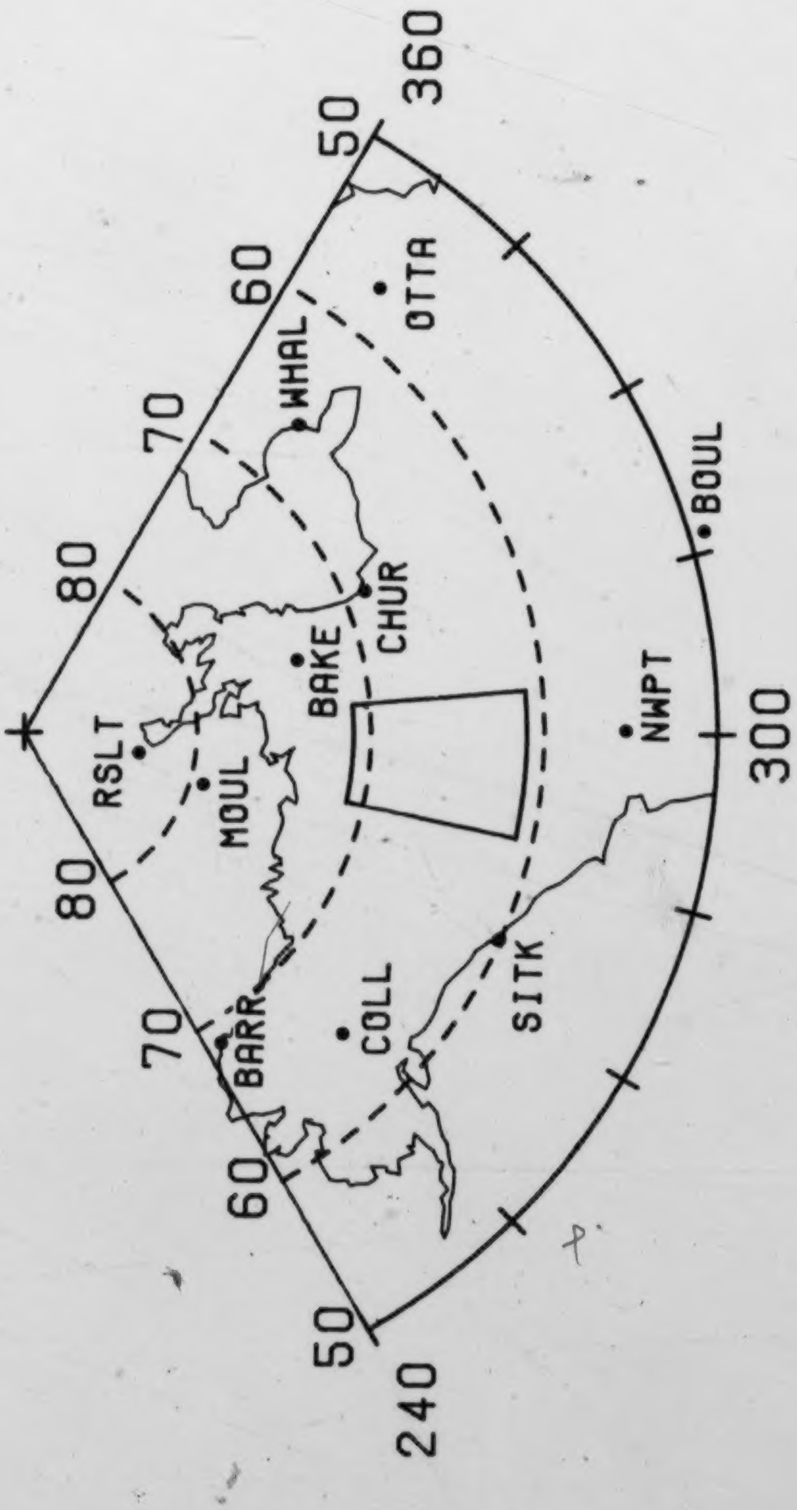
50
360
60
70
80
80
70
60
50
240
300
RSLT
MOUL
BAKE
CHUR
WHAL
OTTA
BOUL
NWPT
SITK
COLL
BARR

TABLE 2.2

LOCATIONS OF CANADIAN AND U.S. OBSERVATORIES

Observatory	Code Name	Geographic Coordinates		Geomagnetic Coordinates	
		LAT.N.	LONG.W.	LAT.N.	LONG.E.
Baker Lake	BAKE	64.30	96.00	73.9	314.8
Barrow	BARR	71.30	156.75	68.5	241.1
Boulder	BOUL	40.14	105.24	49.0	316.5
College	COLL	64.86	147.84	64.6	256.5
Fort Churchill	CHUR	58.80	94.10	68.8	322.5
Great Whale R.	WHAL	55.30	77.75	66.8	347.2
Mould Bay	MOUL	76.20	119.40	79.1	284.7
Newport	NWPT	48.26	117.12	55.1	300.0
Ottawa	OTTA	45.40	75.55	57.0	351.5
Resolute	RSLT	74.70	94.90	83.1	287.7
Sitka	SITK	57.06	135.33	60.0	275.4

2.2 Data Processing.

Analog to digital conversion of the GR type magnetometer records was done by first properly timing the analog records on the 35 mm film. Then the selected events were digitized using the Digital Converter as described by Burke et al (1975) and Alabi (1974). For sorting out the traces and base lines a new Fortran IV editing program was written in order to make use of a new Interactive Graphic (GT40) terminal acquired from DIGITAL by the Computing Center of the University of Alberta. The GT40 was linked to the new Amdahl 470V/6 computer of that Centre.

In several records, one or two traces would fall outside the operating range of the automatic film scanner of the Digital Converter. In these cases a photographic enlargement was made of the film records and the missing trace was hand digitized on a digitizing table of the University of Alberta Computing Center. The resolution of the system was 0.01 inch.

Scale values for the three components of the Gough-Reitzel magnetometers were obtained by field calibrations using a standard magnet. The scale values were about 36 nT for D, 30 nT for H, and 22 nT for Z refered to 1mm of the 35mm film.

Magnetograms from all stations of the array were converted to digital records with sample intervals of one minute, with amplitudes referred to the first minute of the record. These magnetograms were corrected to a centred dipole coordinate system to obtain the final magnetograms used in the modelling of the ionospheric currents.

Timing errors for magnetograms of the GR magnetometer do not exceed one minute. By the use of Pi2 micropulsations, it was possible to reduce timing errors to less than 25 seconds before digitizing. Timing errors for other stations are smaller.

It is estimated that the resolution of the film scanner (Digital Converter) is approximately 1 nT. The standard magnet used for calibrating the GR magnetometer is known to be within 0.4%. At least two, but normally four estimates of the calibration factors were obtained for each magnetic component from the calibration marks at the start and end of every film. An estimate of the standard deviation of the calibrating factors is 1.5%. Therefore it is estimated that the relative magnetic fields obtained from the GR magnetometers have an associated error of about 2%. The estimated error for the fluxgate magnetometers is ±1 nT.

CHAPTER 3

DEVELOPMENT OF A POLAR MAGNETIC SUBSTORM ON SEPTEMBER 11, 1974

3.1 Introduction

From the many substorms recorded with the magnetometer array, one which occurred on September 11, 1974 (Substorm 1) was selected for analysis. The criteria for the selection included the levels of activity before and after the substorm, the magnitude of the substorm, and the indication (by the inspection of the H and Z magnetograms across the array) that the overhead current was within the limits of the array. Maximum values of |H| together with minimum value of |Z| indicate approximately the centre of the current system. Maximum positive and negative values of Z indicate the approximate locations of the current edges (Kisabeth 1972). The substorm of 1974 September 11 was recorded by 25 stations of the array.

Magnetograms of the substorm from 14 stations, a representative subset of the array, are shown in Fig. 3.1. The left-hand stack shows the data from a north-south line of stations in the western part of the array and the right-hand stack refers to a north-south line in the eastern part. The stations are identified in Fig. 2.1. The geographic and geomagnetic coordinates of all stations are listed in

Figure 3.1 Magnetograms of Substorm 1 from 14 stations along two north-south lines near the western and eastern edges of the array. Bars indicate the six time intervals averaged in Figs. 3.5a and 3.5b. The station positions are shown in Fig. 2.1.

SEPTEMBER 11 1974

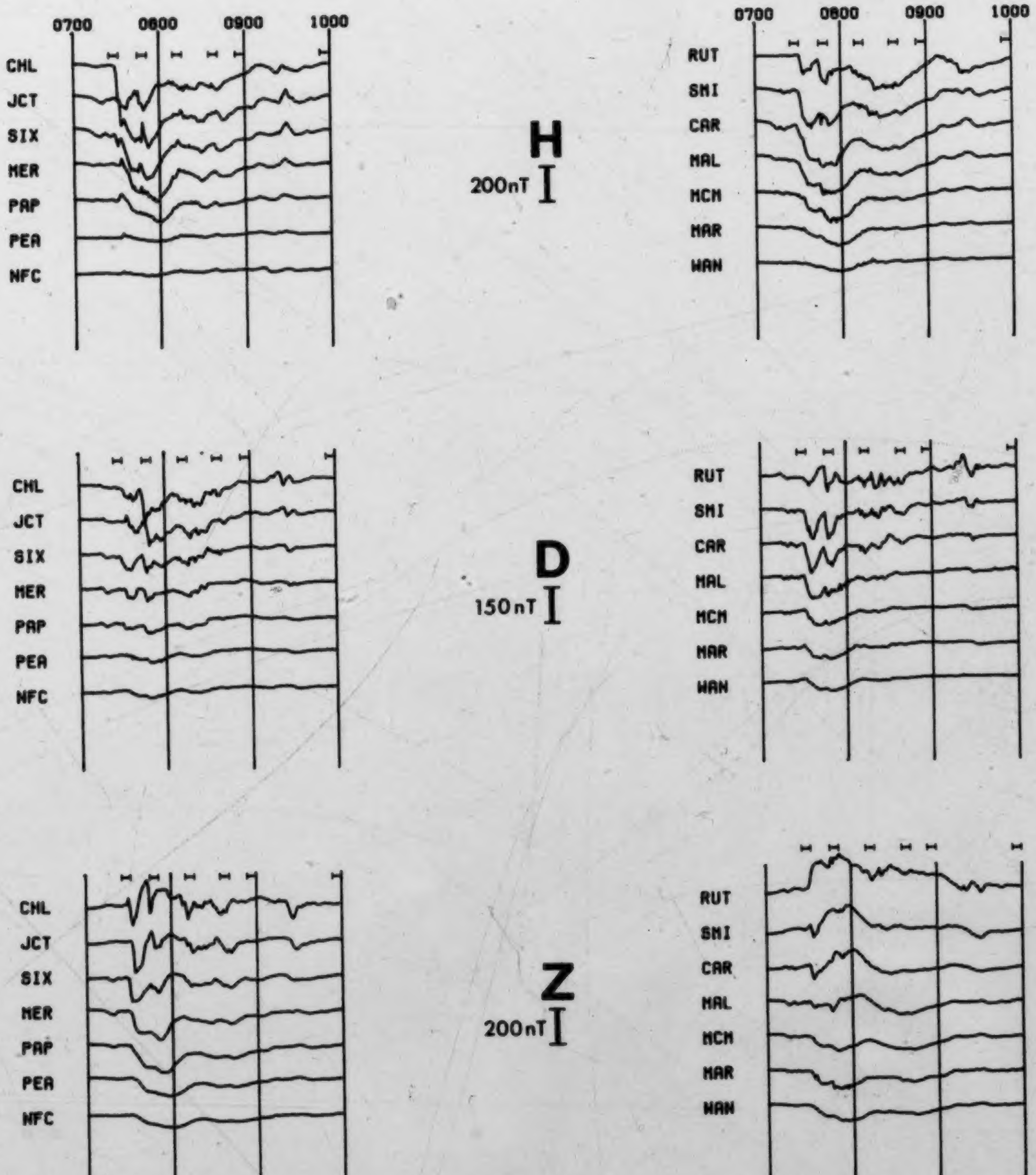

Table 2.1.

3.2 Induced currents in the earth

3.2.1 Electrical conductivity distribution in the earth

As far as electrical conductivity is concerned, the continental regions of the earth can be divided into three sections. In the first section, starting from the surface of the earth, is a conductive layer which consists of sedimentary or metamorphic rocks sometimes containing water. Here the conductivities are variable, in the range 10^{-3} to 10^{-1} S/m. Then comes a section of igneous and metamorphic rocks with a comparatively low conductivity of about 10^{-4} S/m. It is believed that at these depths the pressures are high enough to close cracks and exclude water, but the temperatures are still low. As temperature increases with depth, there is a sharp increase in conductivity between 400 and 600 Km. reaching a value of 1 S/m at about 700 Km.

The broken line in Fig. 2.1 (Chapter 2) represents the boundary of the Canadian shield with respect to the array. To the north east of the broken line the uppermost layer of high conductivity is minimal. To the southwest of the broken line there is a thin Mesozoic sedimentary section of intermediate conductivity.

Induction effects produced by the changing magnetic fields in conductive layers of the earth are large enough to require consideration in the calculation of ionospheric current models. Two simple, idealized earth models can generally be used to include the induction effects in the calculations of ionospheric current systems. These are (A) models where the earth is represented by a body of finite conductivity $\sigma(r)$ (Banks, 1969) and (B) models which reduce the earth to a perfect conductor at depth. Mareshall (1976) shows that for most modelling of substorms it is sufficient to treat the earth as a perfect conductor. The depth of this perfect conductor is a function of the source frequency. The effective depth of induced currents, in a half-space with conductivity a function of depth alone, is proportional to the skin depth and thus to $T^{\frac{1}{2}}$ where T is the dominant period in the disturbance field. Therefore by examining the different events it is possible to estimate the depth of the superconductor. Alternatively, several depths may be tried and one selected for which the model current gives smallest residuals in H and Z. A shallower perfect conductor increases calculated H and reduces Z. The depth of the perfect conductor can, if desired, be made a variable in the fitting of the model.

3.2.2 Maps of Fourier spectral components

In addition to the induction effects in the spherically symmetric approximation to the earth, there are possible local induction effects produced by conductivity anomalies in the low-conductivity crustal depth range. Such local anomalies have been found in many magnetometer array studies.

One technique which has proved useful in such studies is the mapping of amplitudes and phases of Fourier transforms of magnetic variation fields (Reitzel et al. 1970; Gough (1973); Alabi et al. 1975).

Figs 3.2, and 3.4 are the contour maps of the Fourier transforms for two different periods of a polar magnetic substorm recorded by the array on 1974 September 18. Fig 3.3 is the Fourier contour map for 60.2 minute period of another magnetic substorm recorded on September 11, 1974. These contour maps show the fields of both external and internal induced currents. Local conductivity anomalies in the Earth would appear consistently with approximately unchanged positions for different variation events, and could then with some confidence be assigned to internal conductivity structure.

Fig 3.2 shows the results of a Fourier transformation for a period of 120.5 minutes. As would be expected for a westward electrojet, there is a maximum of H under the current system with a very small change in phase (60 minutes=180°). The Z amplitude has a minimum under the current system and maxima north and south of this minimum with a complete reversal (180°) in the phase map.

For the shorter periods 60.2 minutes (Fig 3.3) and 21.1

Figure 3.2 Contour maps of Fourier transform amplitudes (nT) and phases (min) at period 120.5 minutes from Substorm 3 (1974 September 18). Contours are over a map of the array in geographic coordinates in a Lambert conical projection. For the phase, 60.2 min=180°.

T = 120.5 min

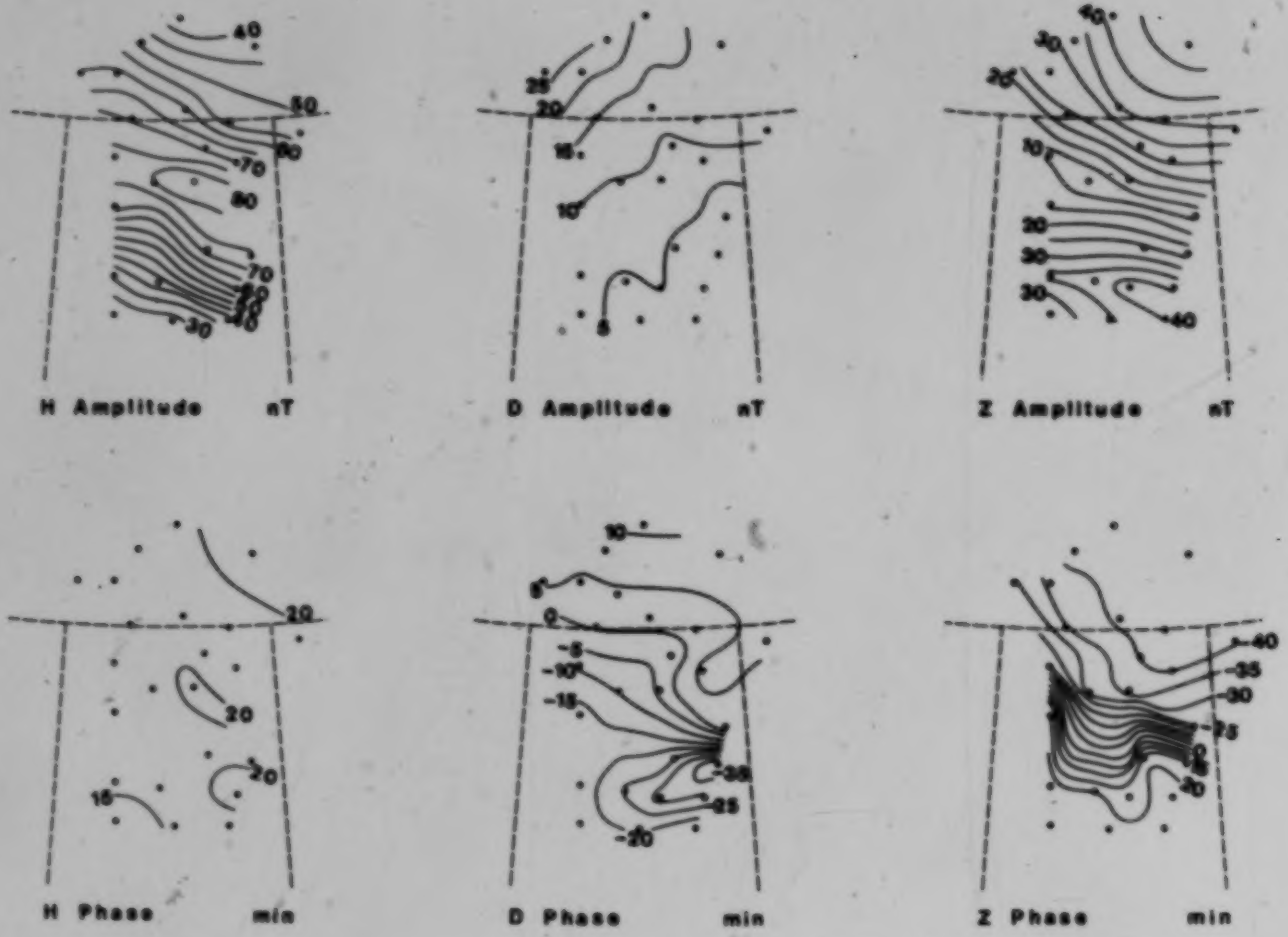
40
50
60
70
80
70
30
H Amplitude nT
25
20
15
10
5
D Amplitude nT
40
30
20
10
20
30
30
40
Z Amplitude nT
20
20
20
15
H Phase min
10
5
0
-5
-10
-15
-30
-25
-20
D Phase min
-40
-35
-30
-25
-20
Z Phase min

Figure 3.3 Contour maps of Fourier transform amplitudes (nT) and phases (min) at period 60.2 minutes from Substorm 1 (1974 September 11). Contours are over a map of the array in geographic coordinates in a Lambert conical projection. For the phase 30.1min=180°.

T = 60.2 min

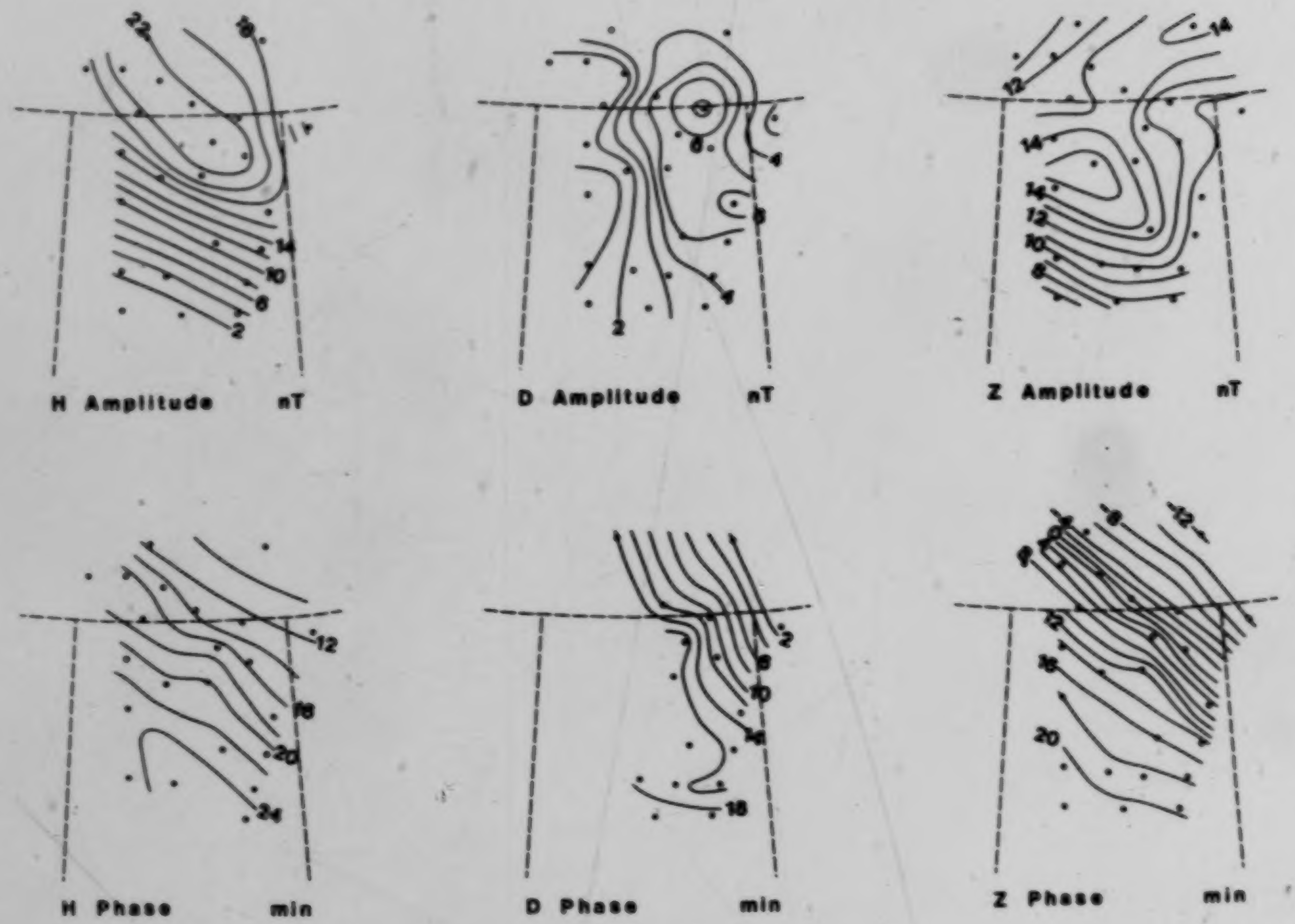
22
18
14
10
6
2
H Amplitude nT
8
4
6
4
2
D Amplitude nT
14
12
14
14
12
10
8
Z Amplitude nT
12
16
20
24
H Phase min
2
6
10
14
18
D Phase min
-12
-8
-4
0
8
12
16
20
Z Phase min

Figure 3.4 Contour maps of Fourier transform amplitudes (nT) and phases (min) at period 21.1 minutes from Substorm 3 (1974 September 18). Contours are over a map of the array in geographic coordinates in a Lambert conical projection. For the phase, 10.6 min=180°.

T = 21.1 min

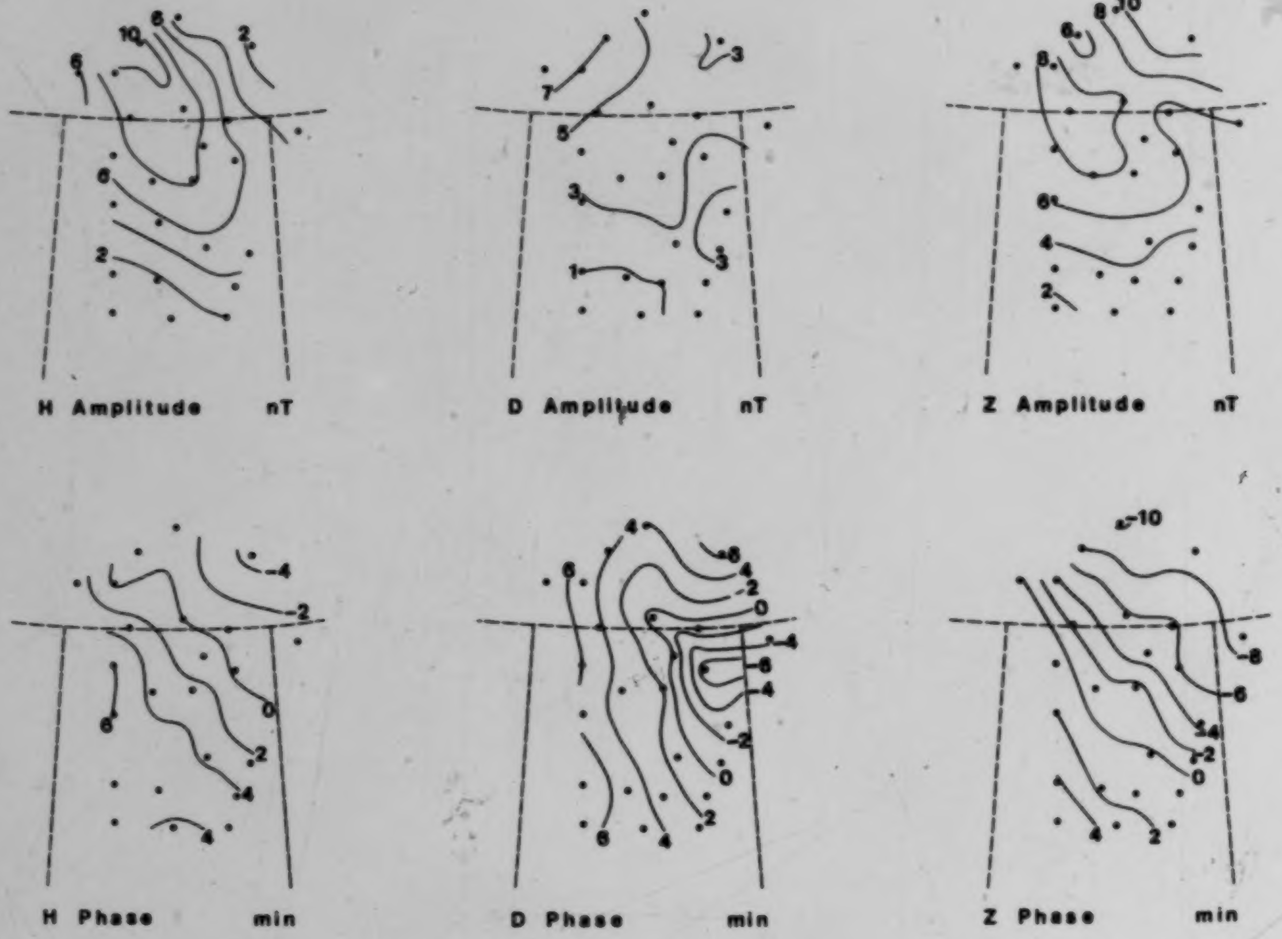
H Amplitude nT
D Amplitude nT
Z Amplitude nT
H Phase min
D Phase min
Z Phase min

minutes (Fig 3.4) the contours display approximately the same characteristics as for 120.5 minutes. It appears from Fig 3.4 that the centre of the current system shifts north when shorter periods are reached. The development of rapidly changing fields observed in the auroral zone during a geomagnetic substorm is, however, better studied in the time domain than in terms of a Fourier transform which integrates over an event. The Fourier transform maps are more sensitive to induced currents which do not shift during the substorm, and have therefore been used to check the possible existence of local anomalies in conductivity. From the several such contour maps studied there is no evidence of significant conductivity anomalies under the region covered by the array.

3.3 Perturbation Fields

Observed field components have been averaged over five-minute intervals to yield "time frames" each of which represents an epoch in the substorm development. Periods of specially rapid change have been scrutinized in two-minute averages, but the timing precision precludes shorter intervals. All time frames here presented represent five-minute averages.

The entire substorm has been plotted in consecutive five-minute time frames, and six representative epochs in the development are reproduced in Figs. 3.5a and 3.5b. These time intervals are indicated in Fig. 3.1.

For all substorms reported the standard deviations of H, D and Z at each epoch are in general within 10% of the total perturbation field averaged in that interval.

In Figs. 3.5 and 3.7-3.11 the tail ends of the arrows are at the 25 stations that recorded the substorm, mapped on a Mercator projection of the centred dipole geomagnetic coordinates already specified in Chapter 2. Thus each map in these figures has its top and bottom aligned with geomagnetic latitudes and its sides along geomagnetic longitudes.

The H, D and Z values were measured from baselines at 05.00 U.T., when conditions were quiet. In the epoch 07.26-07.30, represented in the first time frame of Fig. 3.5a, it is clear that the perturbations were small. Twenty minutes later (Fig. 3.5a frame 2) there are large overhead currents flowing across the array somewhat north of west. Both the horizontal and vertical components locate the centre of the current systems near 67-68° (magnetic) and its southern edge near 65°N (magnetic). In the third frame of Fig. 3.5a the fields resemble those of frame 2, but have amplitudes about half those of frame 2.

In frames 1 and 2 of Fig. 3.5b, prominent eastward horizontal fields appear in the southern part of the array. It will be shown that these fields can be modelled in terms

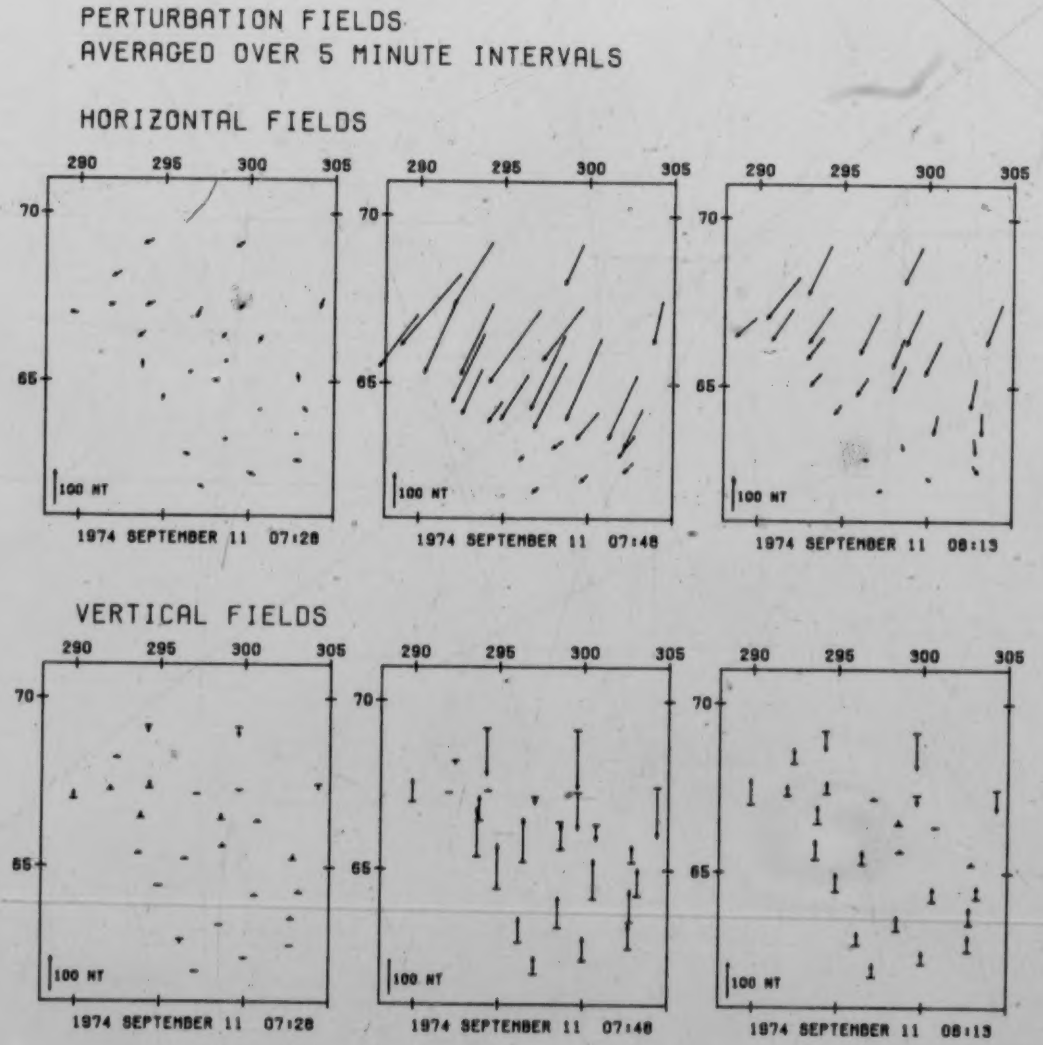

Figure 3.5a Mean perturbation fields over five-minute intervals at three epochs before and during Substorm 1. For the vertical components, northward arrows represent upward fields. Unit: nanotesla.

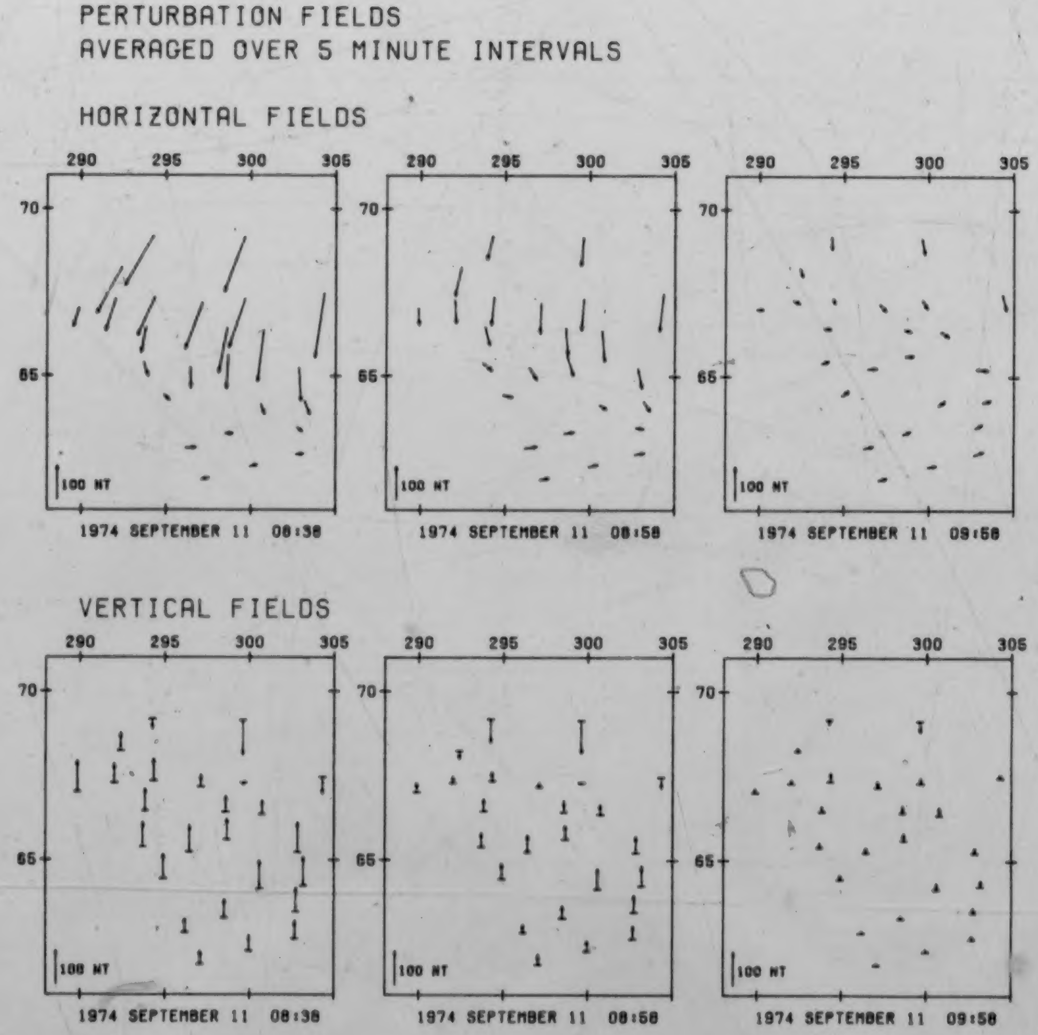

Figure 3.5b Mean perturbation fields over five-minute intervals at three epochs during Substorm 1. For the vertical components, northward arrows represent upward fields. Unit: nanotesla.

of an upward field-aligned current at the west end of the ionospheric current. Frame 3, Fig. 3.5b, which represents the fields one hour after frame 2, shows the gradual decline of the substorm fields in contrast to the sudden onset.

3.4 Model Calculations

The outstanding feature of the perturbation fields is the signature of a strong westward ionospheric current. This leads naturally to consideration of the model of a current loop, used by Kisabeth (1972) and Kisabeth and Rostoker (1977), having field-aligned currents at the east and west ends of the ionospheric current, and closure in the neutral sheet within the magnetotail (Fig. 1.7). For three of the four time-frames modelled, the perturbation fields required introduction of a bend to displace the western end of the ionospheric current to higher latitudes, as is indicated in Fig. 1.7.

The magnetic fields produced at the Earth's surface by the three-dimensional current loop (Fig. 1.7) were calculated from the Biot-Savart law in the manner described by Kisabeth (1972). Provision was made to introduce a bend in the ionosphere segment to give a change of latitude with a cosine dependence on longitude. Kisabeth (1972) and Kisabeth and Rostoker (1977) used a parabolic path for the ionospheric currents to provide for paths having a northward component.

By varying the total current and the position of the ionospheric segment, a least-squares fit was obtained between the calculated and observed magnetic fields. In fitting the perturbation fields at 07.48, 08.13 and 08.38 U.T. (Figs. 3.7-3.9), eight parameters were allowed to change (Fig. 3.6). These were the total current (P1), the latitudes of the northern (P6, P9) and southern (P7, P8) edges of the ionospheric segment at each end, the longitude limits of the bend (P3, P4) and the longitude of the end of the ionospheric segment closer to the array (P5 for 07.48 P2, for the other epochs). The longitude of the further end, to which the calculated fields were rather insensitive, was kept fixed while the eight parameters were adjusted, and was finally itself adjusted to optimize the fit.

In fitting the perturbation fields at 08.58 U.T. (Fig. 3.10) a simple constant-latitude ionospheric segment proved sufficient and four free parameters were allowed to change, viz. the total current (P1), the latitude limits (P6 and P7) and the longitude of the nearer (in this case western) end of the ionospheric current segment (P2). Once again the longitude of the east end (P5) was finally adjusted to optimize the fit.

All calculated fields reported in this chapter correspond to a uniform current density across the ionospheric segment. It is possible that some further improvement in fit could be secured if non-uniform current

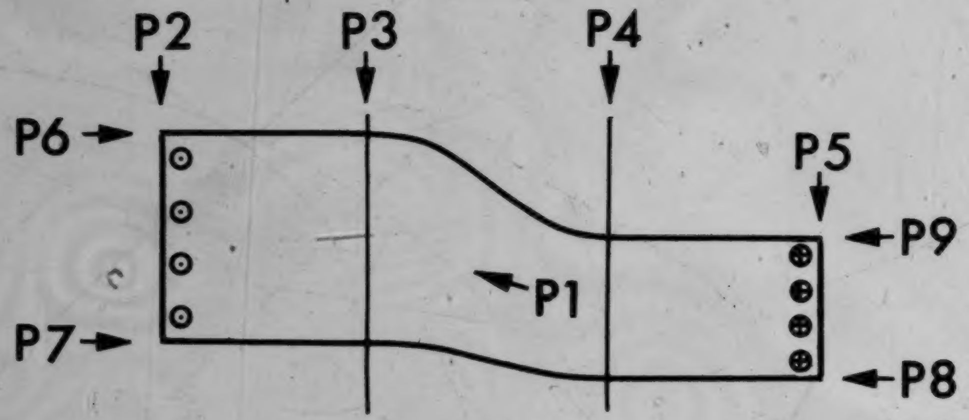

Figure 3.6 Outline of the ionospheric segment of the three-dimensional current loop used to model Substorm 1 indicating the different parameters that control its geometry and current. Birkeland field aligned currents are indicated.

profiles were used. While the field-aligned currents have been modelled as sheets of negligible thickness, tests show that the data are equally well satisfied by field-aligned currents distributed through five degrees of longitude, even when the foot of one field-aligned current lies inside the array (as at 08.58 U.T., Fig. 3.10). In reality the field-aligned currents seem likely to be distributed in longitude.

In all calculations the ionospheric currents were kept at altitude 115 km. Induction in the Earth has been approximated by that in a superconducting sphere at depths chosen empirically to optimize the fits of calculated horizontal and vertical components to those observed. Inspection of Fig. 3.1 shows that the dominant period T is longer for the tail of the event than earlier. The empirical approach as described in section 3.2.1 of this chapter, which is that used by Kisabeth (1975) and by Mareschal (1976), leads to the use of 250 km for the depth of the superconductor in the models of 07.48, 08.13 and 08.38 U.T., and of 600 km at 08.58, in the coda of the substorm.

The least-squares fit was obtained by applying to observed and calculated values, of three magnetic components with equal weights, the iterative subroutine ZXSSQ of the IMSL library.

The models in this chapter approximate observed perturbation fields from the 05.00 U.T. baseline. These are presumably superimposed on some steady-state field corresponding to preexisting currents in the magnetosphere and ionosphere. The latter, if they remained steady through the substorm, would not be seen in the perturbation field.

3.5 Model currents for four epochs of Substorm 1

Observed and calculated fields, and the residuals (observed - calculated), are shown at four representative epochs of the substorm in Figs. 3.7-3.10. The northern and southern limits of the ionospheric segment of the current loop are shown in these maps. Before discussing these further it is worth pointing out that the entire ionospheric segment for each epoch is shown in Fig. 3.11, in relation to the array, with observed horizontal fields only. These are mapped in geomagnetic Mercator projection, as explained earlier. Each ionospheric segment has a downward field-aligned current at the east end and an upward field-aligned current at the west end.

In Figs. 3.7-3.10 the upper frames show total horizontal perturbation fields; in the lower frames the vertical components are shown by upward arrows at stations where Z was upward (negative).

In the interval 07.46-07.50 U.T. (Fig. 3.7) the current attained its greatest value of 0.24×10^6 amperes. The westward component of the observed horizontal field and the trend of the region Z=0 require that the ionospheric current be modelled with a bend to the northwest as shown. The

Figure 3.7 Observed perturbation fields, calculated fields for a model current of best fit, and residuals in the five-minute interval 07.46-07.50 U.T. during Substorm 1. The full length of the ionospheric segment of the current is shown in Fig. 3.11. Total current is 0.24×10^{6} amperes.

IONOSPHERIC CURRENT MODEL
WESTWARD UNIFORM CURRENT 0.24 MA

HORIZONTAL PERTURBATION FIELDS

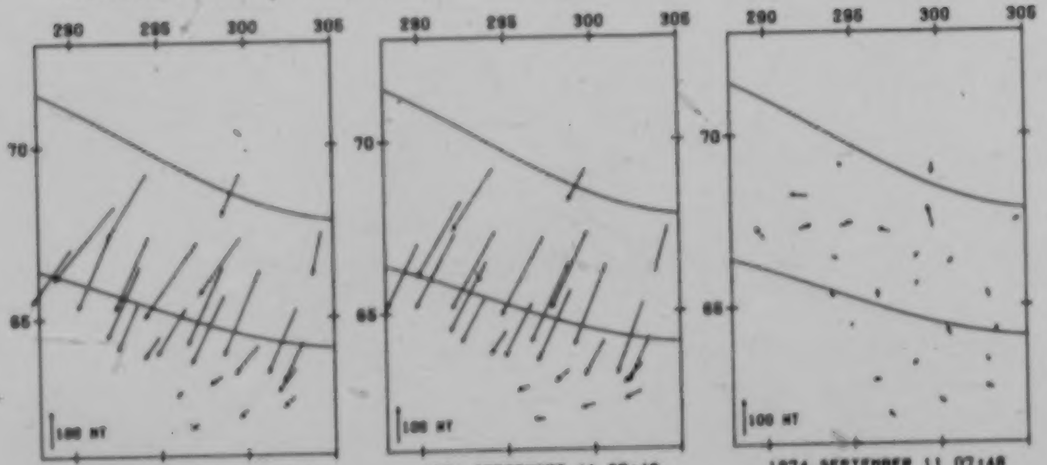

1974 SEPTEMBER 11 07:48
OBSERVED VALUES

1974 SEPTEMBER 11 07:48
CALCULATED VALUES

1974 SEPTEMBER 11 07:48
RESIDUALS

VERTICAL PERTURBATION FIELDS

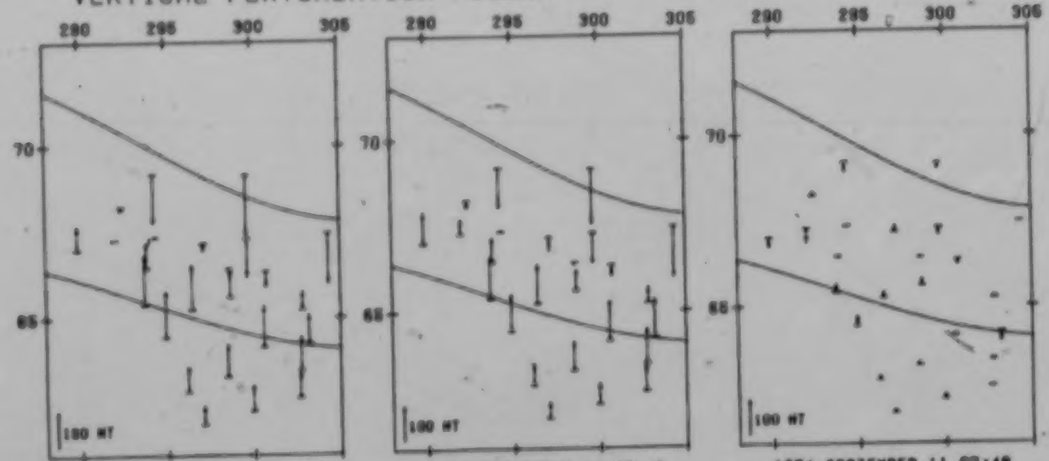

1974 SEPTEMBER 11 07:48
OBSERVED VALUES

1974 SEPTEMBER 11 07:48
CALCULATED VALUES

1974 SEPTEMBER 11 07:48
RESIDUALS

Figure 3.8 Observed perturbation fields, calculated fields and residuals in the five-minute interval 08.11-08.15 U.T. during Substorm 1. The full length of the ionospheric segment of the current is shown in Fig. 3.11. Total current is 0.12×10^6 amperes.

IONOSPHERIC CURRENT MODEL
WESTWARD UNIFORM CURRENT 0.12 MA

HORIZONTAL PERTURBATION FIELDS

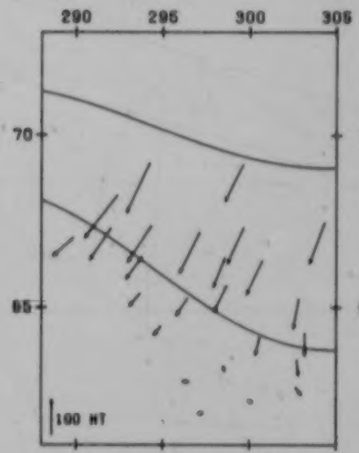

1974 SEPTEMBER 11 08:13
OBSERVED VALUES

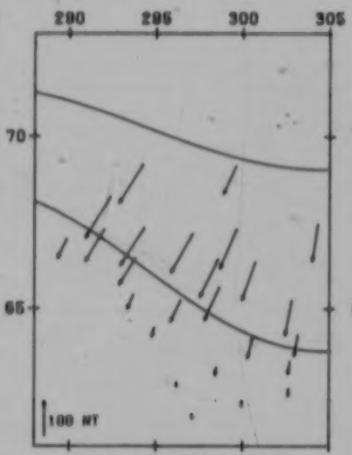

1974 SEPTEMBER 11 08:13
CALCULATED VALUES

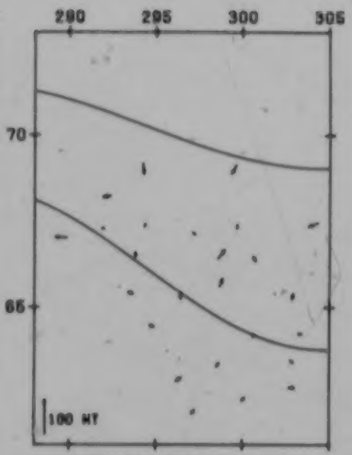

1974 SEPTEMBER 11 08:13
RESIDUALS

VERTICAL PERTURBATION FIELDS

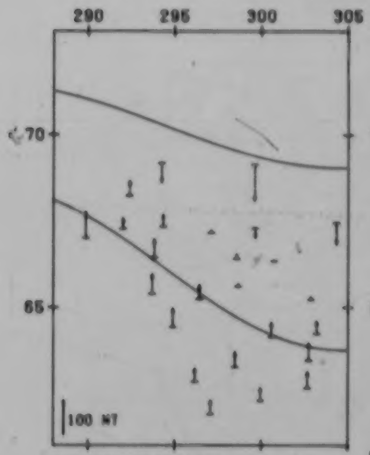

1974 SEPTEMBER 11 08:13
OBSERVED VALUES

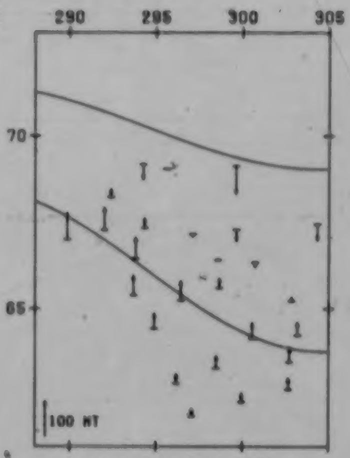

1974 SEPTEMBER 11 08:13
CALCULATED VALUES

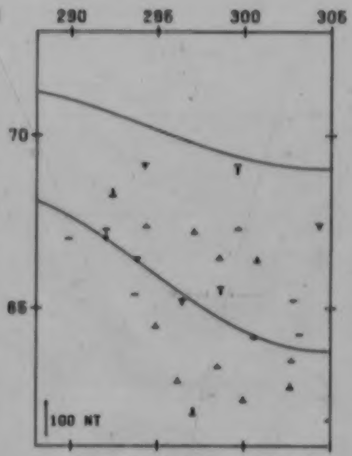

1974 SEPTEMBER 11 08:13
RESIDUALS

Figure 3.9 Observed perturbation fields, calculated fields and residuals in the five-minute interval 08.36-08.40 U.T. during Substorm 1. The full length of the ionospheric segment of the current is shown in Fig. 3.11. Total current is 0.20×10^6 amperes.

IONOSPHERIC CURRENT MODEL
WESTWARD UNIFORM CURRENT 0.20 MA

HORIZONTAL PERTURBATION FIELDS

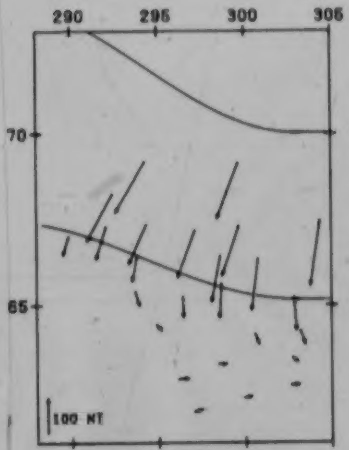

1974 SEPTEMBER 11 08:38
OBSERVED VALUES

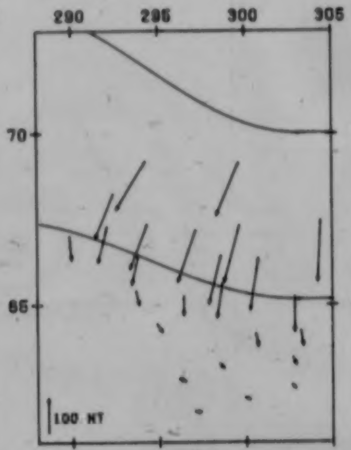

1974 SEPTEMBER 11 08:38
CALCULATED VALUES

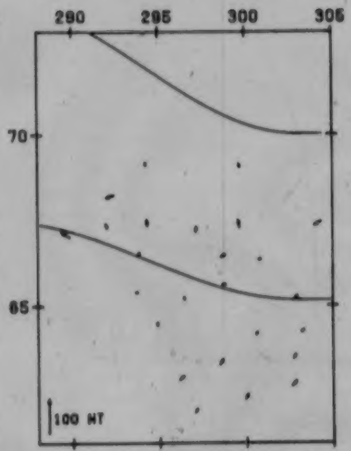

1974 SEPTEMBER 11 08:38
RESIDUALS

VERTICAL PERTURBATION FIELDS

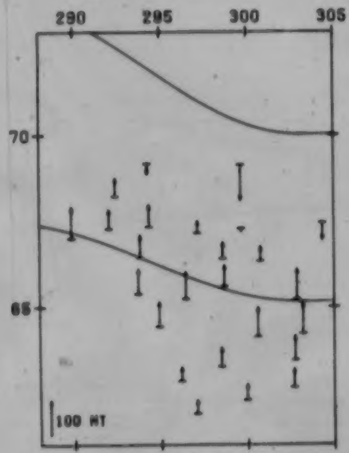

1974 SEPTEMBER 11 08:38
OBSERVED VALUES

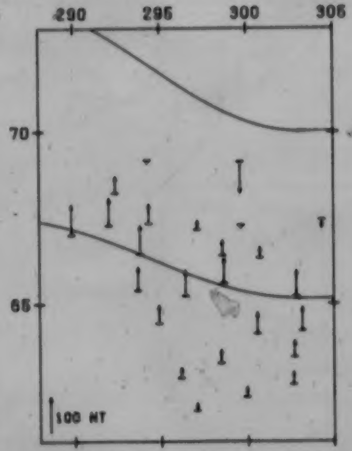

1974 SEPTEMBER 11 08:38
CALCULATED VALUES

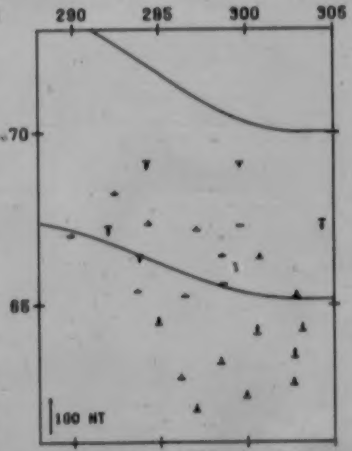

1974 SEPTEMBER 11 08:38
RESIDUALS

Figure 3.10 Observed perturbation fields, calculated fields and residuals in the five-minute interval 08.56-09.00 U.T. during Substorm 1. The full length of the ionospheric segment of the current is shown in Fig. 3.11. Total current is 0.12x10^{6} amperes.

IONOSPHERIC CURRENT MODEL
WESTWARD UNIFORM CURRENT 0.12 MA

HORIZONTAL PERTURBATION FIELDS

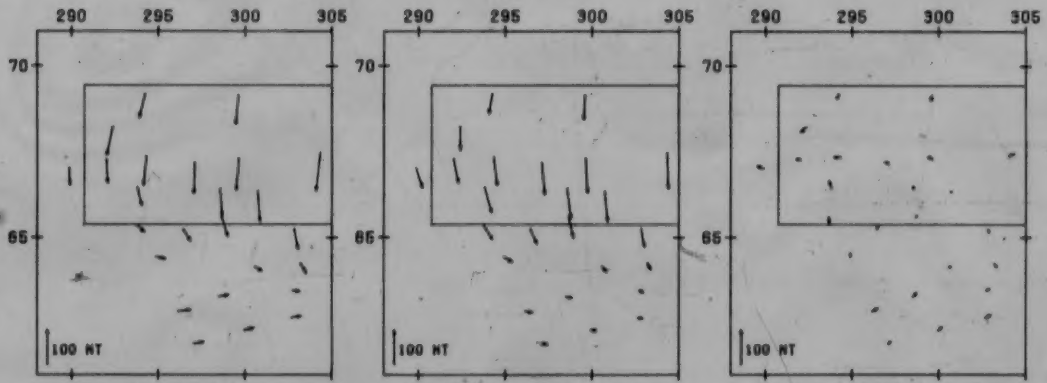

1974 SEPTEMBER 11 08:58
OBSERVED VALUES

1974 SEPTEMBER 11 08:58
CALCULATED VALUES

1974 SEPTEMBER 11 08:58
RESIDUALS

VERTICAL PERTURBATION FIELDS

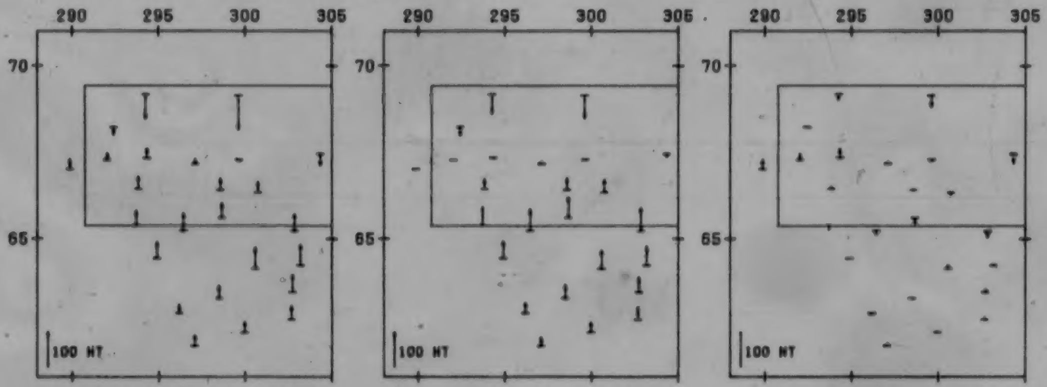

1974 SEPTEMBER 11 08:58
OBSERVED VALUES

1974 SEPTEMBER 11 08:58
CALCULATED VALUES

1974 SEPTEMBER 11 08:58
RESIDUALS

residuals appear quite large, but when normalized to the observed fields, they are smaller than at the other three epochs (Table 3.1). As a measure of goodness of fit the following parameters are used:

$$\varepsilon = \frac{\sum(\text{residual})^2}{\sum(\text{observed total field})^2}$$

and

$$\xi = \frac{\sum(\text{residual})^2}{\sum(\text{observed total field at epoch 07.28})^2}$$

The large and systematic negative residuals of the horizontal fields for three stations in Fig. 3.7 under the centre of the current system suggests that a better fit could be obtained if a nonuniform current density distribution, having increased current density near the centre, had been used in this model.

Between 08.11 and 08.15 U.T. (Fig. 3.8) the total current was half that for 07.46-07.50 U.T., as expected from the magnetograms (Fig. 3.1). The westward components in the horizontal fields once again require a bend displacing the ionospheric current to the northwest. Eastward displacement of the east end of the current loop appears to occur mostly between 07.48 and 08.13 U.T. (Fig. 3.11). The parameters ε and ξ are given in Table 3.1.

TABLE 3.1

STATISTICAL PARAMETERS FOR SUBSTORM 1

1974 SEPTEMBER 11

TIME U.T.	SSQ OBSERVED	SSQ RESIDUAL	ε	ξ
07.28	12595	--	--	--
07.48	953020	21783	0.0229	1.73
08.13	250056	13598	0.0544	1.08
08.38	365283	10761	0.0295	0.85
08.58	140364	9944	0.0708	0.79
09.58	24346	--	--	--

Note: SSQ denotes sum of squares.

In the interval 08.36-08.40 U.T. the total current has risen to 0.20×10^6 amp. and the current loop has moved eastward. The array does not now extend far enough northward to locate the northern edge of the current at all well. It is worthy of note that the model produces small northward H components to fit the observed values, in the southern part of the array. This and the eastward D at southern stations are produced by the upward field-aligned current at the west end of the current system.

Between 08.56 and 09.00 U.T. the total current has dropped to 0.12×10^6 amp. and the fields are quite well fitted by a current loop whose ionospheric segment lies in the constant latitude range of 65-69°N (geomagnetic). The upward field-aligned current sheet at the western end is now within the limits of the array. The relatively large and highly consistent eastward D components in the southern half of the array give specially striking evidence of the upward field-aligned current.

Major changes, during the substorm, in both position and length of the current system are required to fit the two-dimensional array data (Fig. 3.11). At the epoch 07.46-07.50 U.T. the downward field-aligned current sheet at the east end is close enough to the array that its longitude is constrained to lie between 312° and 313° magnetic. This east end is 1° west of local magnetic midnight, as defined by Montbriand (1965). The upward field aligned current is too far to be placed with precision, but is no more than 10° east of the position shown in Fig. 3.11. In the next epoch, 08.11-08.15 U.T., the current system has moved north and neither field-aligned current is close enough to be well located by the array.

In the epoch 08.36-08.40 U.T. the upward field-aligned current sheet is just west of the array and produces strong contributions to the horizontal fields. Once again the further field-aligned current, now that at the east end, produces little effect at the array and cannot be placed accurately. It cannot be closer than the position shown. The current system has moved eastward relative to the previous

Figure 3.11 Ionospheric segments of current loops for Substorm 1, in relation to the magnetometer array, at four epochs, in the Mercator projection of centred-dipole geomagnetic coordinates. GM represents magnetic midnight (see text).

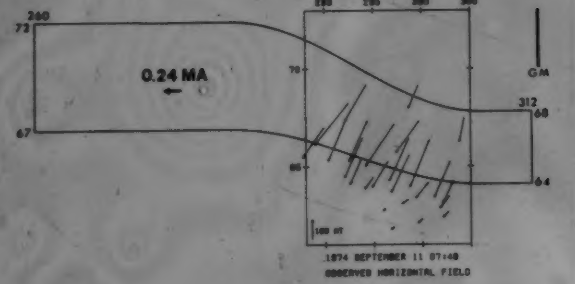

280
72
67
0.24 MA ←
280
285
300
305
70
65
GM
312
68
64
100 NT
1974 SEPTEMBER 11 07:40
OBSERVED HORIZONTAL FIELD

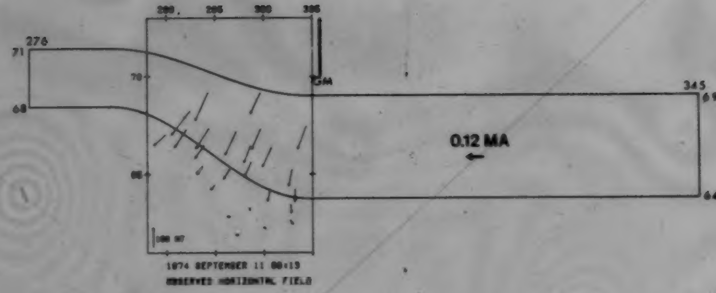

276
71
68
280
285
300
305
70
65
GM
345
69
64
0.12 MA ←
100 NT
1974 SEPTEMBER 11 08:13
OBSERVED HORIZONTAL FIELD

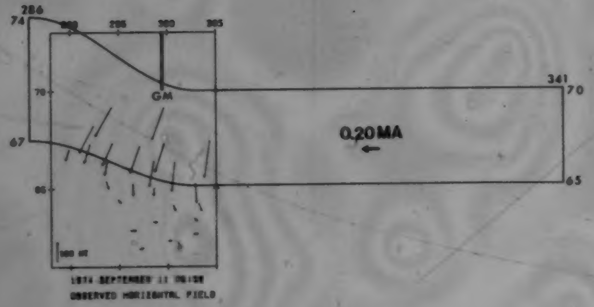

286
74
67
280
285
300
305
70
65
GM
341
70
65
0.20 MA ←
100 NT
1974 SEPTEMBER 11
OBSERVED HORIZONTAL FIELD

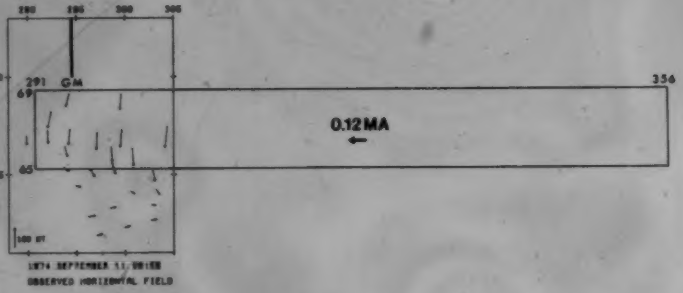

280
285
300
305
70
65
GM
291
69
65
356
0.12 MA ←
100 NT
1974 SEPTEMBER 11
OBSERVED HORIZONTAL FIELD

epoch, and possibly northward, but the array gives little control of the northern edge of the ionospheric current.

In the interval 08.56-09.00 U.T. the current system has moved further east relative to the array. The upward field-aligned current is well located and the downward east end current is not at all well controlled but cannot be much closer than the position shown.

3.6 Discussion

The current loop moved eastward through at least 20° of geomagnetic longitude between 07.48 and 08.58 U.T. relative to the surface of the earth. In this same time interval local geomagnetic midnight (Montbriand 1965) moved westward through 17.5° relative to the array, because of the rotation of the Earth. The current loop therefore moved eastward at least 38° geomagnetic relative to magnetic midnight, in this 70 minute interval.

A second point appears in Fig. 3.11. The bend in the ionospheric part of the current lies within 27° of longitude west of geomagnetic midnight. In the first epoch (Fig. 3.11) the bend corresponds approximately to the shape of the auroral oval (Q = 2). In the final epoch (Fig. 3.11) the current loop ends 5° west of magnetic midnight, and no bend is seen. An association of the bend in the model currents with the Harang discontinuity seems possible (Harang, 1946; Heppner, 1972).

The ionospheric parts of the current systems at the four epochs modelled are shown in Fig. 3.12 in azimuthal equidistant projection of centred geomagnetic dipole coordinates. The ionospheric currents in these four models extend through the longitudes of several Canadian and American magnetic observatories (Table 2.2). The records of 1974 September 11 from these observatories have been examined and are generally consistent with the model currents. Perturbation fields at two epochs, 08.38 and 08.58 U.T., recorded by these observatories are shown in Fig. 3.13 and 3.14. At epoch 08.58 U.T. (Fig. 3.14) the reduced perturbation recorded at WHAL indicates that the eastern end of the current should be placed nearer the array, that the current flow is displaced north at the east end or that WHAL lies within the longitudinal range in which the downward field-aligned current enters the ionosphere. The vertical component at CHUR is positive indicating that the centre of the ionospheric current must lie south of this station. There are discrepancies at some high-latitude observatories, and it is believed that these observatories may be strongly affected by local currents not seen by the array. Incorporation of data from different observatories in the quantitative model calculations, based on the data from the array, has not been attempted.

Figure 3.12 Ionospheric segments of current loops at four epochs of Substorm 1 in azimuthal equidistant projection of centred dipole geomagnetic coordinates, superimposed on a map of the North American mainland. Comparison with Fig. 2.2 shows the close relation to the auroral oval. GM represents magnetic midnight.

7:48 UT

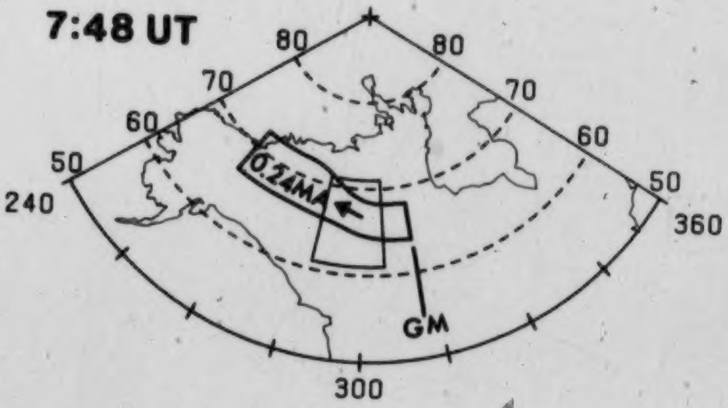
80
80
70
60
50
240
70
60
50
360
300
0.24MA
GM

8:13 UT

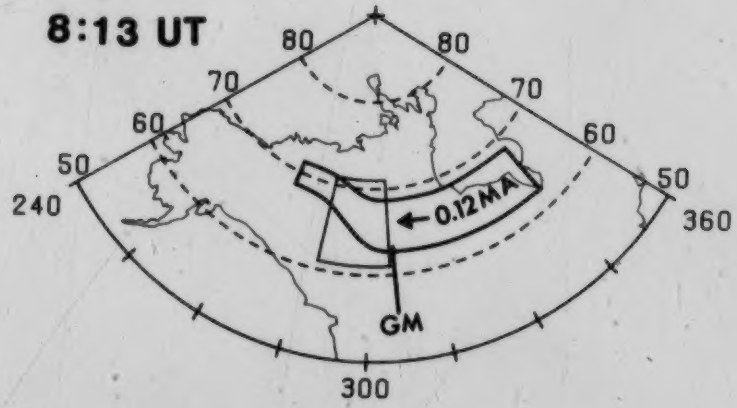
80
80
70
60
50
240
70
60
50
360
300
0.12MA
GM

8:38 UT

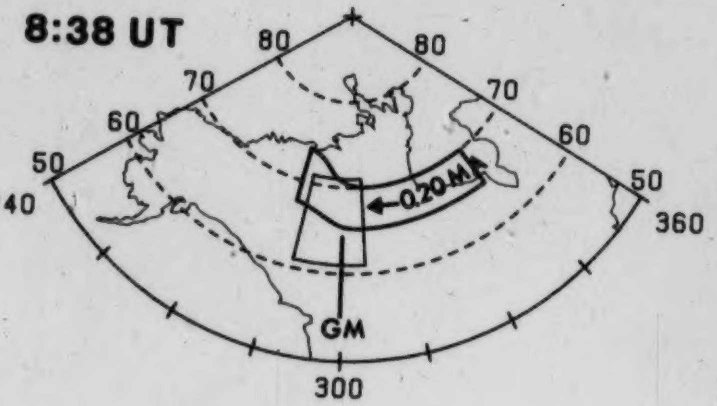
80
80
70
60
50
240
70
60
50
360
300
0.20MA
GM

8:58 UT

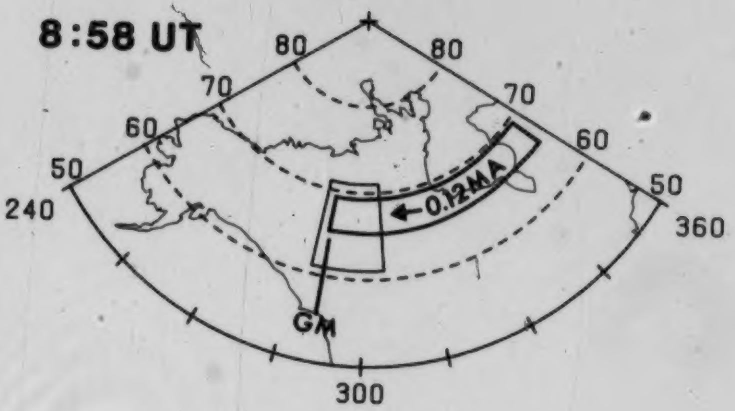
80
80
70
60
50
240
70
60
50
360
300
0.12MA
GM

Figure 3.13 Horizontal perturbation fields recorded by Canadian and U.S. observatories at epoch 08.38 U.T. of Substorm 1 an azimuthal equidistant projection of centred dipole geomagnetic coordintates. Location of the stations are given in table 2.2.

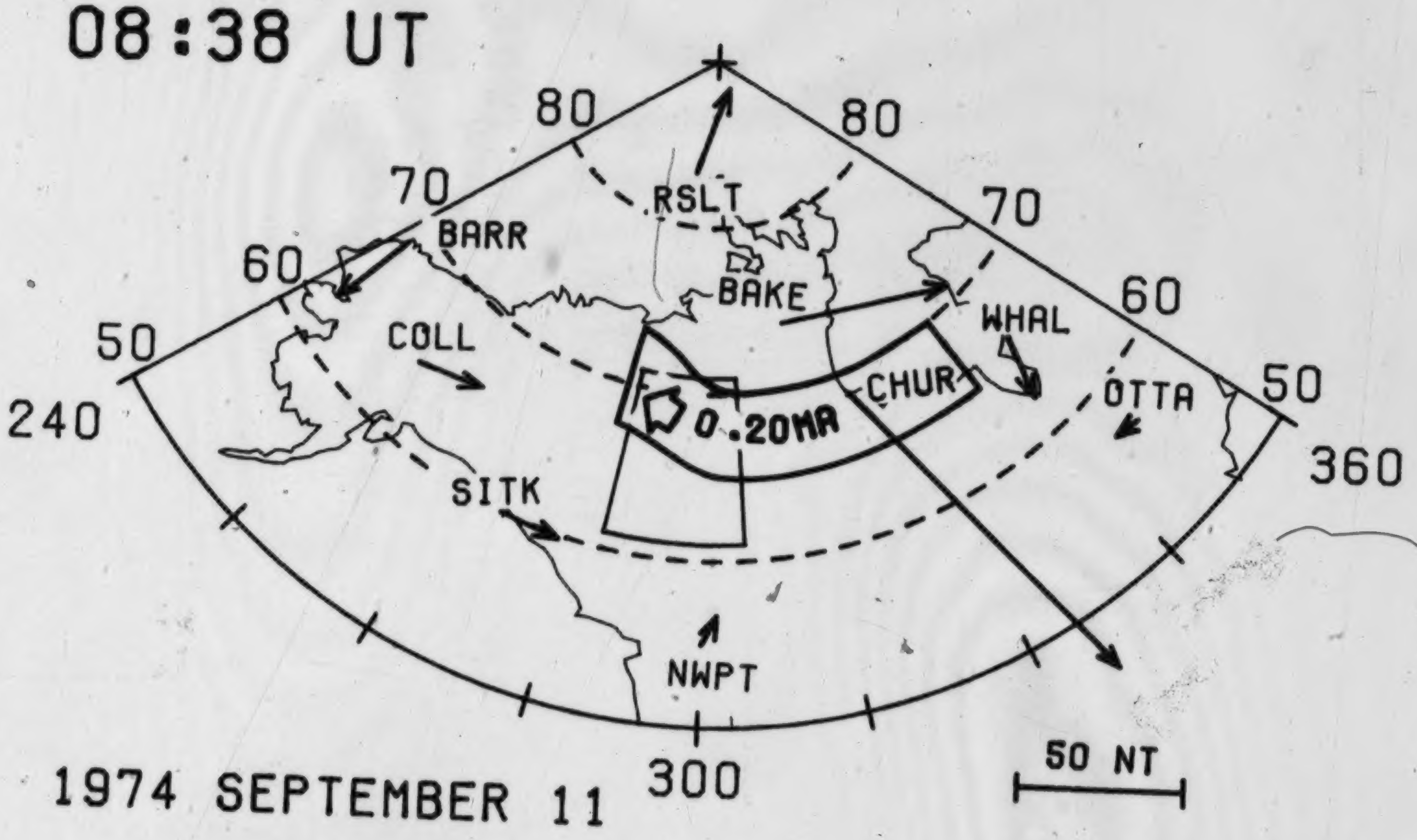
08:38 UT
80
80
70
70
60
60
50
50
240
360
300
RSLT
BARR
BAKE
COLL
WHAL
CHUR
OTTA
0.20MA
SITK
NWPT
50 NT
1974 SEPTEMBER 11

Figure 3.14 Horizontal perturbation fields recorded by Canadian and U.S. observatories at epoch 08.58 U.T. of Substorm 1 in same map projection as Fig. 3.13.

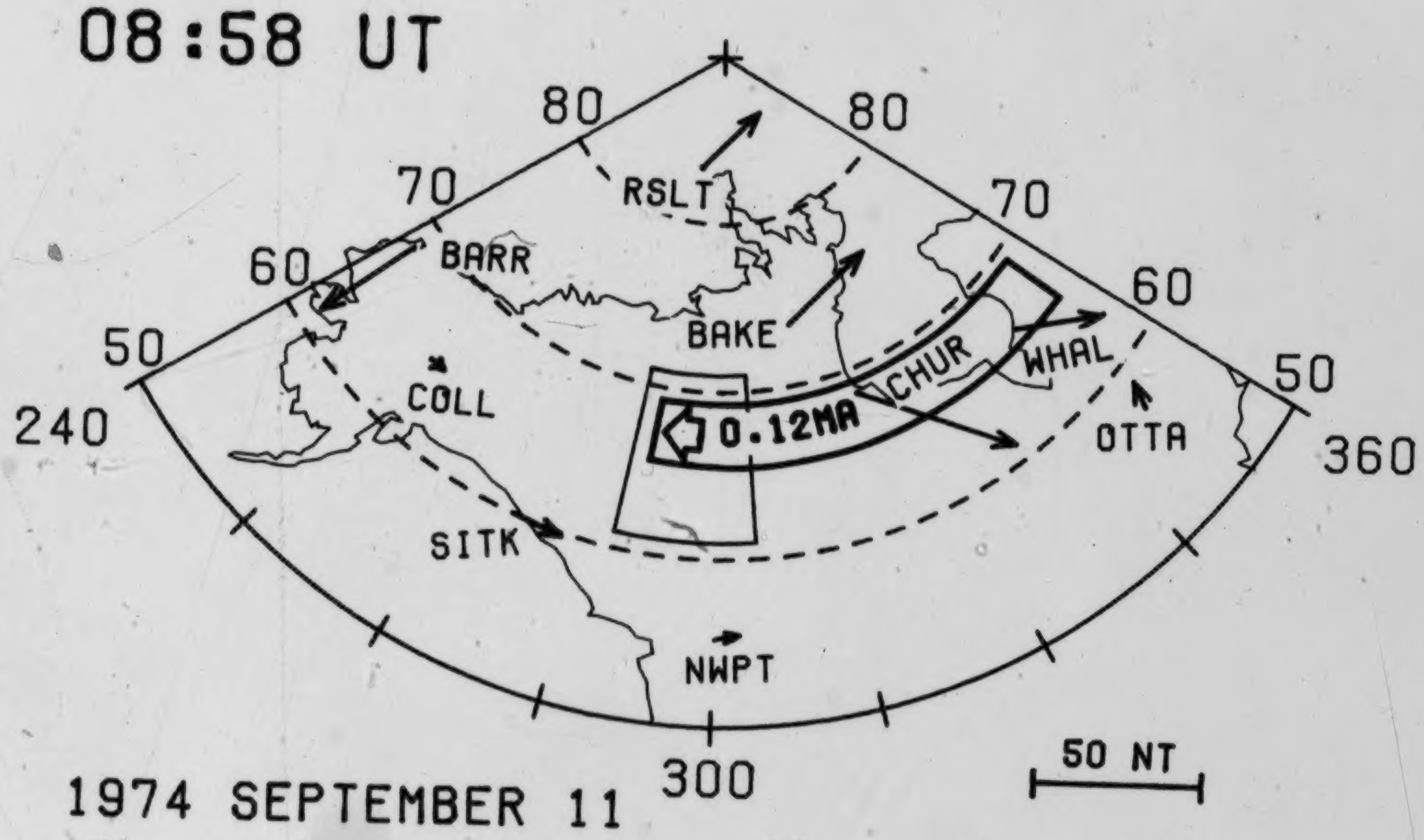
08:58 UT
80
80
70
70
60
60
50
50
240
360
300
RSLT
BARR
BAKE
CHUR
WHAL
OTTA
COLL
SITK
NWPT
0.12MA
50 NT
1974 SEPTEMBER 11

CHAPTER 4

DEVELOPMENT OF TWO POLAR MAGNETIC SUBSTORMS ON SEPTEMBER 7 AND SEPTEMBER 18, 1974

4.1 Introduction

It was shown in Chapter 3 that the perturbation magnetic fields of that substorm could be well fitted by a current loop consisting of a westward electrojet above the array, downward field-aligned current at the east end of this ionospheric current, upward field-aligned current at the west end and closure in the magnetotail (Fig. 1.7 Chapter 1) with constant current density over any cross-section of the current. To obtain a best fit a northward bend in the ionospheric currents west of magnetic midnight was required in most cases. This chapter discusses two substorms which involve westward current in the ionosphere above the array, but which cannot be fitted with uniform current density. More sophisticated treatment of the current model is necessary. The present chapter therefore records two events more complicated in their geometric forms, and an extension of modelling technique to deal with them.

4.2 Observations

The array location in relation to the auroral oval (Q = 2), for local midnight at the array, is shown in Chapter 2

(Fig. 2.2). In the maps of this chapter as in the previous chapter, centred dipole geomagnetic coordinates are shown with the north pole at geographic coordinates 78°.565N., 69°.761W.

The substorms here reported occurred in 1974 on September 7 and September 18 and were recorded by 23 stations. Magnetograms are shown in Fig. 4.1 from 13 stations along north-south profiles near the western and eastern limits of the array for the September 7 event, and in Fig. 4.2 for the September 18 substorm. The station positions are shown in Fig. 2.1 (Chapter 1). It will be seen that the September 7 substorm was of about 3 1/2 hours duration, whereas that of September 18 lasted little more than 1 1/2 hours.

It is convenient at this point to take the discussion of each substorm separately to the final current models.

4.3 Substorm 2: 1974 September 7

4.3.1 Perturbation Fields

The entire substorm was plotted as a series of maps of mean values over consecutive five-minute intervals of the three components H, D and Z, measured from baselines at 01.00 U.T. From these maps eight "time frames" were chosen as representative of the main epochs of the substorm. These eight time intervals are marked in Fig. 4.1, and the mean

Figure 4.1 Magnetograms of Substorm 2 from 13 stations along two north-south lines near the western and eastern edges of the array. Bars indicate the eight time intervals averaged in Figs. 4a and 4b. The station positions are shown in Fig. 2.1.

SEPTEMBER 7 1974

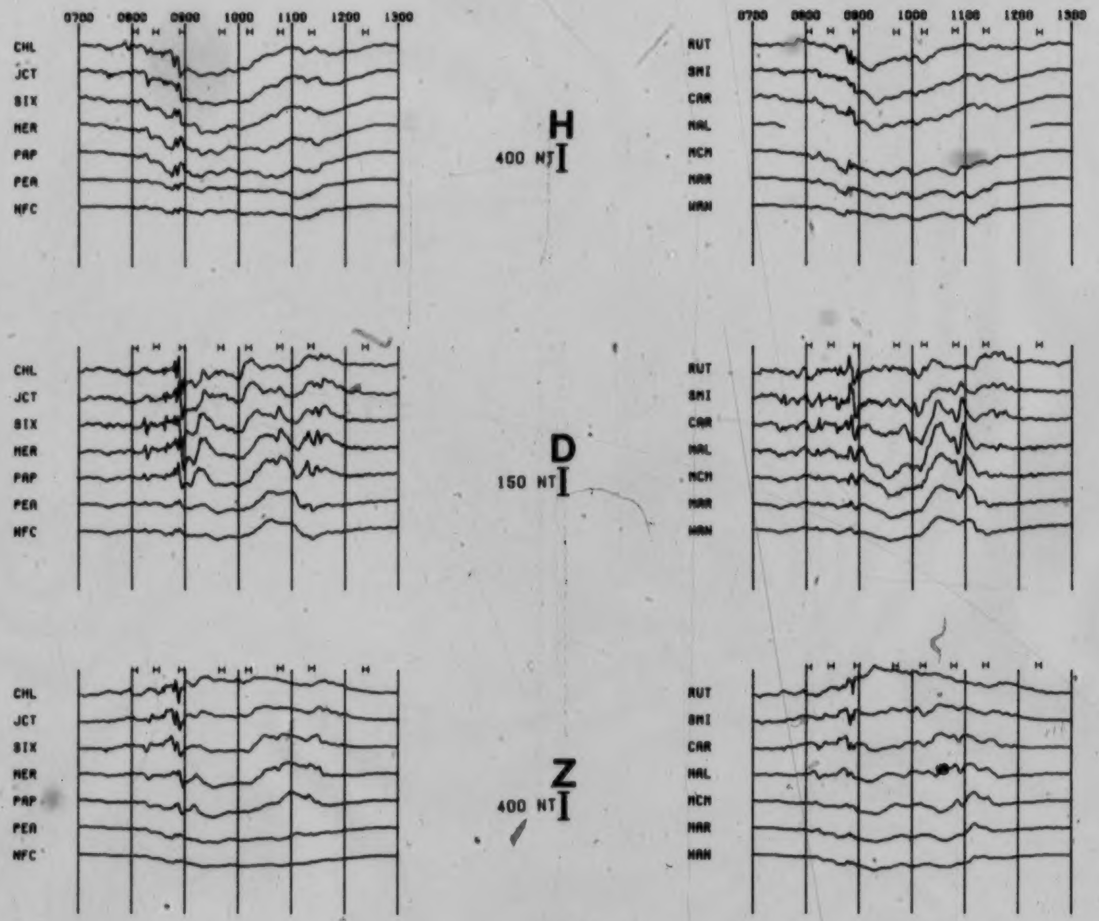

Figure 4.2 Magnetograms of Substorm 3 from 14 stations along two north-south lines near the western and eastern edges of the array. Bars indicate the eight time intervals averaged in Figs. 10a and 10b. The station positions are shown in Fig. 2.1.

SEPTEMBER 18 1974

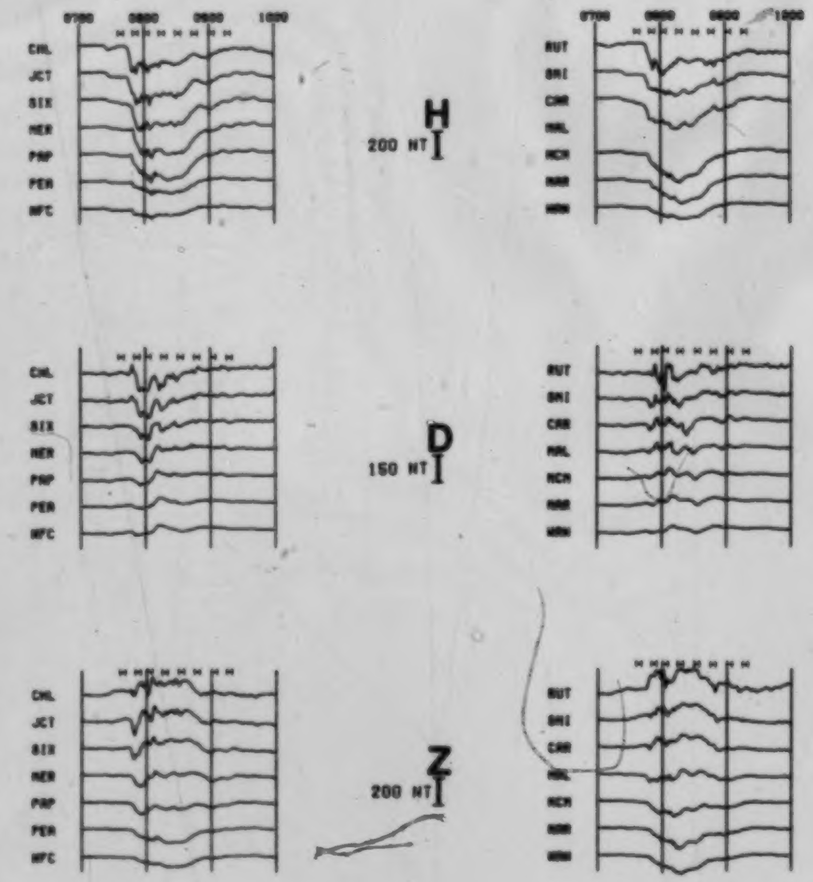

perturbation fields are represented in Figs. 4.3a and 4.3b. In the first time-frame of Fig. 4.3a it will be noted that, at 08.03 U.T., only small random changes had appeared since 01.00 U.T.; the field was quiet for at least seven hours before the substorm commencement, and the choice of baseline appears reasonable.

The time-scale of the substorm is of interest. Figs. 4.1 and 4.3 depict fields and current growing over the first 100 minutes and declining over the next 2 hours.

In six of the seven epochs of the substorm shown in Fig. 4.3 (the exception is at 10.13 U.T.) there are large downward vertical fields at the northern stations of the array, combined with small horizontal fields. Quantitative model calculations show that this combination cannot be modelled by a westward ionospheric current alone, but requires an eastward ionospheric current to the north of the main westward current, or some other current system which gives equivalent fields. This asymmetry in the Z latitudinal profile has been noted by Chen and Rostoker (1974), Kisabeth and Rostoker (1974), Langel (1974). Rostoker and Hron (1975) suggest that in the morning sector an eastward current south of the main westward electrojet produces this asymmetry in Z. As pointed out by Kisabeth (1977) this asymmetry may alternatively be produced by the ends of a north south current system. Throughout this thesis the eastward current north of the main westward electrojet, obtained by the

Figure 4.3a Mean perturbation fields over five-minute intervals at four epochs before and during Substorm 2. For the vertical components, northward arrows represent upward fields. Unit: nanotesla.

PERTURBATION FIELDS
AVERAGED OVER 5 MINUTE INTERVALS

HORIZONTAL FIELDS

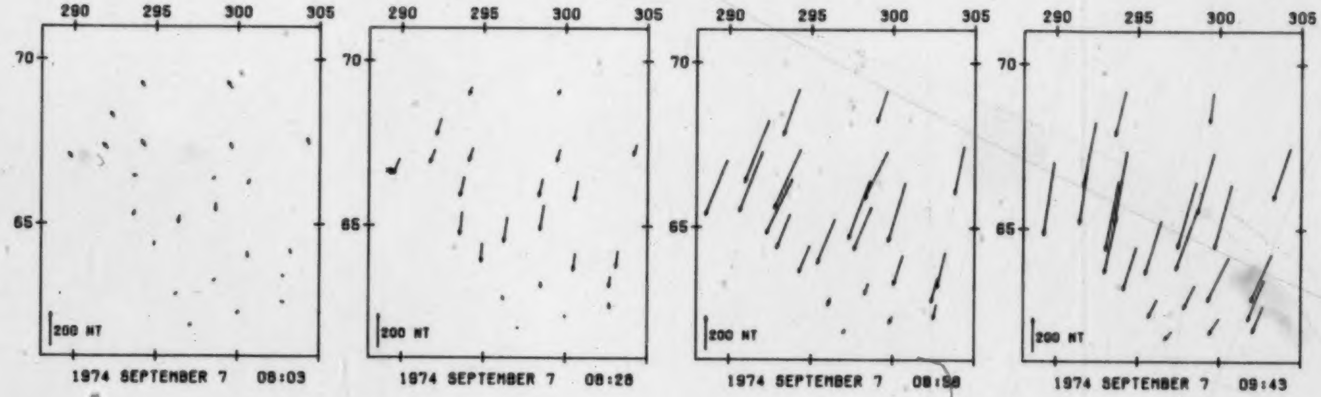

VERTICAL FIELDS

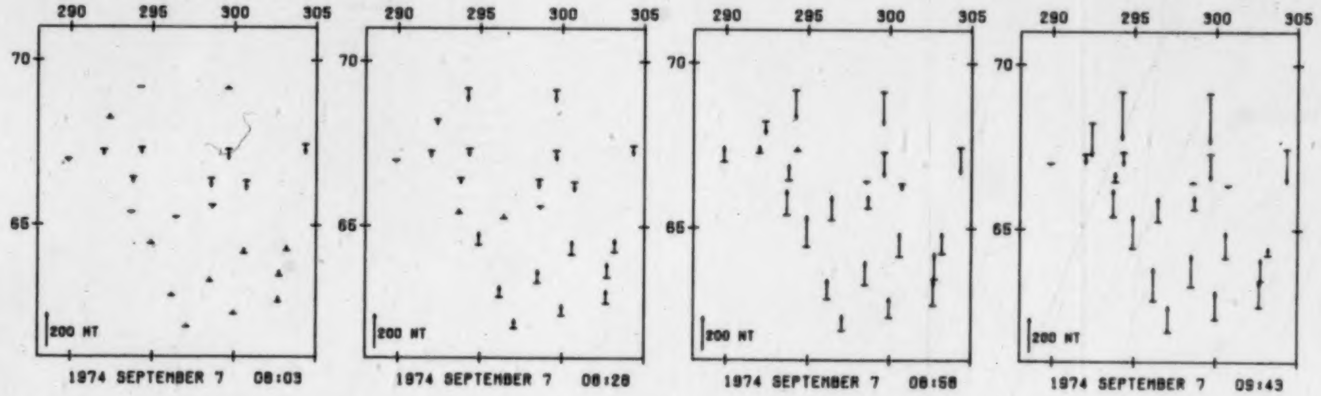

Figure 4.3b Mean perturbation fields over five-minute intervals at four epochs during Substorm 2. For the vertical components, northward arrows represent upward fields. Unit: nanotesla.

PERTURBATION FIELDS
AVERAGED OVER 5 MINUTE INTERVALS

HORIZONTAL FIELDS

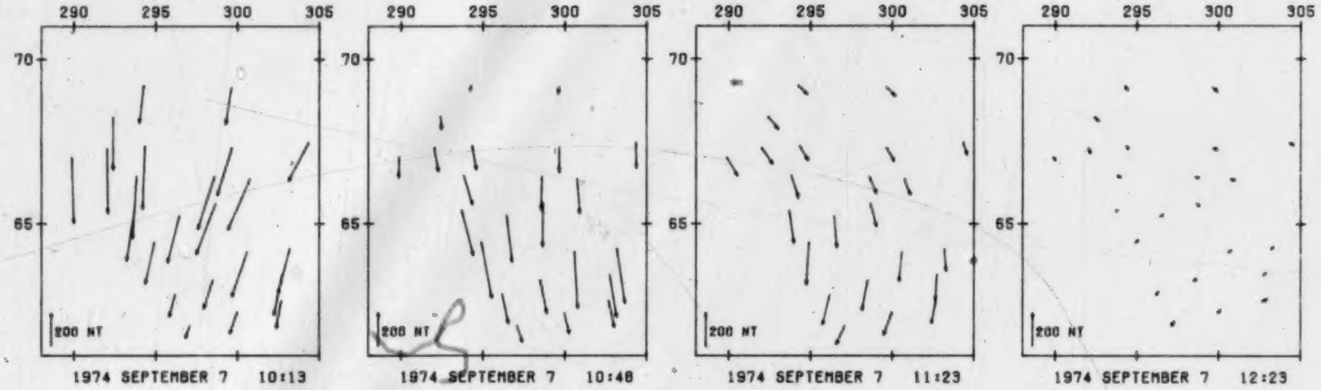

VERTICAL FIELDS

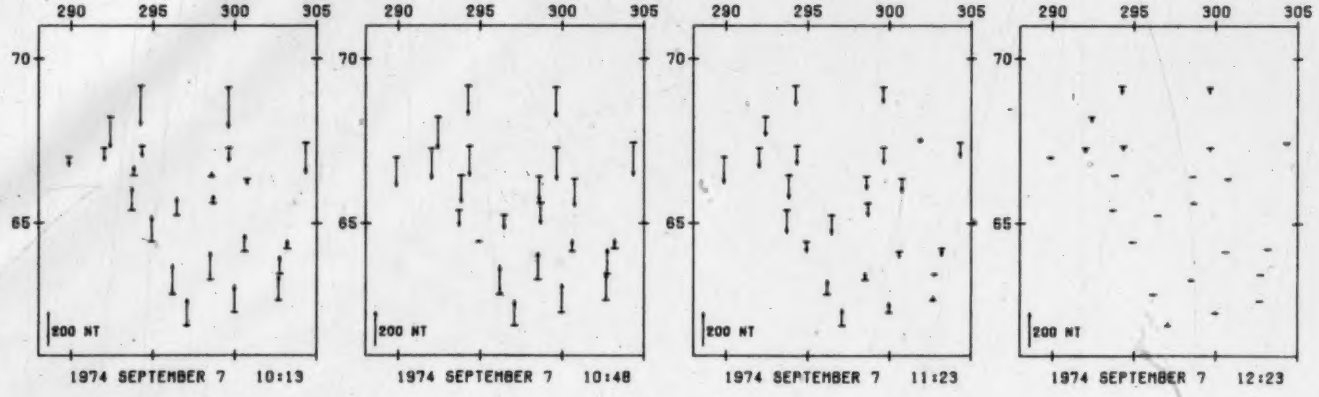

modelling procedure, should be regarded as an equivalent current. Observations north of the array, at the time of the substorms would be needed to properly define the northern current.

At 11.23 U.T. (Fig. 4.3b) the prominent clockwise curvature of the horizontal field, convex to the east, is a consequence of the presence above the array of the downward field-aligned current at the east end of the westward ionospheric electrojet: see also Fig. 4.12.

4.3.2 Inversion of magnetic perturbation fields

The perturbation fields at different epochs of Substorms 2, 3 (this chapter) and 4 (Chapter 5) have been fitted by models of the Kisabeth type (Kisabeth 1972; Kisabeth and Rostoker 1977). The general configuration of the current loop is shown in Fig. 1.7. These substorms could not be modelled by a current of this type with uniform current density across its width. Accordingly a current distribution was estimated by a direct inversion method recently developed by Oldenburg (1976, 1977), based on the linear inverse theory of Backus and Gilbert. A brief sketch of the method follows, but the reader is referred to the original papers (Oldenburg 1976, 1977; Backus and Gilbert 1970) for a complete treatment of the method.

The magnetic field resulting from a Boström (1964) Type 1 current loop with a current density distribution $j(\theta)$ is given by

$$B^m(a,\theta_o,\phi_o) = k \int_{\theta_1}^{\theta_2} j(\theta) \left\{ r \int_\Gamma \sum_{i=1}^{3} dC_{im} \right\} d\theta \qquad (1)$$

at a point on the surface of the earth of radius a at colatitude θ_o and longitude ϕ_o, following the notation of Kisabeth (1972) (Appendix A) and Oldenburg (1976), m takes the values 1, 2 and 3 as the field components Z, H and D are computed, θ_1 and θ_2 define the latitudinal limits of the ionospheric current. The integral sign $\int_\Gamma$ represents integration over the whole loop and dC_{im} represents a 3x3 matrix (Kisabeth 1972).

For an observation of H, Z or D at location $(a,\theta_\ell,\phi_\ell)$ equation (1) may be rewritten as:

$$B_\ell(a,\theta_\ell,\phi_\ell) = \int_{\theta_1}^{\theta_2} j(\theta)\ G_\ell(\theta)d\theta \qquad \ell=1, \ldots N \qquad (2)$$

where $G_\ell(\theta)$ is the 'data kernel' of the ℓth datum B_ℓ. Even though there are infinitely many current densities $j(\theta)$ which satisfy the N constraints (2), there exist properties which are shared by all of these models. In particular a unique average of the current density can be constructed from linear combinations of the observations. This average density, $\langle j(\theta_o)\rangle$ at co-latitude θ_o is shown to be

$$\langle j(\theta_o)\rangle = \sum_{\ell=1}^{N} a_\ell(\theta_o)B_\ell = \int_{\theta_1}^{\theta_2} j(\theta)\ A(\theta,\theta_o)d\theta \qquad (3)$$

where $$A(\theta,\theta_o) = \sum_{\ell=1}^{N} a_\ell(\theta_o)G_\ell(\theta) \qquad (4)$$

$A(\theta,\theta_o)$ is called the averaging function, and $a_\ell(\theta_o)$ are constants that are found by making $A(\theta,\theta_o)$ as 'close as possible' to a Dirac delta function. The deviation of $A(\theta,\theta_o)$ from a Dirac delta distribution can be quantitatively measured by the spread S given by

$$S(\theta_o) = 12 \int_{\theta_1}^{\theta_2} (\theta-\theta_o)^2 A^2(\theta,\theta_o)d\theta \qquad (5)$$

This is the quadratic criterion of Backus and Gilbert (1967) which leads to averaging functions that are not contaminated by sidelobes (Oldenburg 1977). By finding the set of values $a_\ell(\theta_o)$ that minimizes the spread S, we can obtain a current density estimate $\langle j(\theta_o)\rangle$ corresponding to maximum resolution.

Assuming that the errors in the data have a Gaussian distribution with zero mean and standard deviation σ_ℓ, we may express the error in the estimate of $\langle j(\theta_o)\rangle$ as

$$\mathrm{Var}\left[\langle j(\theta_o)\rangle\right] = \sum_{\ell=1}^{N} a_\ell^2(\theta_o)\,\sigma_\ell^2 = \sigma^2(\theta_o) \qquad (6)$$

The most accurate value of $\langle j(\theta_o)\rangle$ is obtained for those values of a_ℓ that minimize equation (6). Thus as equations (5) and (6) cannot be minimized simultaneously, it is necessary to accept a compromise between resolution and accuracy that can be expressed in the quadratic form

$$\eta = S(\theta_o) \cos\psi + \sigma^2(\theta_o)\sin\psi \tag{7}$$

where ψ is the trade-off parameter. For any value of $(0 \leq \psi \leq \pi/2)$ we can find a set of a_ℓ's that minimizes η in equation (7).

There are infinitely many current densities $j(\theta)$ which satisfy the N equations (2). We have used the method of Oldenburg (1977) to choose a specific one, the "flattest" current density, because he has indicated that this model may be relatively insensitive to random errors in the observations. The flattest current density can be found by minimizing the function β given by

$$\beta = \int_{\theta_1}^{\theta_2} [j'(\theta)]^2 \, d\theta \tag{8}$$

subject to the constraints that the observations are reproduced. An additional limitation is included by making the current density zero at the northern and southern limits of the electrojet. This is insured by setting

$$j(\theta_1) = j(\theta_2) = 0 \tag{9}$$

If we define

$$H_j(\theta) = \int_{\theta_1}^{\theta} G_j(u)du \tag{10}$$

The minimization of (8) leads to

$$j'(\theta) = \eta - \sum_{j=1}^{N} b_j \int_{\theta_1}^{\theta_2} H_j(\theta)d\theta \qquad (11)$$

where

$$\eta = \frac{1}{\theta_2-\theta_1} \sum_{j=1}^{N} b_j \int_{\theta_1}^{\theta_2} H_j(\theta)d\theta \qquad (12)$$

the b_j's are the solutions to the following system of equations

$$B_j = \eta \int_{\theta_1}^{\theta_2} H_j(\theta)d\theta + \sum_{i=1}^{N} b_i \int_{\theta_1}^{\theta_2} H_i(\theta)\, H_j(\theta)d\theta \qquad (13)$$

From (11) the current density $j(\theta)$ is easily recovered

The shaded areas of fig 4.4 represent a theoretical current density distribution used to calculate values of the horizontal (H) and vertical (Z) perturbation fields at seven stations (Fig. 4.4a) and four stations (Fig. 4.4b) indicated by arrows. The solid line curve correpsonds to the flattest model of the Oldenburg inversion which resembles the original current distribution only in the region of the stations (62° to 68.5° latitude in Fig. 4.4b). Outside this region (68.5° to 74° latitude) when only four stations are used (Fig. 4.4b) the negative current is not as well resolved as when stations under the current are used (Fig. 4.4a). Nevertheless, both integrated negative currents ($-2.37\text{x}10^4$ amperes) are only 4.9% greater than the theoretical value of $-2.26\text{x}10^4$ amperes. In effect the four stations (Fig. 4.4b) can 'see' the current outside their

Figure 4.4 A test of resolution of current density in a theoretical model with both westward and eastward ionospheric currents shown by shaded areas in a three-dimensional loop including field-aligned currents, (a) using data from seven stations as shown, (b) using data from four stations. Solid line corresponds to the "flattest" model of the Oldenburg inversion. Vertical error bars indicate the accuracy of current estimates which are joined by broken line.

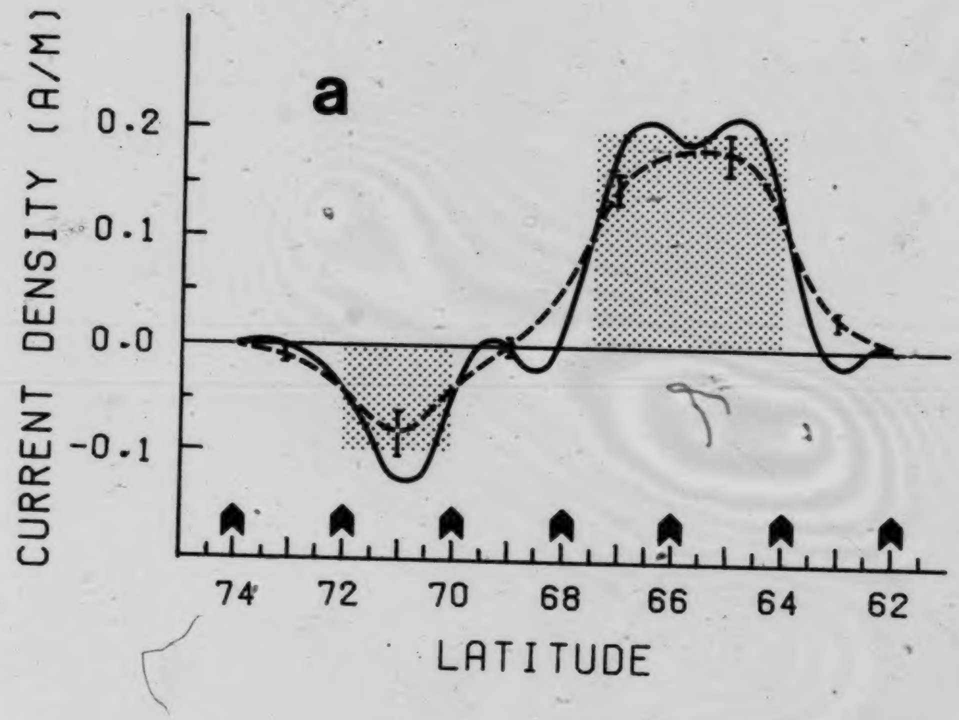
a
CURRENT DENSITY (A/M)
0.2
0.1
0.0
-0.1
74
72
70
68
66
64
62
LATITUDE

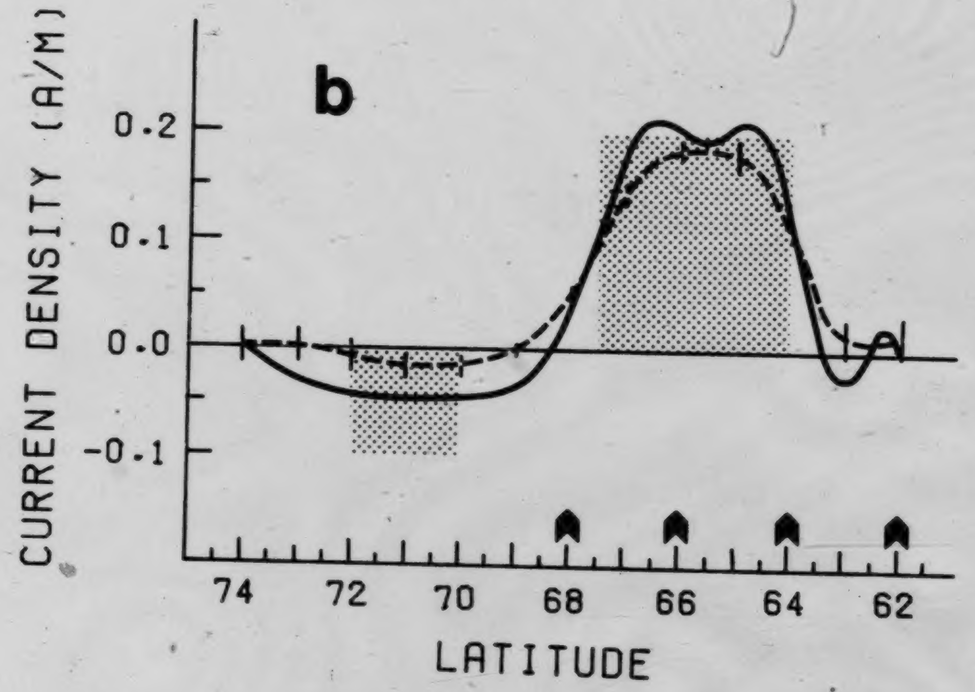
b
CURRENT DENSITY (A/M)
0.2
0.1
0.0
-0.1
74
72
70
68
66
64
62
LATITUDE

latitude ranges, but cannot resolve its shape or position. The integrated positive currents are also within 5% of the theoretical value of 7.92×10^{4} amperes where both sets of stations (Figs. 4.4a and b) resolve it equally well in shape and position.

The broken lines of Fig. 4.4 joins the values of the current density estimates whose accuracies are indicated by vertical bars. In computing those error estimates it was assumed that there was a standard deviation of 3 nT in the observations of H and Z. Corresponding to each vertical bar is a range of latitude (not shown), the spreads of the averaging function. These functions are narrow and well centred (similar to curve II in Fig. 4.5b) above the positions of the estimates in latitudes where there are observations but become wide and off-centred outside those latitudes (Oldenburg, 1976). This displacement in latitude will be further discussed in relation to Fig. 4.5. When the flanks of the current are reached, in the latitudes where there are observations, the averaging functions become one-sided but well centred as in curve III of Fig. 4.5b. In Fig. 4.4 for the region between the stations S is about 1.3 degrees. As the flanks of the current or the limits of the stations are reached, the resolution is reduced. For an estimate of $\langle j(\theta_o)\rangle$ at $\theta_o = 62^o$ S is 2.8 degrees. For estimates outside the limits of the stations (Fig. 4.4b) the values of S increase from about 2^o at $\theta_o = 69^o$ to about 25^o at $\theta_o = 73^o$. Here the resolution and significance of current

Figure 4.5 (a) An inversion by Oldenburg's method from fields observed at five stations, at 08.33 U.T. on 1974 September 18, to a current density distribution (solid line). The broken line joins points where current density estimates were made with an averaging function discussed in the text.
(b) Averaging functions for evaluation of current density estimates at three different latitudes (shown by arrows) of the inversion shown in (a). Note that curve I is wide and off centre as compared to curve II which is over the range of the stations. Area under each averaging function is 1.

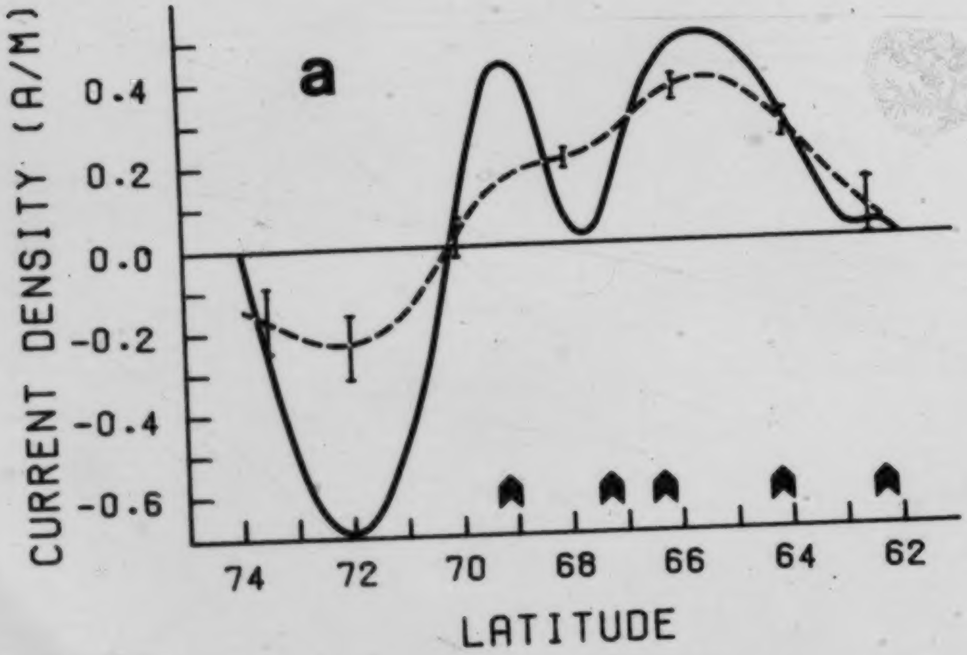
a
CURRENT DENSITY (A/M)
0.4
0.2
0.0
-0.2
-0.4
-0.6
74
72
70
68
66
64
62
LATITUDE

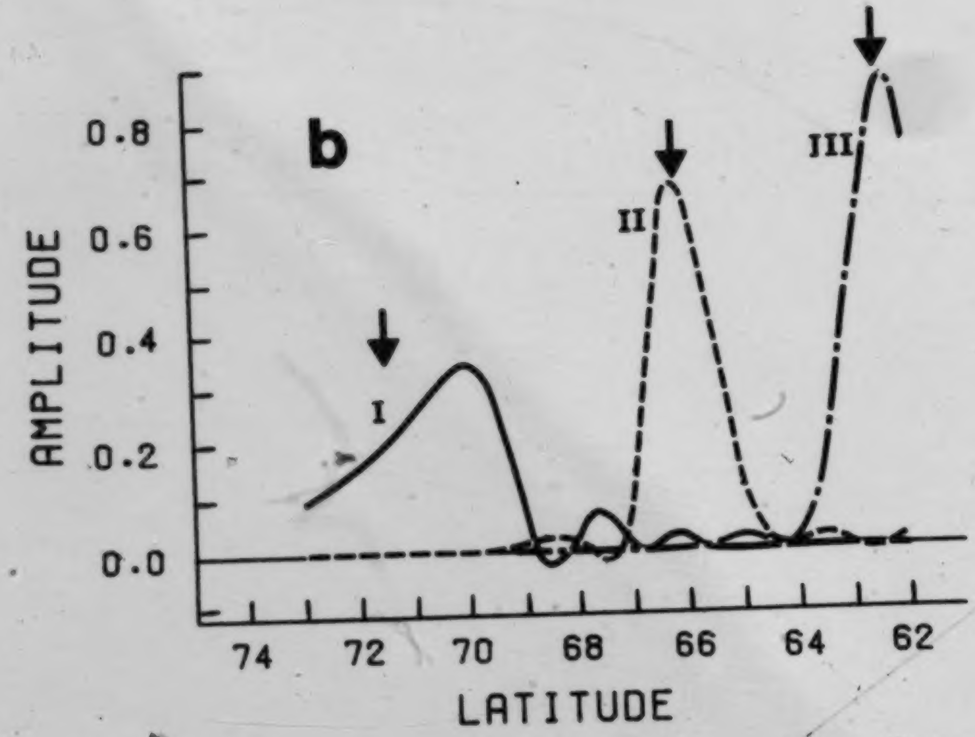
b
AMPLITUDE
0.8
0.6
0.4
0.2
0.0
I
II
III
74
72
70
68
66
64
62
LATITUDE

density estimates are limited because the averaging function becomes very flat and is not centred at θ_o, as curve I of Fig. 4.5b. The box-car theoretical model of Fig. 4.4 provides a specially severe test.

Fig. 4.5a shows the result of inversion of the perturbation fields recorded by a line of five stations of the array at epoch 08.33 U.T., 1974 September 18. Here the current density distribution shows the existence of a large eastward (negative) current to the north of the main westward (positive) current. The eastward current flows north of the array and therefore is not well resolved. While the current density estimates are not very significant, it is clear that an equivalent eastward current system existed to the north of the main westward current.

The standard deviations of the data, related to the error bars on the current density estimates, include not only observational errors, but also departures of the observed fields from those calculated from the model current system. The sums of squared residuals in Tables 4.2 and 4.4 allow estimation of such standard deviations. For 08.33 U.T. on September 18, $\sigma = 18.8$ nT. The error bars on the dashed curve in Fig. 4.5a correspond to this value. The eastward current north of the array is clearly significant, though its shape is not well resolved.

Fig. 4.5b shows typical averaging functions corresponding to evaluation of current density estimates at latitudes indicated by the arrows. The value of the spread for the wide and off centred averaging funtion (curve I) is 5.7°. This value reduces to 1° for a well centred and narrow averaging function as shown in curve II (Fig. 4.5b). Near the flanks of the electrojet the averaging function shown by curve III in Fig. 4.5b has a spread S of 1.1°. These averaging functions when convolved with any current density distribution (e.g. the flattest model) that produces the observations will give a unique value of the current density estimate.

When applying this inversion method to the analysis of the array observations, only a representative subset of stations forming a line across the ionospheric current were used. The reason for this is that the inversion technique attempts to fit the data exactly. This produces a current density distribution containing larger oscillations as the number of stations is increased. For the epochs of Substorms 2, 3 and 4 where this method was used, H and Z observations from 5 to 7 stations of the array were used.

In the few cases where the array was completely within the bend of the ionospheric current a small rotation of the horizontal components was made in order to ensure that the observed fields used in the inversion program would properly represent the array observations. This rotation is necessary because the inversion calculations require currents that flow at a constant latitude, and make no provision for tilts or bends of the electrojet.

4.3.3 Model calculations

The perturbation fields at six epochs of Substorm 2 have been fitted by models of the Kisabeth type (Kisabeth 1972, Kisabeth and Rostoker 1977). The general configuration of the current loop is shown in Fig. 1.7. The substorm of September 7 could not be modelled by a current of this type with uniform current density across its width. Accordingly a current distribution was estimated by the direct inversion method described in section 4.3.2.

In four of the six epochs of Substorm 2 which have been modelled, the Oldenburg inverse method led to models with substantial eastward ionospheric currents to the north of the main westward current. The resolution test just described shows that the observed fields require the presence of significant equivalent eastward currents. They have been connected, in these models, to field-aligned currents arbitrarily placed in the same longitudes as those found for the main westward current: thus the least-squares fitting program moves a pair of field-aligned currents at the east end of the loop, or another pair at the west end, to optimize the fit.

The magnetic fields produced at the Earth's surface by the three-dimensional current loop (Fig. 1.7) were calculated from the Biot-Savart law in the manner described by Kisabeth (1972) (Appendix A). Where eastward currents appeared, in the ionospheric segments, to the north of the westward electrojet, two complete loops of current, in opposite senses, formed the model. Provision was made to introduce a bend in the ionosphere segment to give a change of latitude with a cosine dependence on longitude. By varying certain parameters (Fig. 4.6) of the ionospheric current segment, a least-squares fit was obtained between the calculated and observed magnetic perturbation fields. The width of the current system was kept constant as obtained with the inversion technique described earlier, but a constant factor multiplying all current densities was allowed to change as a parameter (P1; Fig. 4.6) of the least-squares fit. For all cases where a bend was needed, the bounding longitudes (P3 and P4) of the bend were allowed to vary as parameters. The fourth and fifth parameters were the latitudes of the southern edges of the eastern (P8) and western (P7) section of the current system. For epoch 09.43 the eastern end of the ionopheric current section was allowed to move with the eastern limit of the bend. For epoch 10.48 U.T. no bend was considered, and only four parameters were allowed to change, namely the total current (P1), the western end (P2) of the ionospheric current system and both its northern (P9) and southern (P8) latitudinal limits. At epoch 11.23 U.T. the only parameters varied were the total current (P1) and the eastern longitudinal end (P5) of the current system.

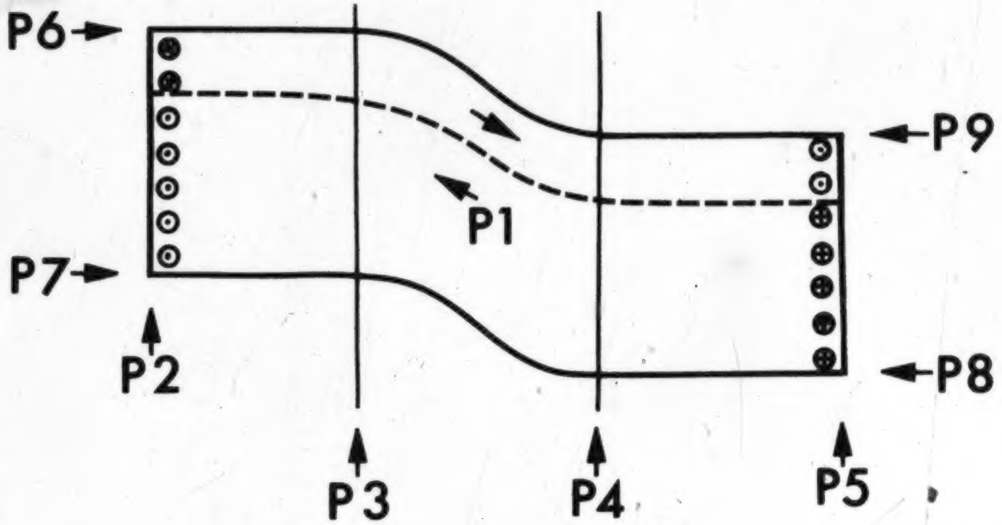

Figure 4.6 Outline of the ionospheric segment of the three-dimensional current loop used to model Substorm 2 and 3, indicating the different parameters that control the geometry and current. Birkeland field aligned currents are indicated.

Table 4.1 summarizes the parameters that were varied at different epochs in their substorm.

TABLE 4.1

PARAMETERS OF THE IONOSPHERIC SEGMENT
VARIED FOR SUBSTORM 2 (refered to Fig. 4.6)

epoch	independent parameters	dependent parameters
08.28	P1,P3,P4,P7,P8	P6,P9
08.58	P1,P3,P4,P7,P8	P6,P9
09.43	P1,P3,P4,P7,P8	P5,P6,P9
10.13	P1,P3,P4,P7,P8	P6,P9
10.48	P1,P2,P8,P9	
11.23	P1,P5	

While the field-aligned currents have been modelled as sheets of negligible thickness, the data could equally well be satisfied by field-aligned currents distributed through several degrees of longitude, as was shown in Chapter 3. In reality the field-aligned currents seem likely to be distributed in longitude.

In all calculations the ionospheric currents were kept at altitude 115 km. Induction in the Earth has been approximated by that in a superconducting sphere at depths chosen empirically to optimize the fits of calculated horizontal and vertical components to those observed. This choice was based upon tests outlined in Chapter 3.

The least-squares fit was obtained by applying to observed and calculated values, of three magnetic components with equal weights, the iterative subroutine ZXSSQ of the

IMSL library.

The models of Substorm 2 approximate observed perturbation fields from 01.00 U.T. baseline. These are presumably superimposed on some steady-state field corresponding to preexisting currents in the magnetosphere and ionosphere.

4.3.4 Model currents for six epochs of Substorm 2

Figures 4.7 to 4.12 show observed and calculated fields and the residuals (observed-calculated) at six representative epochs of Substorm 2. The northern and southern limits of the ionospheric currents, and the boundary between westward and eastward currents, are indicated. The main purpose in presenting the results of model fitting in this way, is to show the residuals as vectors. In Fig. 4.13 shows the complete ionospheric segments of the model currents at six epochs, in Mercator projection of centred dipole geomagentic coordinates, together with the current density distribution at each epoch found from the Olbenburg inversion. As numerical measures of goodness of fit we use the parameters

Figure 4.7 Observed perturbation fields, calculated fields for model currents of best fit, and residuals in the five-minute interval 08.25-08.30 U.T. during Substorm 2. For Z, northward arrows represent upward Z. The full length of the ionospheric segment, and the distribution of current density across the width of the current, are shown in Fig. 4.13.

IONOSPHERIC CURRENT MODEL WESTWARD CURRENT 0.14 MA

HORIZONTAL PERTURBATION FIELDS

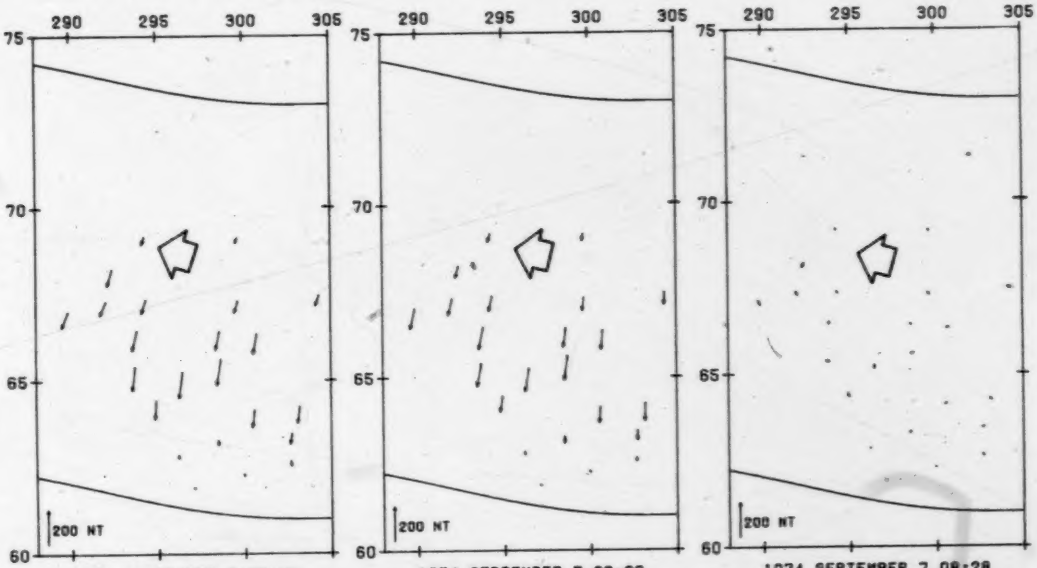
290
295
300
305
75
70
65
60
200 NT

1974 SEPTEMBER 7 08:28
OBSERVED VALUES

1974 SEPTEMBER 7 08:28
CALCULATED VALUES

1974 SEPTEMBER 7 08:28
RESIDUALS

VERTICAL PERTURBATION FIELDS

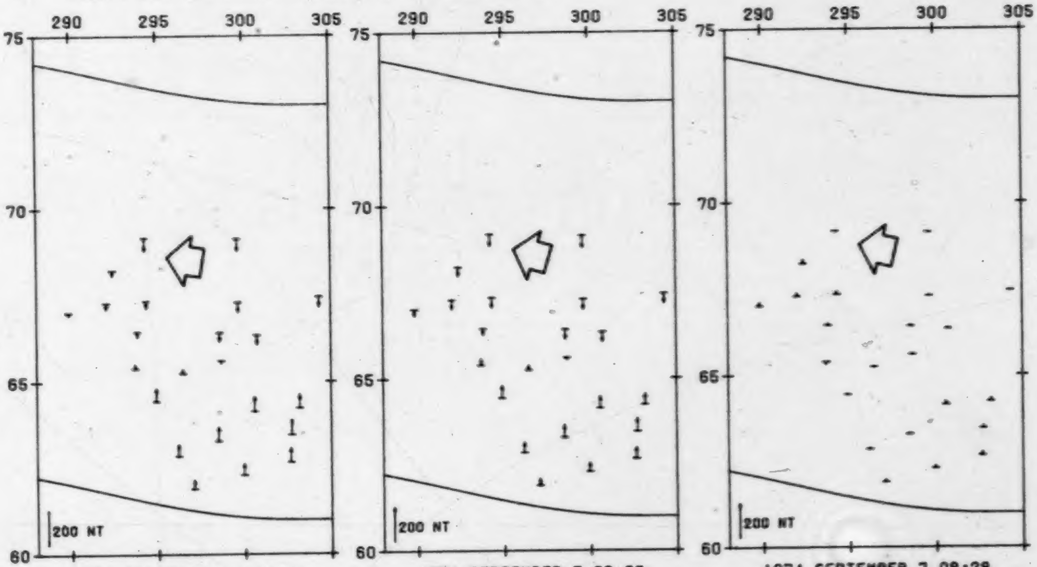
290
295
300
305
75
70
65
60
200 NT

1974 SEPTEMBER 7 08:28
OBSERVED VALUES

1974 SEPTEMBER 7 08:28
CALCULATED VALUES

1974 SEPTEMBER 7 08:28
RESIDUALS

Figure 4.8 Observed perturbation fields, calculated fields for model currents of best fit, and residuals in the five-minute interval 08.56-09.00 U.T. during Substorm 2. For Z, northward arrows represent upward Z. The full length of the ionospheric segment, and the distribution of current density across the width of the current, are shown in Fig. 4.13.

IONOSPHERIC CURRENT MODEL EASTWARD CURRENT 0.22 MA
WESTWARD CURRENT 0.41 MA

HORIZONTAL PERTURBATION FIELDS

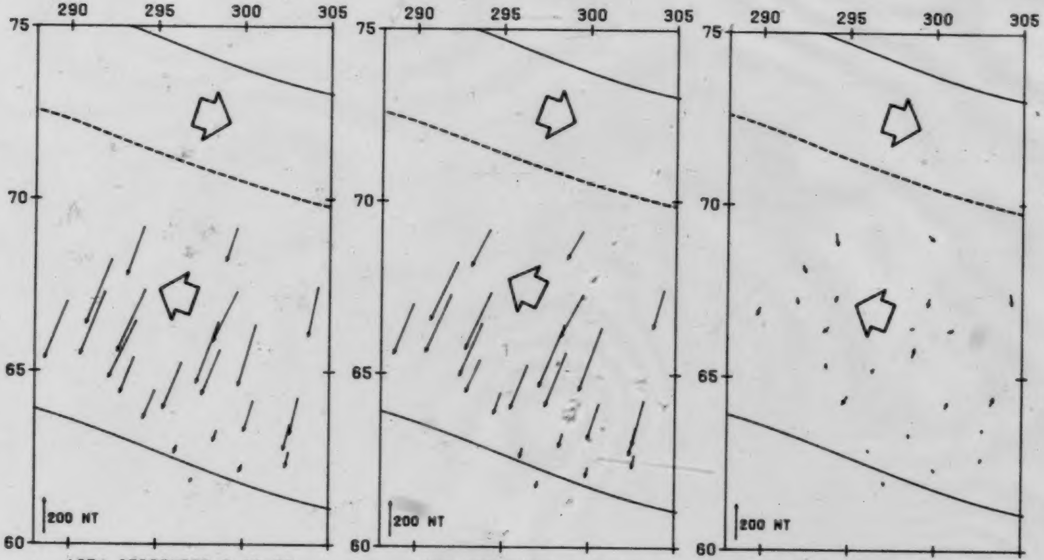

1974 SEPTEMBER 7 08:58
OBSERVED VALUES

1974 SEPTEMBER 7 08:58
CALCULATED VALUES

1974 SEPTEMBER 7 08:58
RESIDUALS

VERTICAL PERTURBATION FIELDS

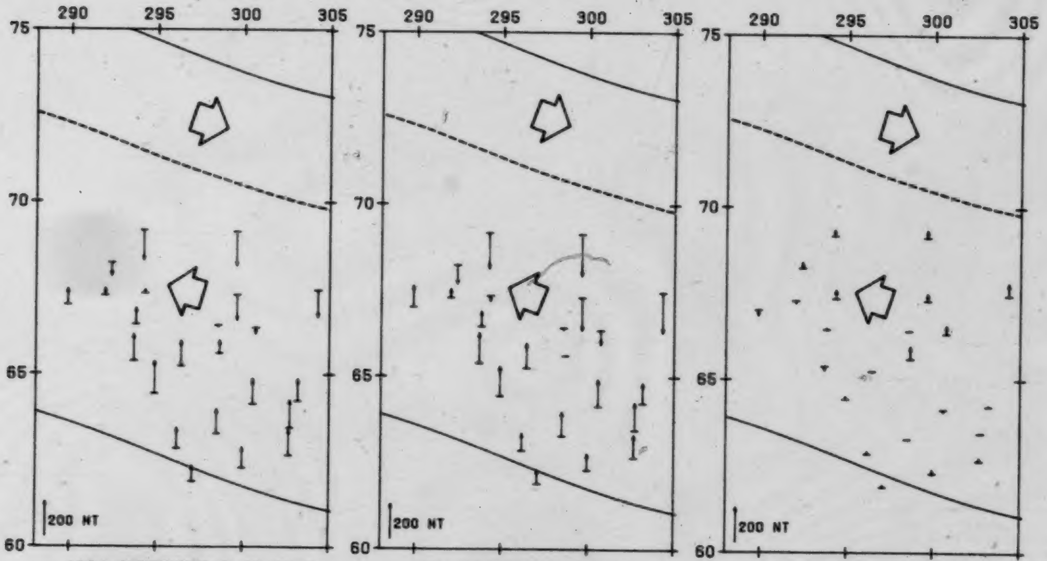

1974 SEPTEMBER 7 08:58
OBSERVED VALUES

1974 SEPTEMBER 7 08:58
CALCULATED VALUES

1974 SEPTEMBER 7 08:58
RESIDUALS

Figure 4.9 Observed perturbation fields, calculated fields for model currents of best fit, and residuals in the five-minute interval 09.41-09.45 U.T. during Substorm 2. For Z, northward arrows represent upward Z. The full length of the ionospheric segment, and the distribution of current density across the width of the current, are shown in Fig. 4.13.

IONOSPHERIC CURRENT MODEL

EASTWARD CURRENT 0.08 MA

WESTWARD CURRENT 0.54 MA

HORIZONTAL PERTURBATION FIELDS

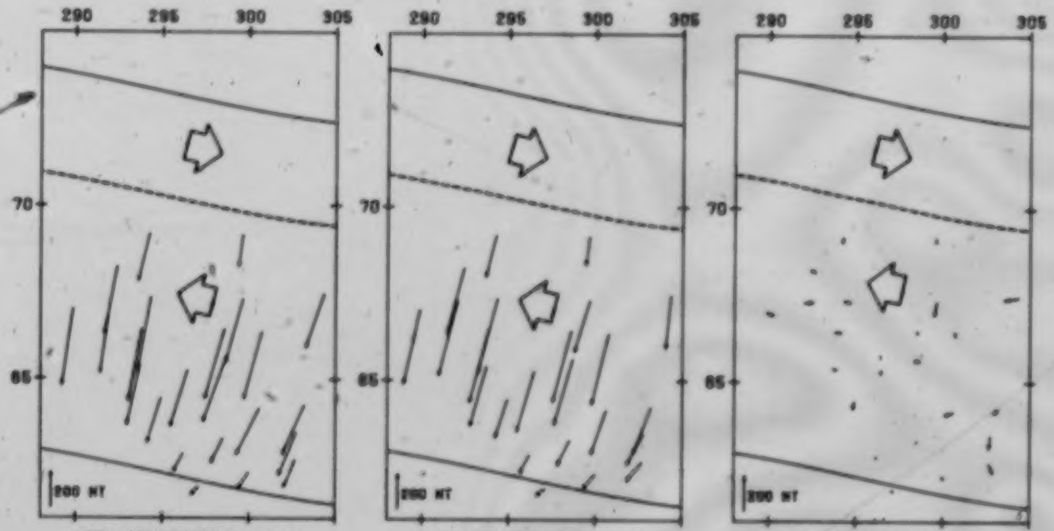
290
295
300
305
70
65
200 NT

1974 SEPTEMBER 7 09:43
OBSERVED VALUES

1974 SEPTEMBER 7 09:43
CALCULATED VALUES

1974 SEPTEMBER 7 09:43
RESIDUALS

VERTICAL PERTURBATION FIELDS

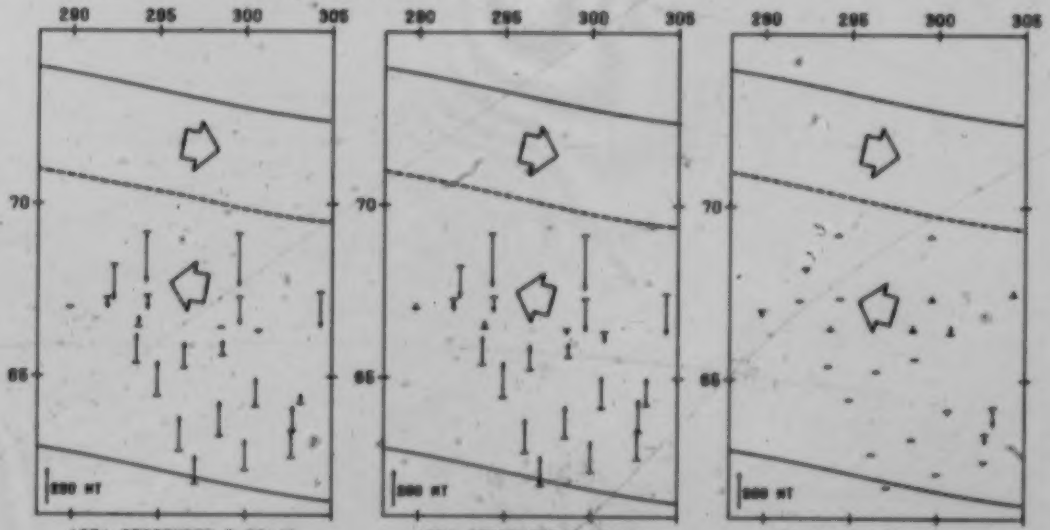
290
295
300
305
70
65
200 NT

1974 SEPTEMBER 7 09:43
OBSERVED VALUES

1974 SEPTEMBER 7 09:43
CALCULATED VALUES

1974 SEPTEMBER 7 09:43
RESIDUALS

Figure 4.10 Observed perturbation fields, calculated fields for model currents of best fit, and residuals in the five-minute interval 10.11-10.15 U.T. during Substorm 2. For Z, northward arrows represent upward Z. The full length of the ionospheric segment, and the distribution of current density across the width of the current, are shown in Fig. 4.13.

IONOSPHERIC CURRENT MODEL   WESTWARD CURRENT 0.50 MA

HORIZONTAL PERTURBATION FIELDS

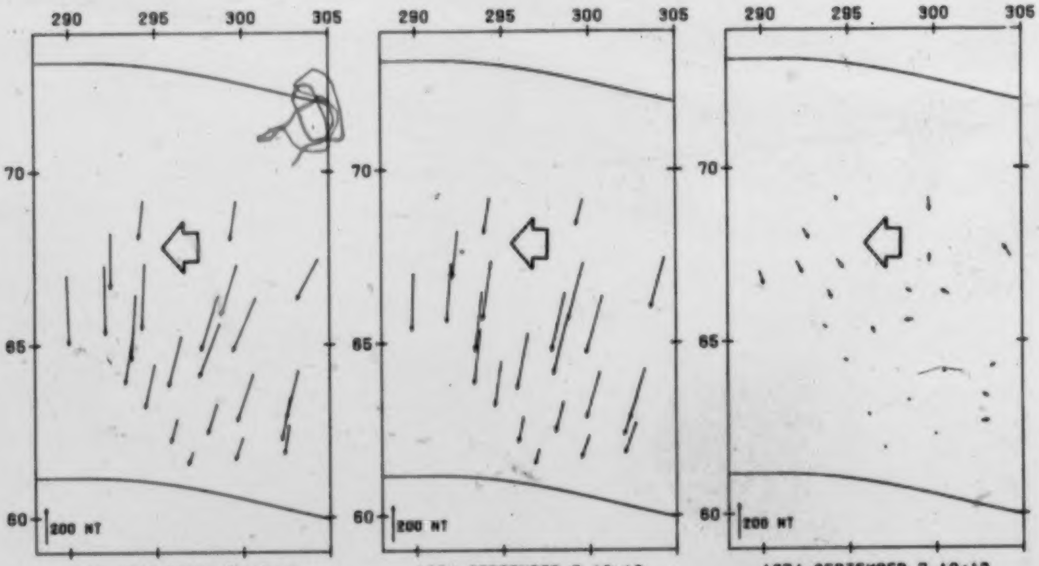

1974 SEPTEMBER 7 10:13
OBSERVED VALUES

1974 SEPTEMBER 7 10:13
CALCULATED VALUES

1974 SEPTEMBER 7 10:13
RESIDUALS

VERTICAL PERTURBATION FIELDS

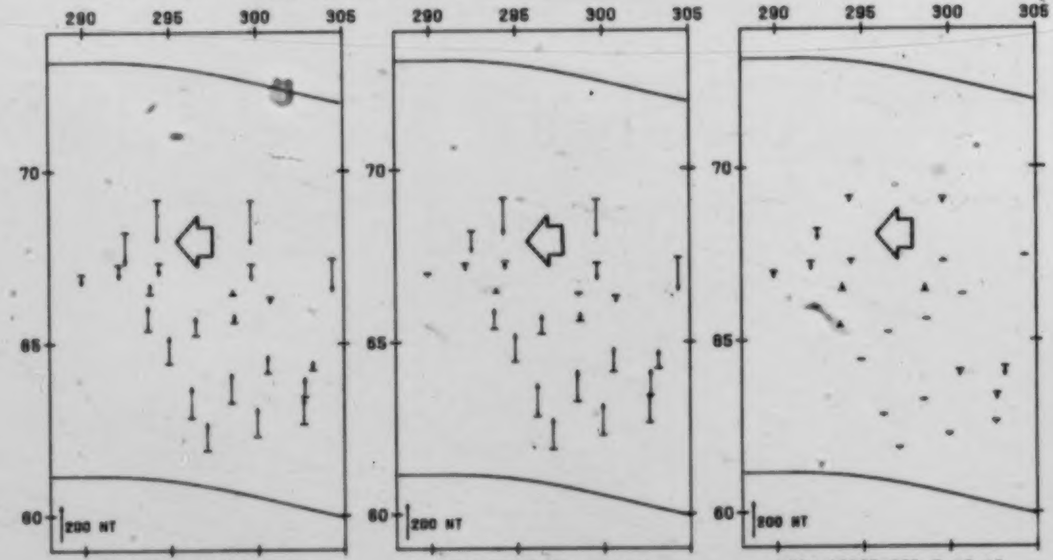

1974 SEPTEMBER 7 10:13
OBSERVED VALUES

1974 SEPTEMBER 7 10:13
CALCULATED VALUES

1974 SEPTEMBER 7 10:13
RESIDUALS

Figure 4.11 Observed perturbation fields, calculated fields for model currents of best fit, and residuals in the five-minute interval 10.46-10.50 U.T. during Substorm 2. For Z, northward arrows represent upward Z. The full length of the ionospheric segment, and the distribution of current density across the width of the current, are shown in Fig. 4.13.

IONOSPHERIC CURRENT MODEL EASTWARD CURRENT 0.10 MA

WESTWARD CURRENT 0.34 MA

HORIZONTAL PERTURBATION FIELDS

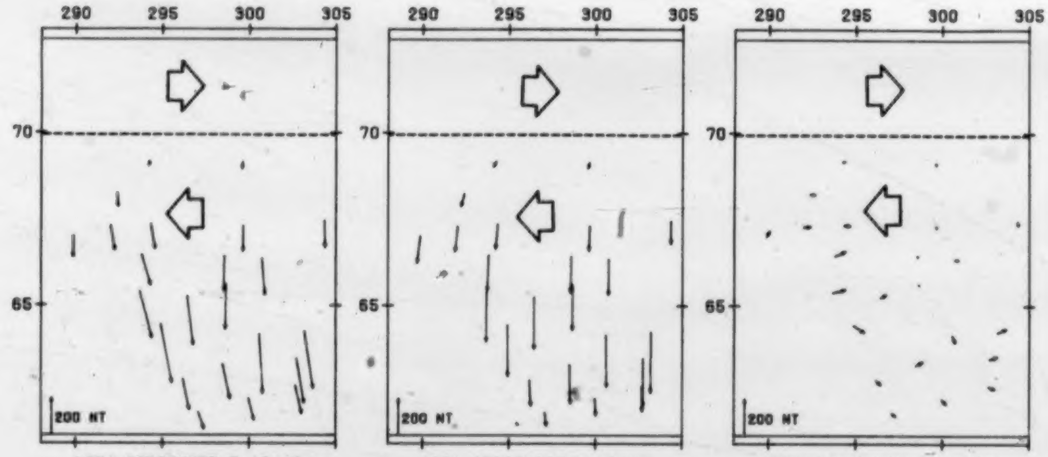

1974 SEPTEMBER 7 10:48
OBSERVED VALUES

1974 SEPTEMBER 7 10:48
CALCULATED VALUES

1974 SEPTEMBER 7 10:48
RESIDUALS

VERTICAL PERTURBATION FIELDS

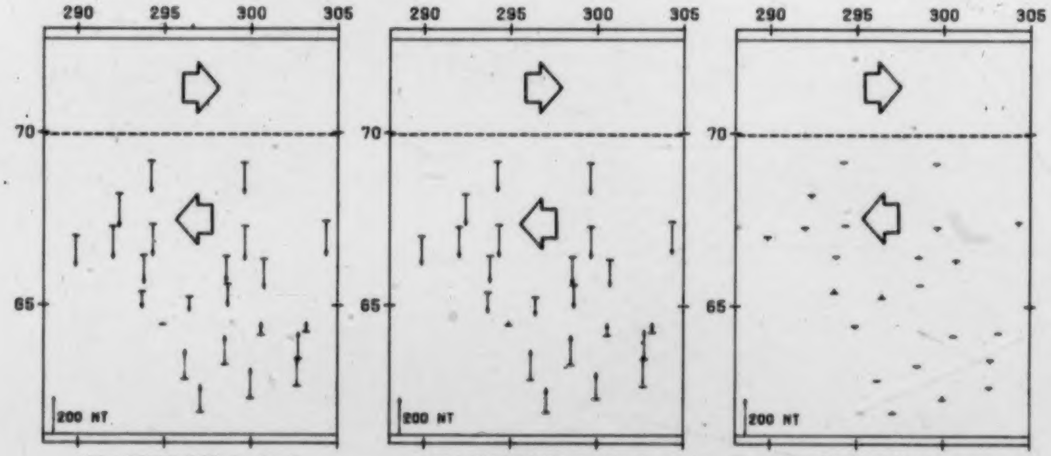

1974 SEPTEMBER 7 10:48
OBSERVED VALUES

1974 SEPTEMBER 7 10:48
CALCULATED VALUES

1974 SEPTEMBER 7 10:48
RESIDUALS

Figure 4.12 Observed perturbation fields, calculated fields for model currents of best fit, and residuals in the five-minute interval 11.21-11.25 U.T. during Substorm 2. For Z, northward arrows represent upward Z. The full length of the ionospheric segment, and the distribution of current density across the width of the current, are shown in Fig. 4.13.

IONOSPHERIC CURRENT MODEL

EASTWARD CURRENT 0.09 MA

WESTWARD CURRENT 0.34 MA

HORIZONTAL PERTURBATION FIELDS

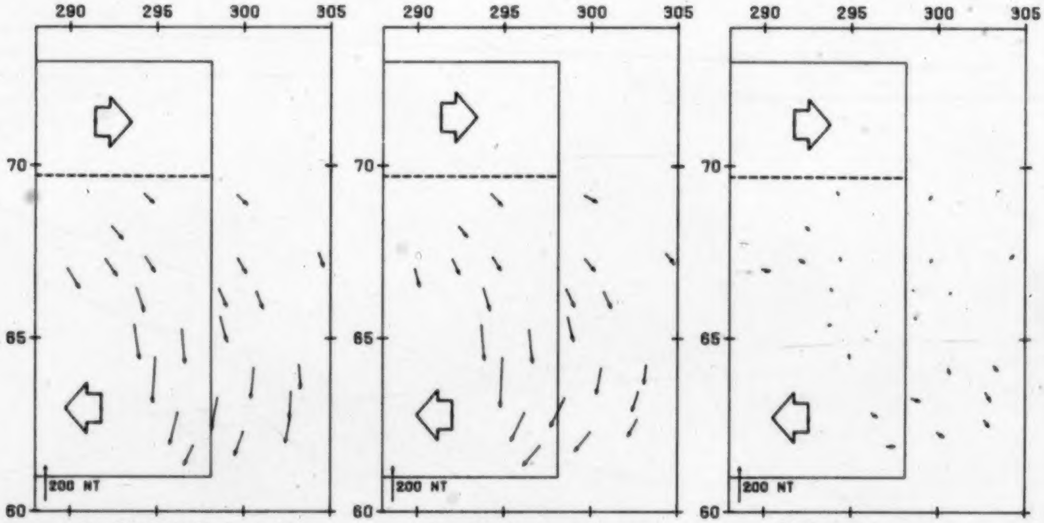

1974 SEPTEMBER 7 11:23
OBSERVED VALUES

1974 SEPTEMBER 7 11:23
CALCULATED VALUES

1974 SEPTEMBER 7 11:23
RESIDUALS

VERTICAL PERTURBATION FIELDS

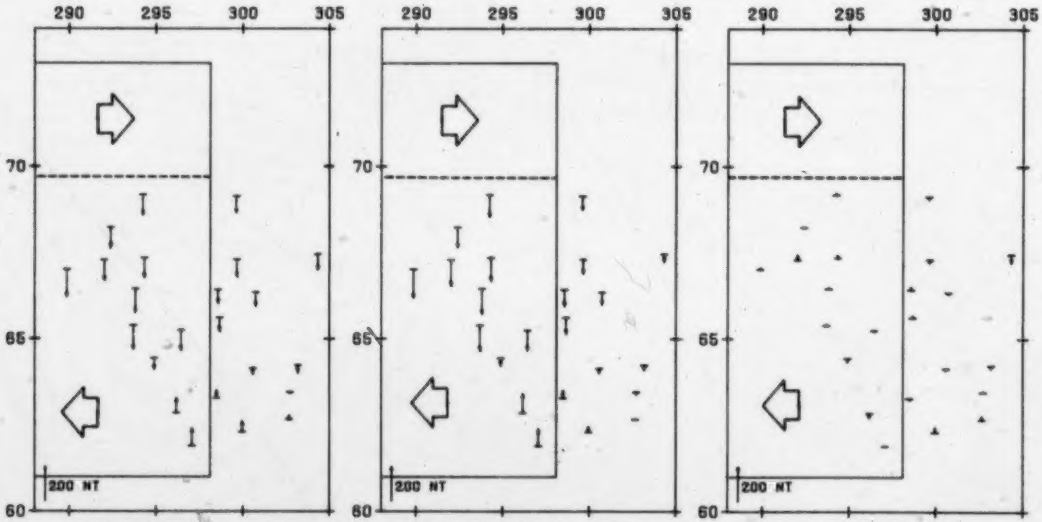

1974 SEPTEMBER 7 11:23
OBSERVED VALUES

1974 SEPTEMBER 7 11:23
CALCULATED VALUES

1974 SEPTEMBER 7 11:23
RESIDUALS

$$\varepsilon = \frac{\Sigma\,(\text{residual})^2}{\Sigma\,(\text{observed total field})^2}$$

and

$$\xi = \frac{\Sigma\,(\text{residual})^2}{\Sigma\,(\text{observed total field at 08.03 U.T.})^2}$$

and these parameters are listed for the six epochs in Table 4.2.

TABLE 4.2

STATISTICAL PARAMETERS FOR SUBSTORM 2
1974 SEPTEMBER 7

TIME U.T.	SSQ OBSERVED	SSQ RESIDUAL	ε	ξ
08.03	41771	--	--	--
08.28	264115	8432	0.0319	0.20
08.58	2023347	55332	0.0273	1.33
09.43	2946832	49535	0.0168	1.19
10.13	2277832	61887	0.0272	1.48
10.48	1546696	41219	0.0266	0.99
11.23	683507	29006	0.0424	0.69
12.23	21585	--	--	--

Note: SSQ denotes sum of squares

Residuals of the horizontal field at epoch 10.48 U.T. (Fig. 4.11) indicate that possibly a better fit could be achieved if the western end of the current system were nearer to the array. This could result if a larger number of iterations were allowed in the least square fit. Nevertheless the fits are very satisfactory.

At the first and fourth epochs, at 08.28 and 10.13 U.T., no appreciable eastward ionospheric current is indicated by the inverse calculation (Fig. 4.13). At the other four epochs eastward currents are required, and as modelled cover a latitude range about one-third of that in which westward current flows. As the eastward currents lie north of the array, they could be varied in width, with appropriate adjustment of total current, and still satisfy the data. Calculations of the H and Z components, due solely to an eastward current typical of those modelled north of the array (71°-74° N.), give values of about 77 nT for Z at northern stations and about 34 nT for H. Such contributions to perturbation fields cannot be attributed to baseline errors, which would in any case need to be made at northern stations only. Thus eastward currents, or equivalent currents elsewhere giving the same fields, are required to the north of the westward currents at four epochs of Substorm 2. At 08.58 U.T. the eastward current at 220,000 amperes is about half the westward current of 410,000 amperes. Although the eastward currents lie just outside the array, the array records strong contributions from them, increasing Z and reducing H at northern stations.

Figure 4.13 Ionospheric segments of current loops, in relation to the magnetometer array, at six epochs of Substorm 2, in Mercator projection of centred-dipole geomagnetic coordinates. GM represents magnetic midnight. The distributions of current density across the width of the current are shown.

IONOSPHERIC CURRENT MODEL

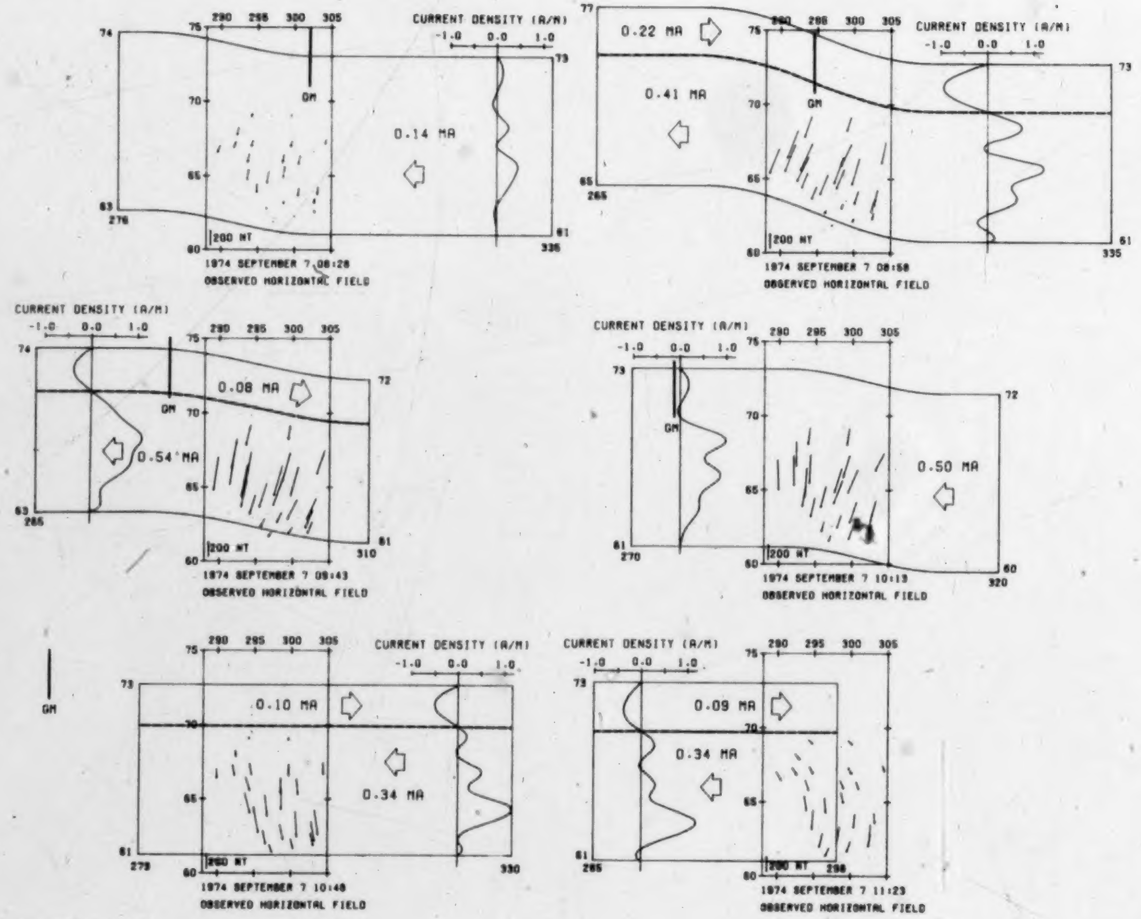

A bend in the ionospheric currents to the northwest is required to fit both horizontal and vertical fields, at the first four epochs modelled (Fig. 4.13). Such a bend therefore appears during the first two hours of the substorm. Straight ionospheric currents at constant geomagnetic latitude characterize the final hour of the substorm (Fig. 4.13, epochs 10.48 and 11.23 U.T.).

Geomagnetic midnight (Montbriand 1965) is shown for the first five epochs in Fig. 4.13. Relative to the Earth's surface, the current system moves westward between 08.28 and 09.43 U.T., then eastward until 10.48 U.T., and finally rapidly westward between 10.48 and 11.23 U.T.. Relative to geomagnetic midnight, however, the current configuration moves monotonically eastward, at varying speeds.

4.4 Substorm 3: 1974 September 18

4.4.1 Perturbation Fields

Twenty-three stations recorded this substorm. Baseline values for the three components were taken at 06.00 U.T., and it will be noted in Fig. 4.2 that the fields were essentially undisturbed until well after 07.00 U.T. Mean perturbation fields from the 06.00 U.T. values were mapped, as horizontal and vertical components, for consecutive five-minute intervals through the substorm, and eight representative epochs are shown in Figs. 4.14a and 4.14b.

Figure 4.14a Mean perturbation fields over five-minute intervals at four epochs before and during Substorm 3. For the vertical components, northward arrows represent upward fields. Unit: nanotesla.

PERTURBATION FIELDS
AVERAGED OVER 5 MINUTE INTERVALS

HORIZONTAL FIELDS

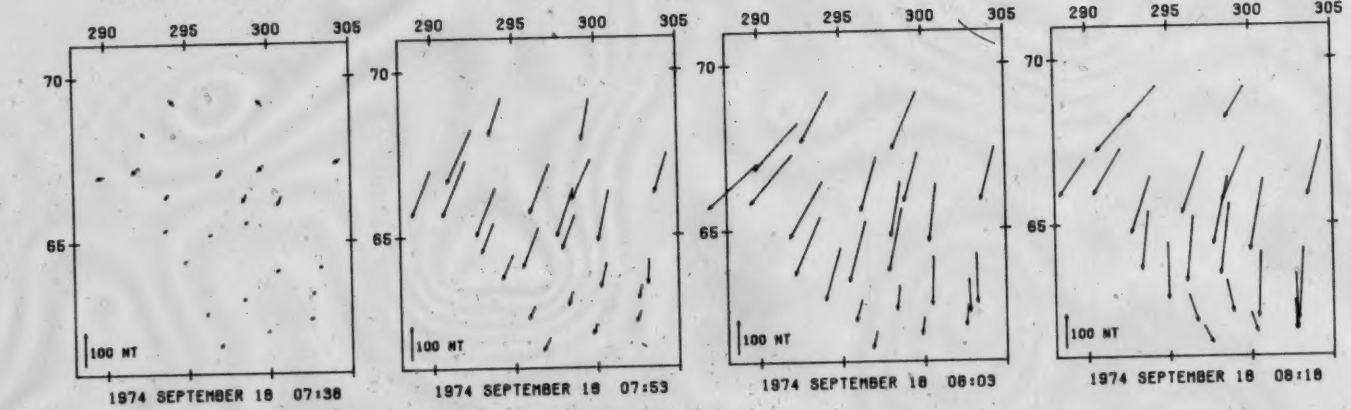

VERTICAL FIELDS

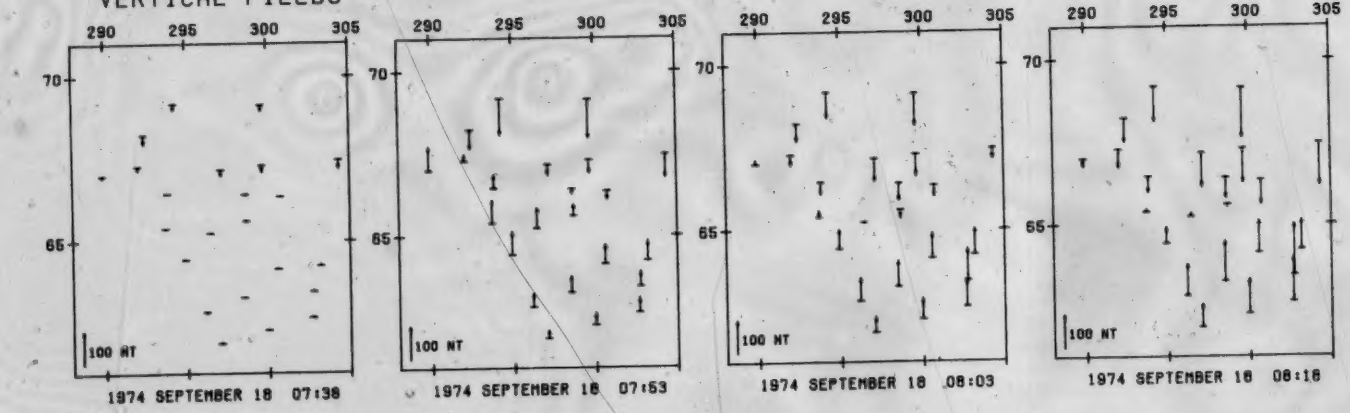

Figure 4.14b Mean perturbation fields over five-minute intervals at four epochs during Substorm 3. For the vertical components, northward arrows represent upward fields. Unit: nanotesla.

PERTURBATION FIELDS
AVERAGED OVER 5 MINUTE INTERVALS

HORIZONTAL FIELDS

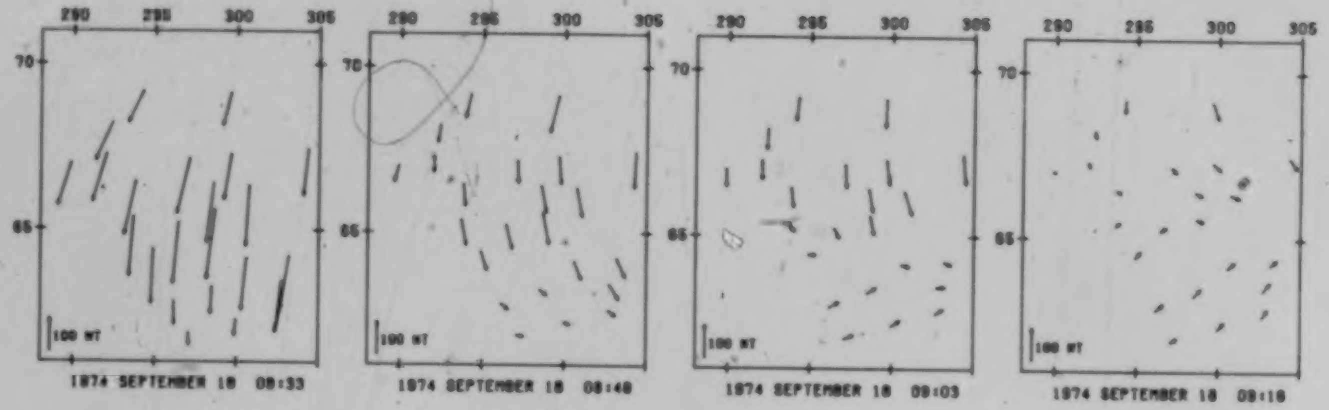

VERTICAL FIELDS

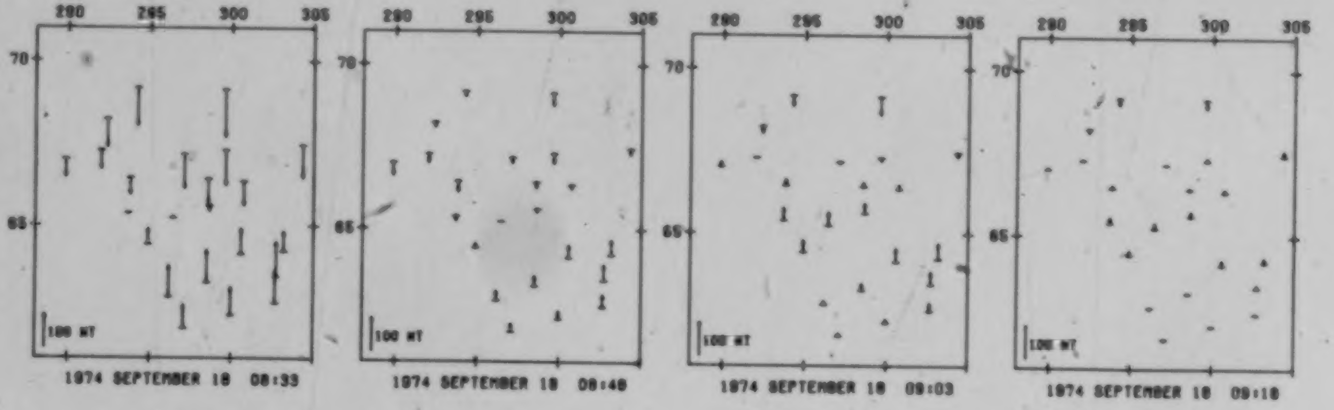

Comparison of Figs. 4.14 with Figs. 4.3 shows that Substorm 3 had about half the perturbation field amplitudes of Substorm 2, and about half the duration.

Two distinct patterns in the perturbation fields can be seen in Fig. 4.14a and 4.14b. The first shows horizontal fields diverging toward the south-southwest (08.03 U.T.); the second shows pronounced curvature, convex to the west, in the horizontal fields (08.18, 08.48). It will be shown that the first arises when a pronounced bend in the ionospheric currents, toward the northwest, lies above the array; the second when the upward field-aligned current, at the west end of the ionospheric current, lies above the array. In the coda of the substorm, at 09.03 and 09.18 U.T., the southern stations recorded horizontal perturbation fields directed to the east-northeast. Such fields could represent a combination of current loops having westward and southward ionospheric segments (Boström (1964) Types 1 and 2). Alternatively the westward ionospheric current could be flanked, on its south side, by an eastward current. Rostoker and Hron (1975) have proposed an eastward current in this position, in the morning sector. It will be shown that considerable eastward ionospheric currents, to the north of the westward current, are required to model all observed fields of Substorm 3. If, in the coda, an eastward current lies south of the westward current, then the latter is flanked by eastward ionospheric currents on both sides, at 09.03 and 09.18 U.T.

4.4.2 Model calculations

The perturbation fields at six epochs of Substorm 3 have been fitted by models of the type already described for Substorm 2. Fig. 1.7 illustrates the current loop. It was again found essential to employ currents of densities varying across their widths, and the Oldenburg (1976, 1977) inversion technique was again applied. All six models include equivalent eastward currents north of the westward ionospheric currents, and of comparable magnitudes. In each model, the eastward ionospheric segment terminates in field-aligned current sheets which are arbitrarily placed in the same longitudes as the field-aligned currents supplying the westward ionospheric current segments.

As for Substorm 2 and the substorm of September 11 (Chapter 3), the field components produced by each model current-loop were calculated from the Biot-Savart law in the manner of Kisabeth (1972), and parameters (Fig. 4.6) of the current loop were iteratively adjusted to optimize a least-squares fit to the observations. For the three epochs (07.53, 08.03 and 08.33 U.T.) that required a bend for best fit, the total current (P1, Fig. 4.6) and both longitudinal limits (P3 and P4) of the bend were allowed to change. For epoch 07.53 the southern limit of the eastern end (P8) of the current was made an additional parameter for the fit. For the three epochs (08.18, 08.48 and 09.03 U.T.) that do not require a bend, a best fit was obtained by allowing the total current (P1) and the western longitudinal end (P2) of the current to change. Table 4.3 lists these parameters.

TABLE 4.3

PARAMETERS OF THE IONOSPHERIC SEGMENT VARIED FOR SUBSTORM 3 (refered to Fig. 4.6)

epoch	independent parameters	dependent parameters
07.53	P1,P3,P4,P7,P8	P6,P9
08.03	P1,P3,P4,P7,P8	P6,P9
08.18	P1,P2	
08.33	P1,P3,P4,P7,P8	P6,P9
08.48	P1,P2	
09.03	P1,P2	

The ionospheric currents were placed at altitude 115 km and induction effects were included, to first order, by assuming a superconducting earth at depth 250 km. This depth is believed appropriate to the greater short-period content of the spectrum of Substorm 3, compared with Substorm 2. Other details of the model calculations were the same as those for Substorm 2.

4.4.3 Model currents at six epochs of Substorm 3

Observed perturbation fields are shown in Figs. 4.15 to 4.20 with calculated fields for models giving best fit, at the six representative epochs. The residuals are also shown. Fig. 4.21 shows the complete ionospheric segments of the model currents at six epochs, with the observed horizontal perturbation fields and the current density distributions

Figure 4.15 Observed perturbation fields, calculated fields for model currents of best fit, and residuals in the five minute interval 07.51-07.55 U.T. during Substorm 3. For Z, northward arrows represent upward Z. The full length of the ionospheric segment, and the distribution of current density across the width of the current, are shown in Fig. 4.21.

IONOSPHERIC CURRENT MODEL EASTWARD CURRENT 0.27 MA

WESTWARD CURRENT 0.20 MA

HORIZONTAL PERTURBATION FIELDS

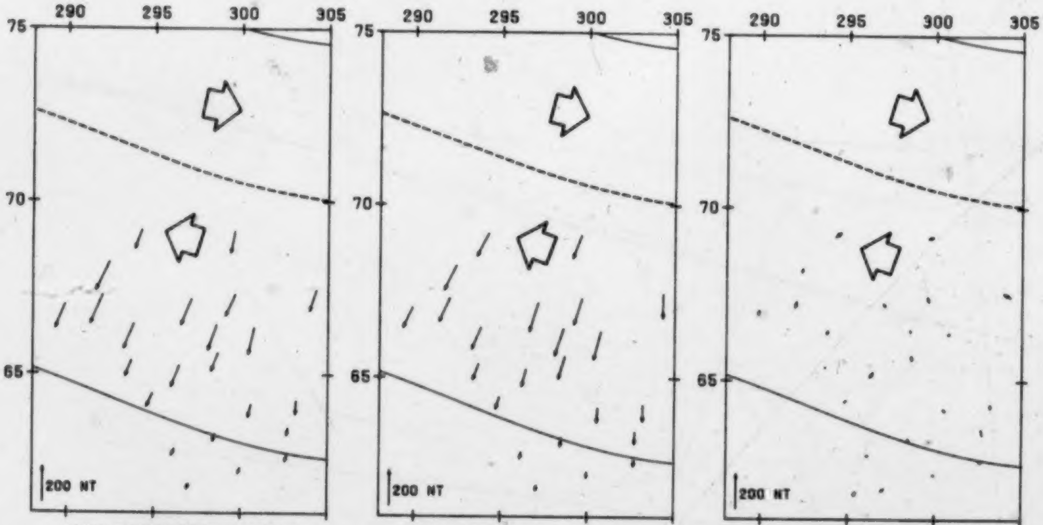

1974 SEPTEMBER 18 07:53
OBSERVED VALUES

1974 SEPTEMBER 18 07:53
CALCULATED VALUES

1974 SEPTEMBER 18 07:53
RESIDUALS

VERTICAL PERTURBATION FIELDS

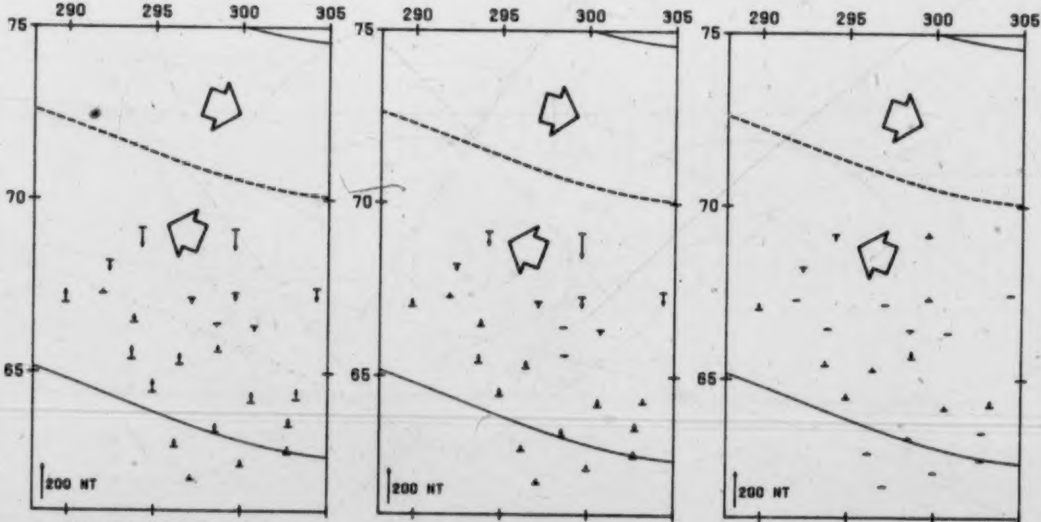

1974 SEPTEMBER 18 07:53
OBSERVED VALUES

1974 SEPTEMBER 18 07:53
CALCULATED VALUES

1974 SEPTEMBER 18 07:53
RESIDUALS

Figure 4.16 Observed perturbation fields, calculated fields for model currents of best fit, and residuals in the five minute interval 08.01-08.05 U.T. during Substorm 3. For Z, northward arrows represent upward Z. The full length of the ionospheric segment, and the distribution of current density across the width of the current, are shown in Fig. 4.21.

IONOSPHERIC CURRENT MODEL   EASTWARD CURRENT 0.21 MA

WESTWARD CURRENT 0.25 MA

HORIZONTAL PERTURBATION FIELDS

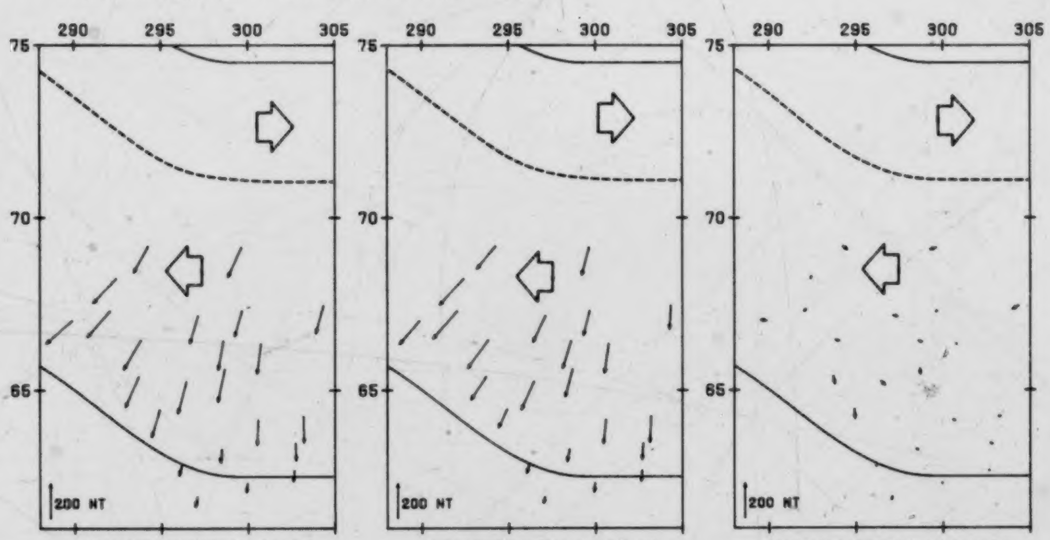

1974 SEPTEMBER 18 08:03
OBSERVED VALUES

1974 SEPTEMBER 18 08:03
CALCULATED VALUES

1974 SEPTEMBER 18 08:03
RESIDUALS

VERTICAL PERTURBATION FIELDS

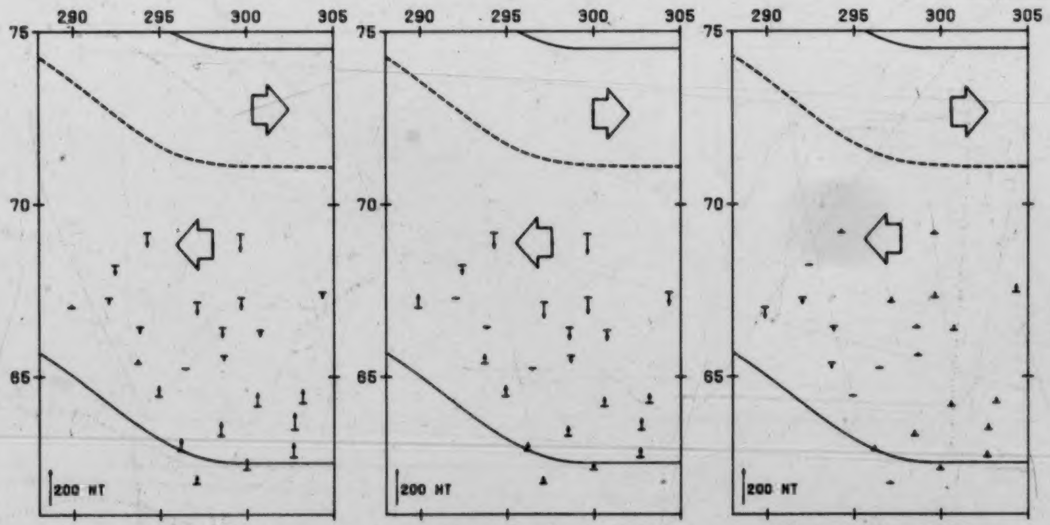

1974 SEPTEMBER 18 08:03
OBSERVED VALUES

1974 SEPTEMBER 18 08:03
CALCULATED VALUES

1974 SEPTEMBER 18 08:03
RESIDUALS

Figure 4.17 Observed perturbation fields, calculated fields for model currents of best fit, and residuals in the five minute interval 08.16-08.20 U.T. during Substorm 3. For Z, northward arrows represent upward Z. The full length of the ionospheric segment, and the distribution of current density across the width of the current, are shown in Fig. 4.21.

IONOSPHERIC CURRENT MODEL EASTWARD CURRENT 0.13 MA

WESTWARD CURRENT 0.32 MA

HORIZONTAL PERTURBATION FIELDS

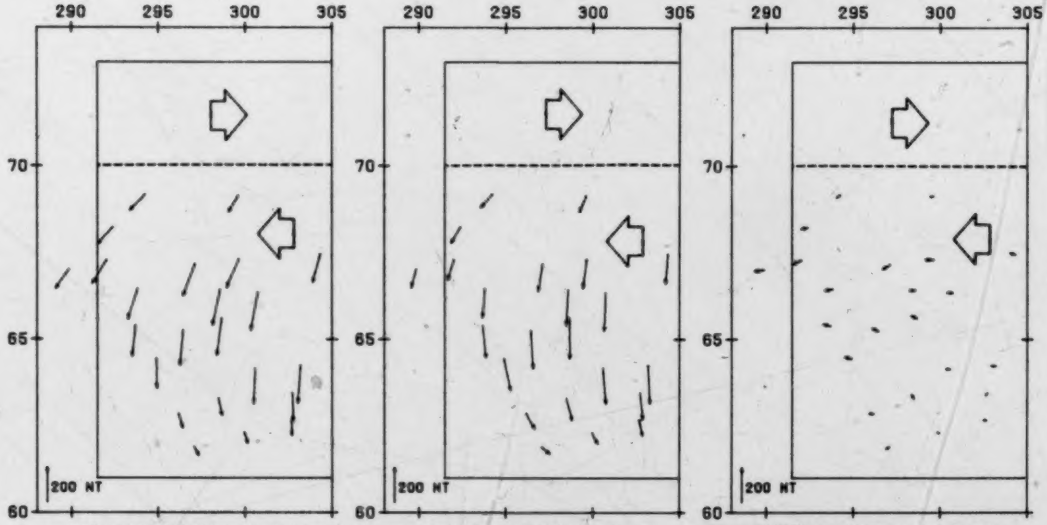

1974 SEPTEMBER 18 08:18
OBSERVED VALUES

1974 SEPTEMBER 18 08:18
CALCULATED VALUES

1974 SEPTEMBER 18 08:18
RESIDUALS

VERTICAL PERTURBATION FIELDS

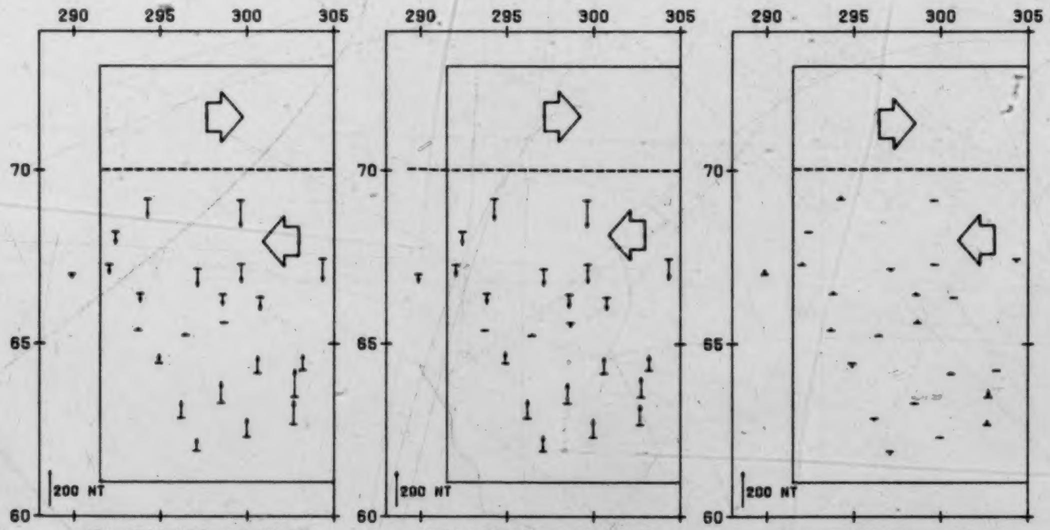

1974 SEPTEMBER 18 08:18
OBSERVED VALUES

1974 SEPTEMBER 18 08:18
CALCULATED VALUES

1974 SEPTEMBER 18 08:18
RESIDUALS

Figure 4.18 Observed perturbation fields, calculated fields for model currents of best fit, and residuals in the five minute interval 08.31-08.35 U.T. during Substorm 3. For Z, northward arrows represent upward Z. The full length of the ionospheric segment, and the distribution of current density across the width of the current, are shown in Fig. 4.21.

IONOSPHERIC CURRENT MODEL EASTWARD CURRENT 0.18 MA

WESTWARD CURRENT 0.22 MA

HORIZONTAL PERTURBATION FIELDS

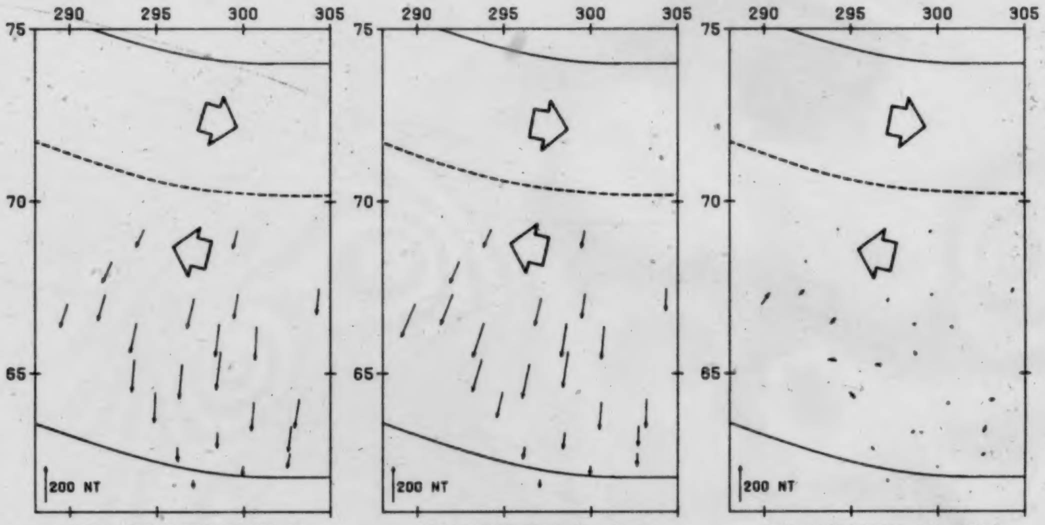

1974 SEPTEMBER 18 08:33
OBSERVED VALUES

1974 SEPTEMBER 18 08:33
CALCULATED VALUES

1974 SEPTEMBER 18 08:33
RESIDUALS

VERTICAL PERTURBATION FIELDS

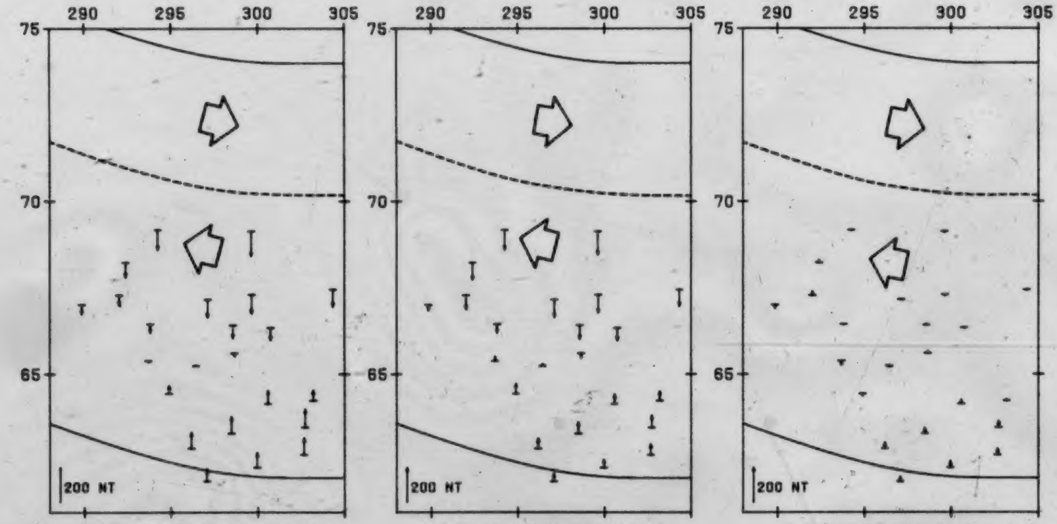

1974 SEPTEMBER 18 08:33
OBSERVED VALUES

1974 SEPTEMBER 18 08:33
CALCULATED VALUES

1974 SEPTEMBER 18 08:33
RESIDUALS

Figure 4.19 Observed perturbation fields, calculated fields for model currents of best fit, and residuals in the five minute interval 08.46-08.50 U.T. during Substorm 3. For Z, northward arrows represent upward Z. The full length of the ionospheric segment, and the distribution of current density across the width of the current, are shown in Fig. 4.21.

IONOSPHERIC CURRENT MODEL EASTWARD CURRENT 0.11 MA

WESTWARD CURRENT 0.18 MA

HORIZONTAL PERTURBATION FIELDS

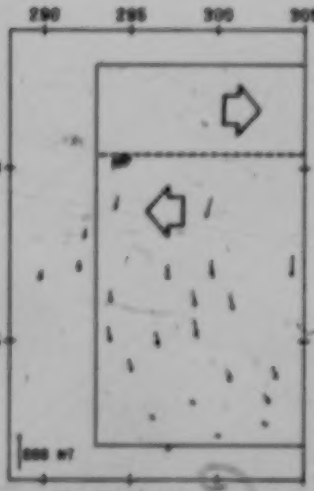

1974 SEPTEMBER 10 08:40
OBSERVED VALUES

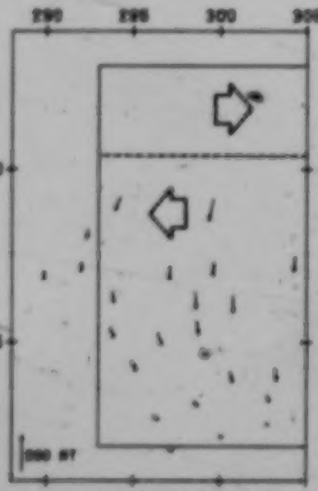

1974 SEPTEMBER 10 08:40
CALCULATED VALUES

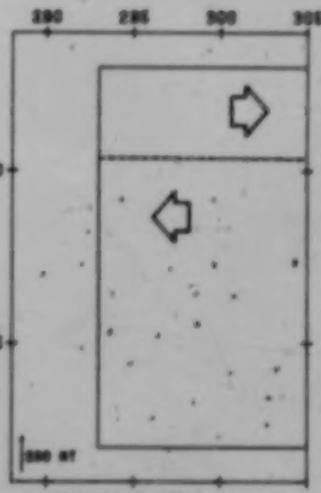

1974 SEPTEMBER 10 08:40
RESIDUALS

VERTICAL PERTURBATION FIELDS

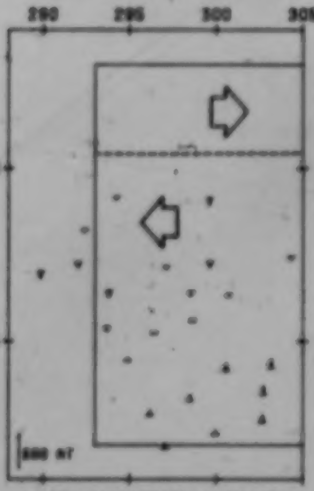

1974 SEPTEMBER 10 08:40
OBSERVED VALUES

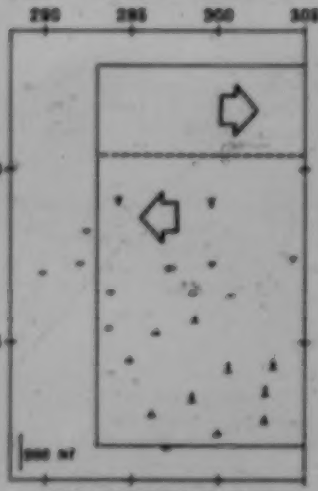

1974 SEPTEMBER 10 08:40
CALCULATED VALUES

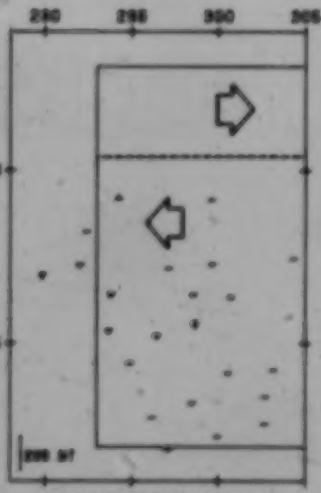

1974 SEPTEMBER 10 08:40
RESIDUALS

Figure 4.20 Observed perturbation fields, calculated fields for model currents of best fit, and residuals in the five minute interval 09.01-09.05 U.T. during Substorm 3. For Z, northward arrows represent upward Z. The full length of the ionospheric segment, and the distribution of current density across the width of the current, are shown in Fig. 4.21.

IONOSPHERIC CURRENT MODEL EASTWARD CURRENT 0.08 MA

WESTWARD CURRENT 0.11 MA

HORIZONTAL PERTURBATION FIELDS

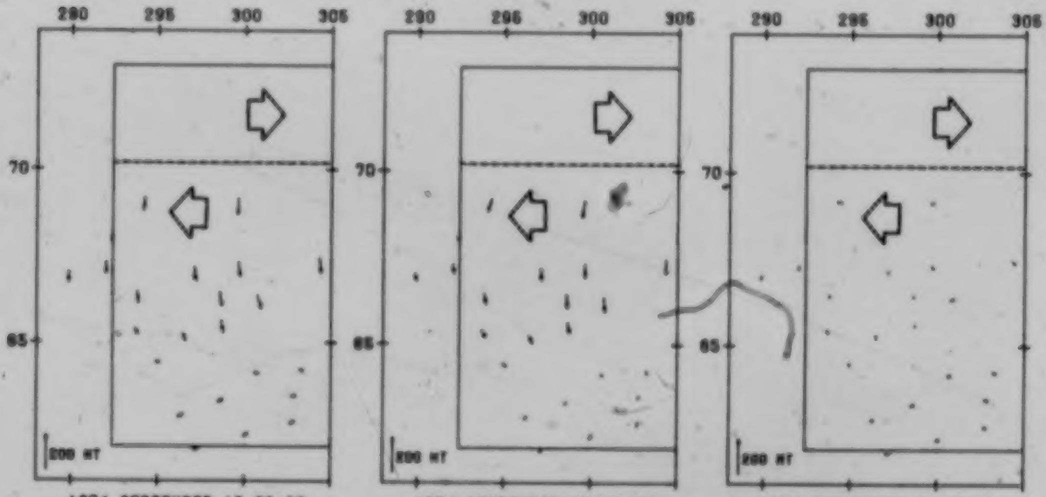
290
295
300
305
70
65
200 NT

1974 SEPTEMBER 18 09:03
OBSERVED VALUES

1974 SEPTEMBER 18 09:03
CALCULATED VALUES

1974 SEPTEMBER 18 09:03
RESIDUALS

VERTICAL PERTURBATION FIELDS

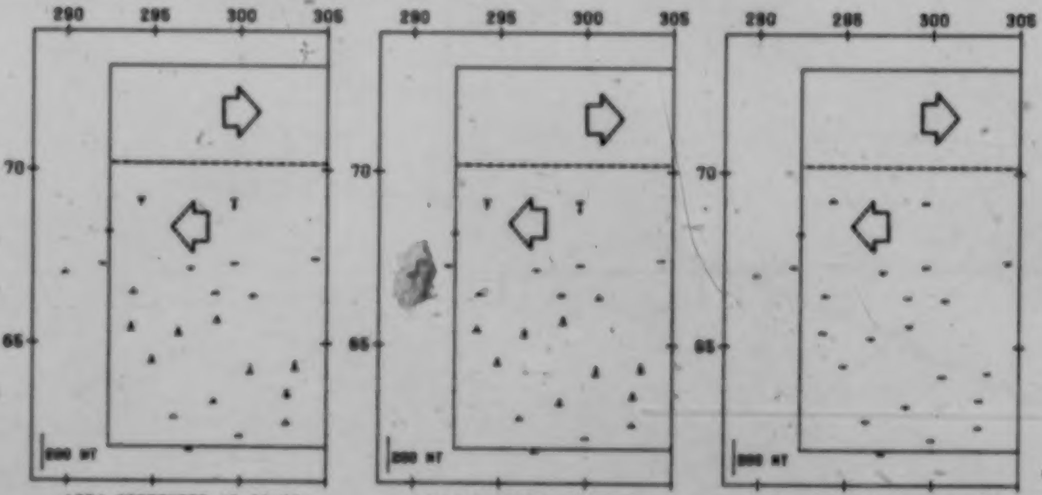
290
295
300
305
70
65
200 NT

1974 SEPTEMBER 18 09:03
OBSERVED VALUES

1974 SEPTEMBER 18 09:03
CALCULATED VALUES

1974 SEPTEMBER 18 09:03
RESIDUALS

found from the Oldenburg inverse calculations. The least-squares parameters ε and ξ are listed in Table 4.4.

TABLE 4.4

STATISTICAL PARAMETERS FOR SUBSTORM 3
1974 SEPTEMBER 18

TIME U.T.	SSQ OBSERVED	SSQ RESIDUAL	ε	ξ
07.38	9053	--	--	--
07.53	379253	20744	0.0547	2.291
08.03	635231	30051	0.0473	3.318
08.18	785459	31524	0.0401	3.482
08.33	634425	24429	0.0385	2.698
08.48	124383	10131	0.0815	1.119
09.03	84903	6546	0.0771	0.023
09.18	21505	--	--	--

Note: SSQ denotes sum of squares, ξ is refered to 07.38

This short-lived substorm was characterized by rapid east-west shifts of the current system between two types (Fig. 4.21). In one type (at 07.53, 08.03 and 08.33 U.T.) the field-aligned currents are both 15° or more away from the array to east and west, and a bend in the ionospheric currents above the array produces horizontal fields which diverge to the south-southwest. In the other type, at 08.18, 08.48 and 09.03 U.T., the ionospheric currents lie at constant geomagnetic latitude, so that they are straight in the Mercator projection of Fig. 4.21, and the west-end field-aligned currents (upward for the westward ionospheric current and downward for the eastward current to the north) lie above the array, producing strong curvature in the horizontal perturbation fields. Figs. 4.15, 4.16 and 4.18 illustrate the fitting of a model of the first type, Figs. 4.17, 4.19 and 4.20 the second type. These two very different fields were recorded at times only 15 minutes apart. The fits of the three components (H and D contributing to the horizontal components) are considered satisfactory.

The substantial eastward ionospheric current north of the westward current, which is comparable to the westward current at each epoch and larger at 07.53, is not an artefact of the inversion and is not a consequence of error in baseline values. The distribution of current density within the eastward current is not well defined by the array, because this current is north of the array, but the total eastward current is well determined and steep northward gradients, near the broken lines in Fig. 4.21, are required to account for the large Z/H ratios at northern stations of the array. The forward model calculations cannot give unique solutions and naturally do not distinguish between real ionospheric currents and its equivalent in

Figure 4.21 Ionospheric segments of current loops, in relation to the magnetometer array, at six epochs of Substorm 3, in a Mercator projection of centred-dipole geomagnetic coordinates. GM represents magnetic midnight. The distributions of current density across the width of the current are shown.

IONOSPHERIC CURRENT MODEL

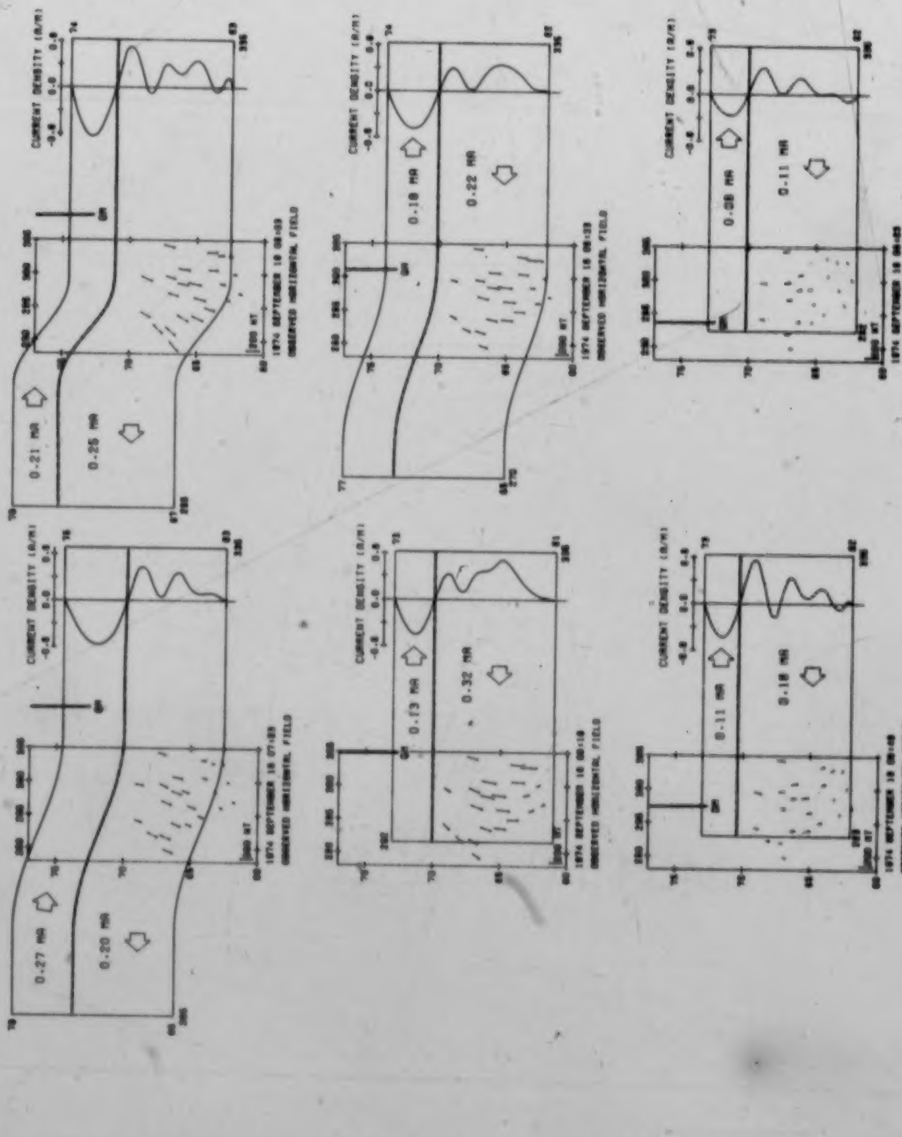

terms of observed fields. The locations of the associated field-aligned currents, at the same longitudes as those of the westward currents, are arbitrary, as has been said.

The bends in the ionospheric currents to the northwest, when seen (at 07.53, 08.03 and 08.33 U.T., Fig. 4.21), are within 30° of longitude west of geomagnetic midnight, as was the case in Substorm 1 (1974 September 11,) (Chapter 3). In the case of Substorm 2 (this chapter) the bend was sometimes west and sometimes east of magnetic midnight. In all three cases the ionospheric currents flowed without change of geomagnetic latitude, once the current system and the array were entirely in the morning sector.

4.5 A comparison of polar magnetic Substorms 2 and 3

The ionospheric segments of the three-dimensional current systems (of the type illustrated in Fig. 1.7) are mapped in azimuthal equidistant projection, centred on the geomagnetic dipole, at the six epochs studied, for Substorm 2 (1974 September 7) in Fig. 4.22 and for that of Substorm 3 (1974 September 18) in Fig. 4.23.

The current systems extend to the geomagnetic longitudes of Canadian and American permanent geomagnetic observatories, and flow above Churchill and Baker Lake at some epochs. The records of observatories near the current systems have been scaled, with careful attention to baselines, and the perturbation fields at these

Figure 4.22 Ionospheric segments of current loops at six epochs of Substorm 2, in azimuthal equidistant projection of centred-dipole geomagnetic coordinates, superimposed on a map of the North American mainland. GM represents geomagnetic midnight.

08:28 UT

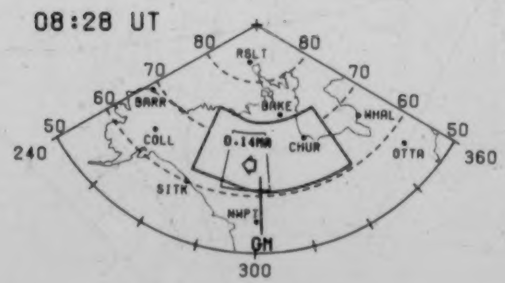
80
80
RSLT
70
70
60
BARR
BAKE
WHAL
60
50
50
240
COLL
0.14MA
CHUR
OTTA
360
SITK
NWPT
GM
300

08:58 UT

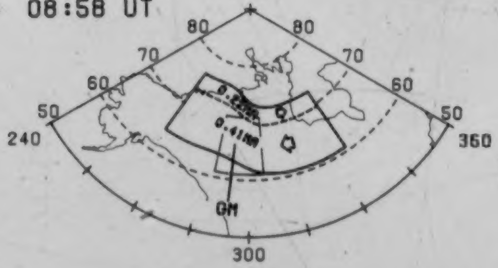
80
80
70
70
60
60
50
50
240
0.41MA
360
GM
300

09:43 UT

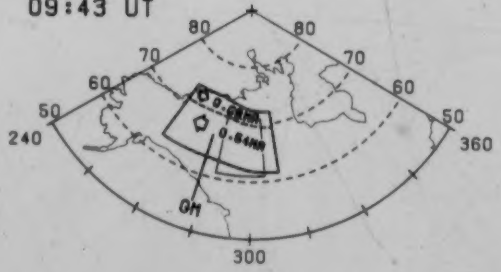
80
80
70
70
60
60
50
50
240
0.64MA
360
GM
300

10:13 UT

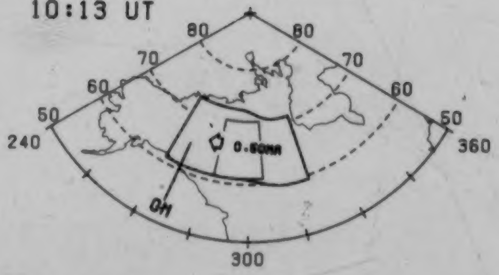
80
80
70
70
60
60
50
50
240
0.60MA
360
GM
300

10:48 UT

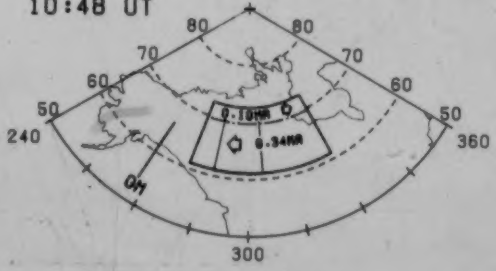
80
80
70
70
60
60
50
50
240
0.10MA
0.34MA
360
GM
300

11:23 UT

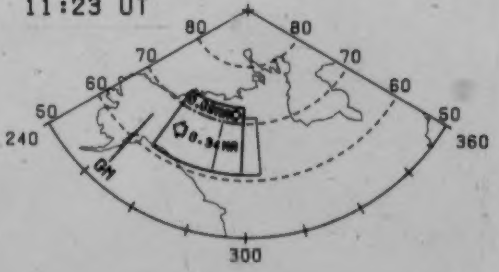
80
80
70
70
60
60
50
50
240
0.34MA
360
GM
300

Figure 4.23 Ionospheric segments of current loops at six epochs of Substorm 3, in azimuthal equidistant projection of centred-dipole geomagnetic coordinates, superimposed on a map of the North American mainland. GM represents geomagnetic midnight.

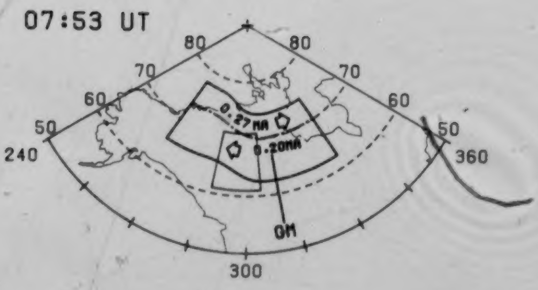
07:53 UT
80
80
70
70
60
60
50
50
240
360
0.27MA
0.20MA
GM
300

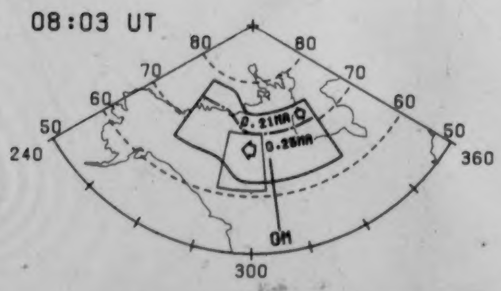
08:03 UT
80
80
70
70
60
60
50
50
240
360
0.21MA
0.25MA
GM
300

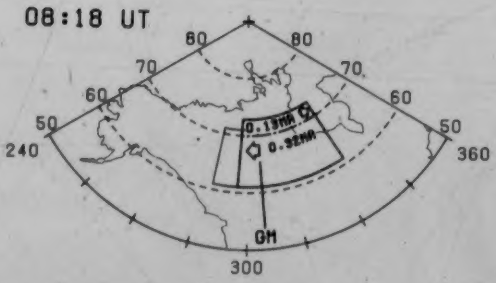
08:18 UT
80
80
70
70
60
60
50
50
240
360
0.13MA
0.32MA
GM
300

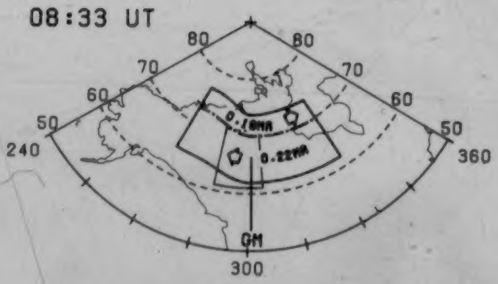
08:33 UT
80
80
70
70
60
60
50
50
240
360
0.16MA
0.22MA
GM
300

08:48 UT
80
80
70
70
60
60
50
50
240
360
0.11MA
0.10MA
GM
300

09:03 UT
80
80
70
70
60
60
50
50
240
360
0.08MA
0.11MA
GM
300

Figure 4.24 Horizontal perturbation fields recorded by Canadian and U.S. observatories at epoch 08.58 U.T. of Substorm 2 in azimuthal equidistant projection of centred dipole geomagnetic coordinate. Location of stations are given in table 2.2.

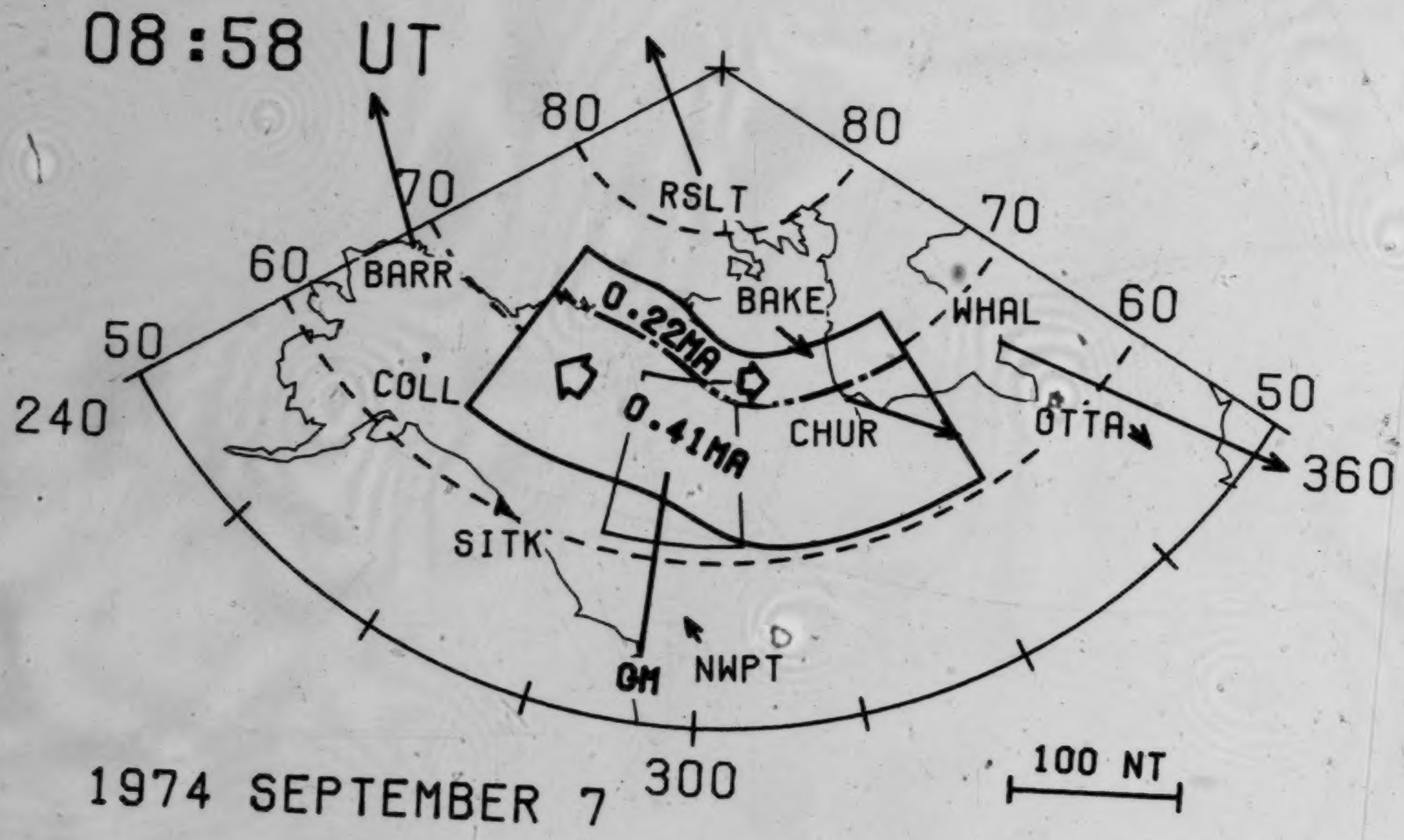
08:58 UT
80
80
70
70
60
60
50
50
240
360
300
RSLT
BARR
BAKE
WHAL
COLL
0.22MA
0.41MA
CHUR
OTTA
SITK
GM
NWPT
100 NT
1974 SEPTEMBER 7

Figure 4.25 Horizontal perturbation fields recorded by Canadian and U.S. observatories at epoch 11.23 U.T. of Substorm 2 in azimuthal equidistant projection of centred dipole geomagnetic coordinate. Location of stations are given in table 2.2. Magnitude of perturbation at COLL (College) is two times the magnitude shown.

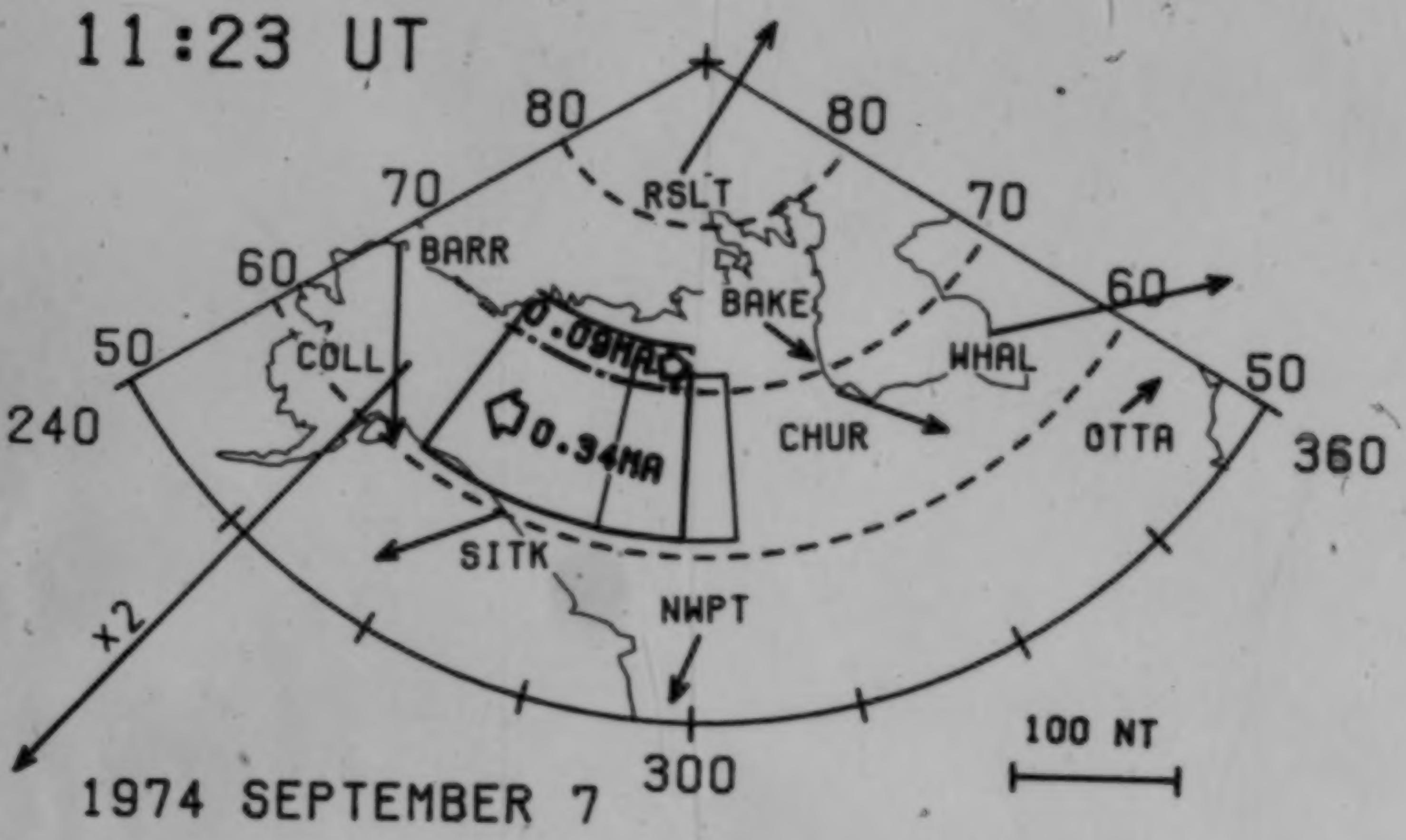
11:23 UT
80
80
70
70
60
60
50
50
240
360
300
RSLT
BARR
BAKE
COLL
WHAL
0.09MA
0.34MA
CHUR
OTTA
SITK
NWPT
x2
100 NT
1974 SEPTEMBER 7

Figure 4.26 Horizontal perturbation fields recorded by Canadian and U.S. observatories at epoch 08.03 U.T. of Substorm 3 in azimuthal equidistant projection of centred dipole geomagnetic coordinate. Location of stations are given in table 2.2.

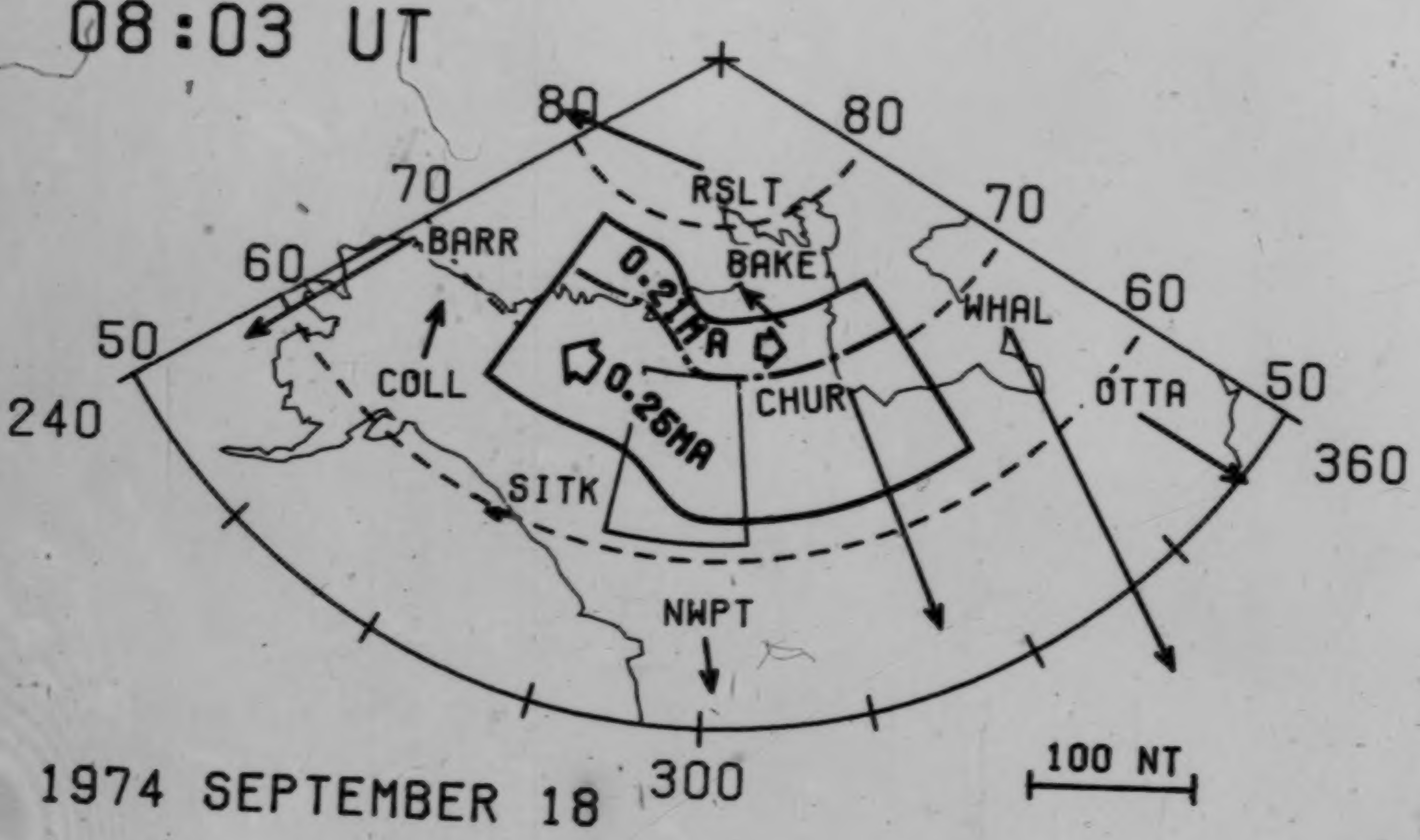
08:03 UT
80
80
70
70
60
60
50
50
240
360
300
RSLT
BAKE
BARR
COLL
WHAL
OTTA
CHUR
SITK
NWPT
0.21MA
0.25MA
100 NT
1974 SEPTEMBER 18

Figure 4.27 Horizontal perturbation fields recorded by Canadian and U.S. observatories at epoch 08.48 U.T. of Substorm 3 in azimuthal equidistant projection of centred dipole geomagnetic coordinate. Location of stations are given in table 2.2.

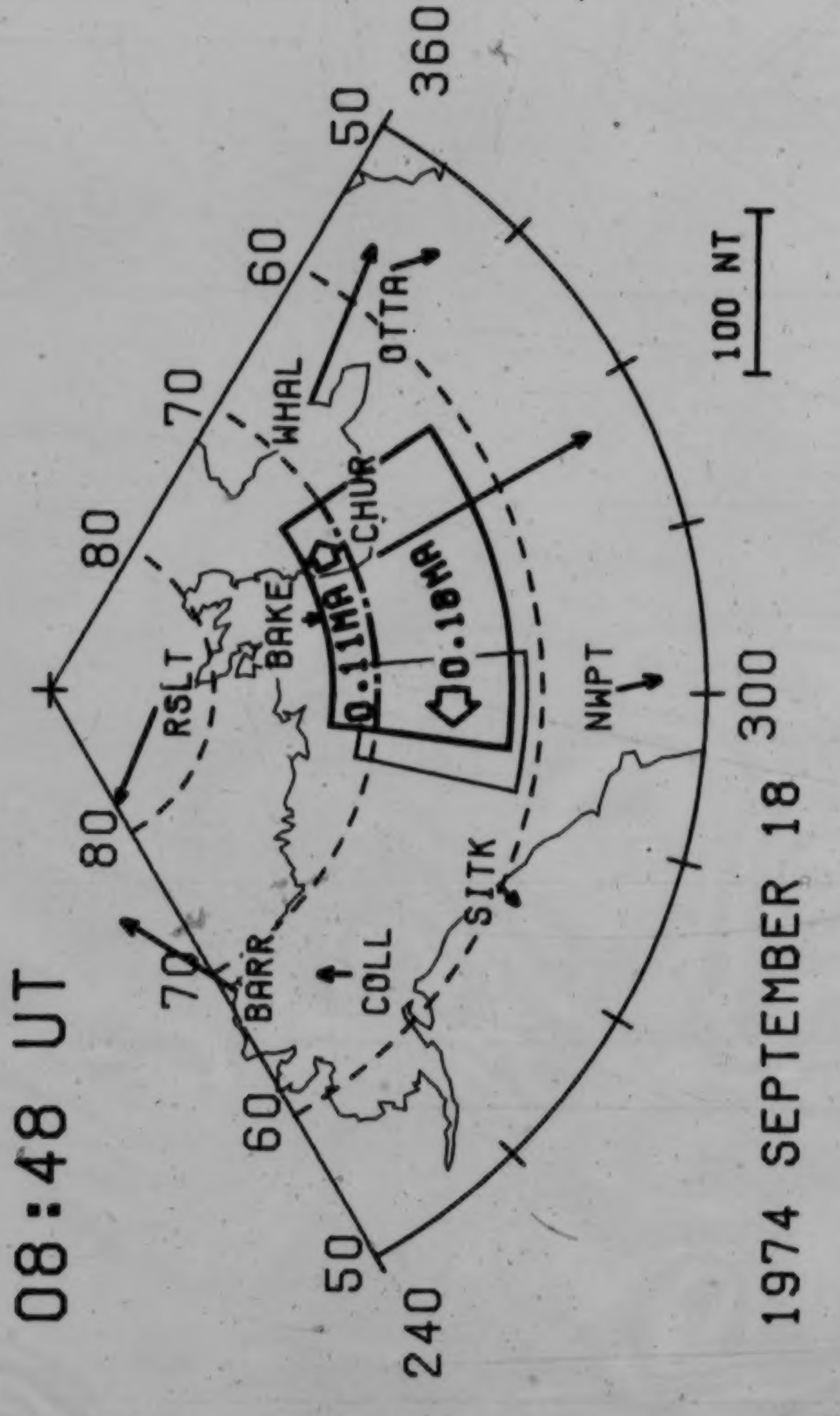
08:48 UT
1974 SEPTEMBER 18
100 NT
50
60
70
80
80
70
60
50
240
300
360
RSLT
BAKE
CHUR
WHAL
OTTA
NWPT
SITK
COLL
BARR
0.11MA
0.18MA

observatories have been mapped, but only four are shown here in Fig. 4.24 to 4.27. In general the perturbation fields at the observatories are consistent with the model currents, but do not add much to the array data. The problem is, as mentioned in Chapter 3, that the substorm fields have scale lengths smaller than the distances between the observatories, whereas the spacing of stations in the array is smaller than the scale lengths of the fields. Thus Churchill and Baker Lake, near the west coast of Hudson's Bay, generally have perturbation fields consistent with the models when these show currents above those observatories, but Great Whale River on the eastern shore of Hudson's Bay always lay east of our current systems and recorded obviously unrelated fields. College, Alaska was in general west of the current systems and usually showed fields unrelated to those systems, but at one epoch (September 7, 11.23 U.T. Fig. 4.25) this observatory recorded a negative H field of more than 680 nT, stronger than any field seen by the array, and it may be that the model for that epoch should be extended westward. This is confirmed by the AL indices. Equally well, College may have recorded another, simultaneous event. Resolute Bay and Mould Bay lie far north of the model currents, and usually recorded positive H perturbations which are not predicted by the models, though they may be related. Observatories such as Sitka and Newport recorded small perturbations consistent with the model currents. Figs. 4.7 to 4.12 and 4.15 to 4.20 illustrate the rapid drop in the substorm fields south of the overhead currents; because of this the United States observatories outside Alaska can in general add little to the array data. No attempt has been made to use observatory data in modelling the currents.

Substorm 2 (Fig. 4.22) generated the largest fields and had the longest duration of the three. The ionospheric current system moved slowly westward over the array, and eastward about 18° relative to geomagnetic midnight, between 08.28 and 10.13 U.T. In the next 35 minutes the current system moved about 10° eastward relative to the ground and about 18° eastward relative to geomagnetic midnight, then in its coda moved rapidly westward relative to both. The relatively brief Substorm 3 (Fig. 4.23) has been modelled with ionospheric current segments having the east end always at constant longitude and rapid variations in the longitude of the west end. (The east end was too far from the array to be well fixed for this event, and some variation of its longitude may actually have occurred). At some epochs the current system stretched westward to about 265-270°, simultaneously developing a northwestward bend (see also Fig. 4.21). The large negative H recorded at WHAL (Fig. 4.26) suggests that the current at 08.03 U.T. extended further east. The positive H at BAKE in this same epoch gives some confirmation of an eastward ionospheric current to the north of the main westward electrojet. At other epochs the current system shortened, with its upward field-aligned currents above the array, and simultaneously became 'straight' (i.e. in constant latitude range).

Equivalent eastward ionospheric currents are required to model the observed fields, in Substorms 2 and 3. In Substorm 2 (Fig. 4.22) the eastward currents had magnitudes between zero and 0.54 of the westward currents. At two epochs, 08.28 and 10.13, the currents in the northern part of the zone are small (Fig. 4.13). In using Figs. 4.22 and 4.23 one should remember the non-uniform current distribution across the width (cf. Figs. 4.13 and 4.21): a "uniform current of best fit" would be narrower than the current outlines shown. Eastward currents north of the westward ionospheric currents are required at all epochs of Substorm 3. The ratio eastward/westward total currents lay in the range 0.4 to 1.4, so that the eastward currents were always comparable to the westward. Westward currents, of uniform density across their widths, gave good fits to the observed fields of Substorm 1, (Chapter 3) which thus does not appear to have involved eastward ionospheric current.

CHAPTER 5

DEVELOPMENT OF A POLAR MAGNETIC SUBSTORM ON AUGUST 14, 1974

5.1 Introduction

In the two previous chapters three substorms have been modelled with Boström Type 1 current loops with mainly westward ionospheric currents. The current models obtained for Substorms 2 and 3 (Chapter 4) required in most cases the existence of an eastward current or equivalent current system to the north of the main westward current where the longitudinal limits of both the eastward and westward currents, were arbitrarily kept the same.

In this chapter a substorm is discussed which involves an eastward current in the ionosphere above the array but which, like the substorms considered in Chapter 4, cannot be fitted with a uniform current density. Furthermore, magnetic records from the northern stations of the array give definite indications of the existence of a westward ionospheric current to the north of the eastward electrojet. Rostoker and Kisabeth (1973) showed that during substorm activity the westward electrojet often penetrated into the evening sector poleward of the eastward electrojet which would be in agreement with the array observations here reported. The possibility indicated by Rostoker and Kisabeth

(1973), that the westward current to the north may be an extension of the westward electrojet into the morning sector, immediately suggests that a more flexible treatment of the current model is necessary, with different longitudes for the ends of the eastward and westward ionospheric currents. This chapter therefore records an exercise in forward modelling, to fit the observed perturbation fields, one step more complicated than those discussed in Chapter 4.

5.2 Observations

The substorm here reported occurred in 1974 on August 14 and was recorded by 18 stations. Magnetograms are shown in Fig. 5.1 from 10 stations along north-south profiles near the western and eastern limits of the array. The station positions are shown in Fig. 2.1. This event on August 14 (Substorm 4) is long-lived, with a duration of about 6 hours and smaller amplitudes, at most epochs, than those of Substorms 1, 2 and 3 (Chapters 3 and 4). Kp and AE indices are given in Appendix B. The three-hour range Kp indices for this event are 2-, 2+, 1 and 1- for the first 12 hours of August 14, 1974. In the maps of this chapter, as in the previous chapters, centred dipole geomagnetic coordinates are shown with the north pole at geographic coordinates 78.565°N., 69.761°W.

Figure 5.1 Magnetograms of Substorm 4 from 10 stations along two north-south lines near the western and eastern edges of the array. Bars indicate the eight time intervals averaged in Figs. 5.2a and 5.2b. The station positions are shown in Fig. 2.1.

AUGUST 14 1974

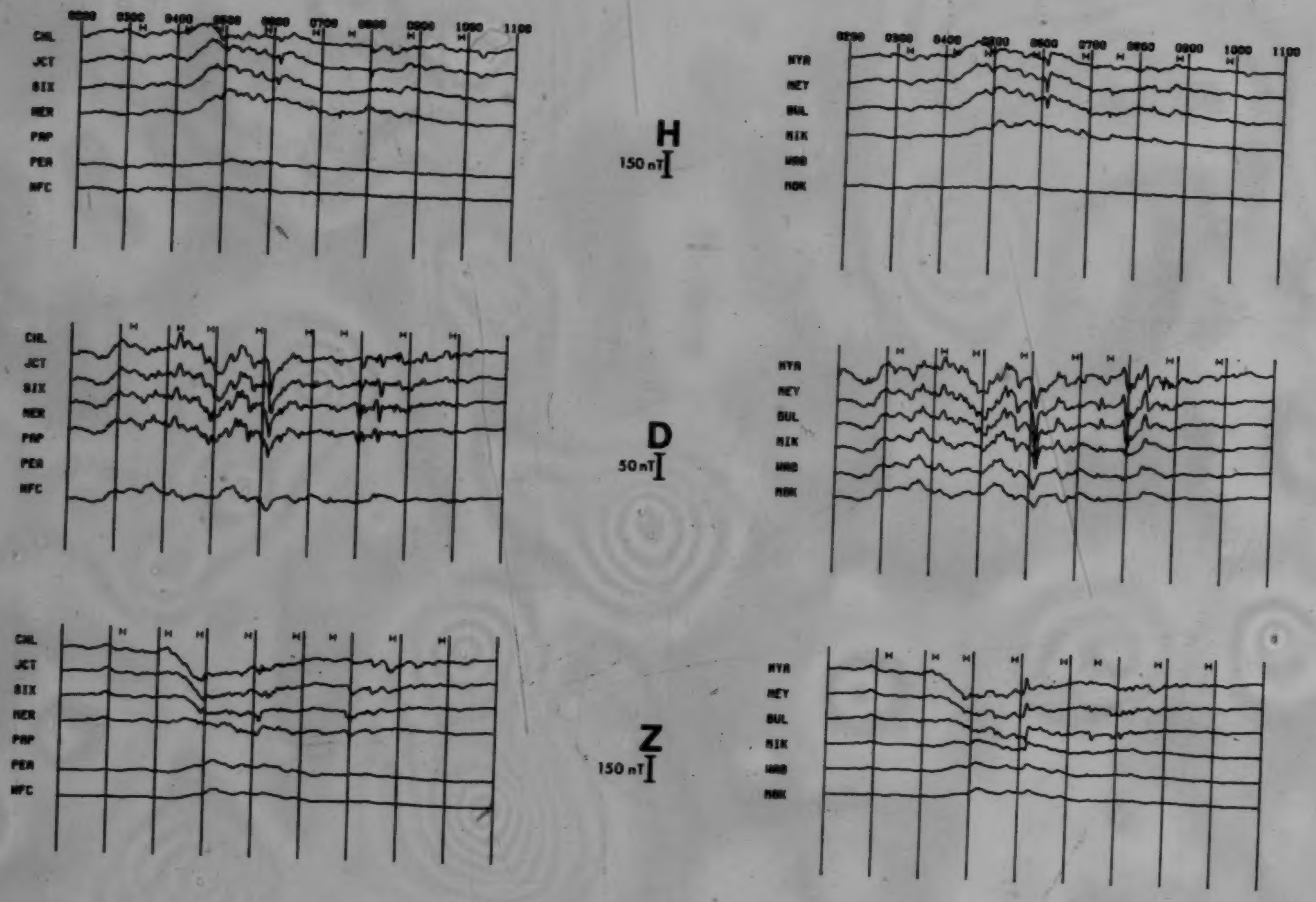

5.3 Perturbation Fields

The entire substorm was plotted as a series of maps of mean values over consecutive five-minute intervals of the three components H, D and Z. From these maps eight "time frames" were chosen as representative of the main epochs of the substorm. These eight time intervals are marked in Fig 5.1 by horizontal bars, and the mean perturbation fields are represented in Figs. 5.2a and 5.2b.

The H, D and Z values were measured from baselines at 23:00 U.T. on 1974 August 13. Although magnetic activity was relatively low at the end of August 13 and on August 14 (the latter selected as one of the five quiet days of the month), selection of the baseline was difficult.

The choice of the baseline at 23.00 U.T. (1974 August 13) appears reasonable when compared to other quiet periods within five days from the event in question, and inspection of AE indices supports this choice. In the first time frame of Fig. 5.2a and in the last of Fig. 5.2b it will be noted that there is a consistent northeast pattern in the horizontal fields with nearly zero vertical fields across the array (except for the northern most station at 03.18 U.T.). Comparing these two time frames with that at 04.13 U.T. (Fig 5.2a) it becomes clear that the current distributions producing the perturbation fields at 03.18, at 04.13 and 10.53 U.T. are similar in character. Growth and decline of the substorm perturbations across the array were

Figure 5.2a Mean perturbation fields over five-minute intervals at four epochs before and during the polar magnetic Substorm 4. For the vertical components, northward arrows represent upward fields. Unit: nanotesla.

PERTURBATION FIELDS
AVERAGED OVER 5 MINUTE INTERVALS

HORIZONTAL FIELDS

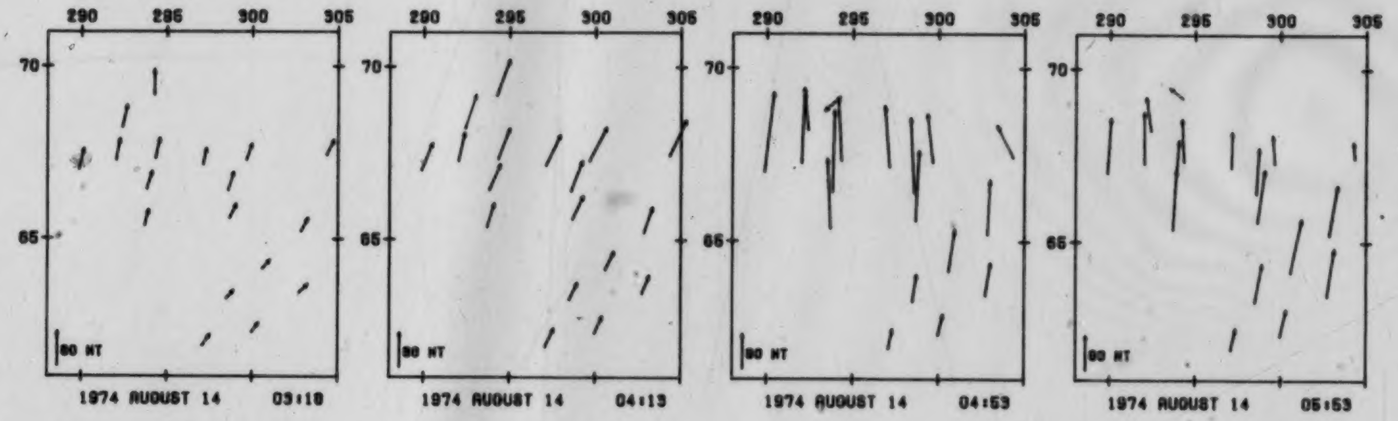

VERTICAL FIELDS

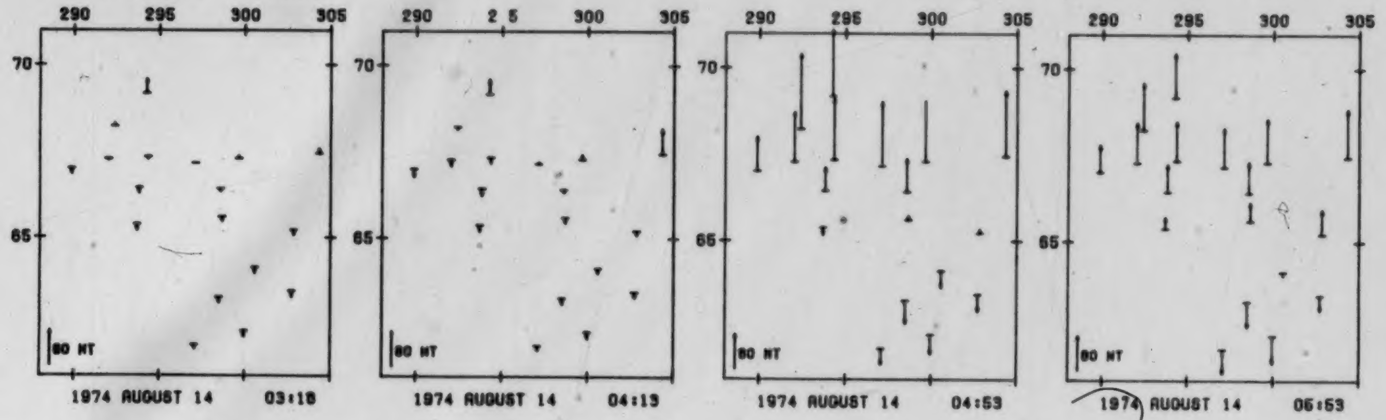

Figure 5.2b Mean perturbation fields over five-minute intervals at four epochs during the polar magnetic Substorm 4. For the vertical components, northward arrows represent upward fields. Unit: nanotesla.

PERTURBATION FIELDS
AVERAGED OVER 5 MINUTE INTERVALS

HORIZONTAL FIELDS

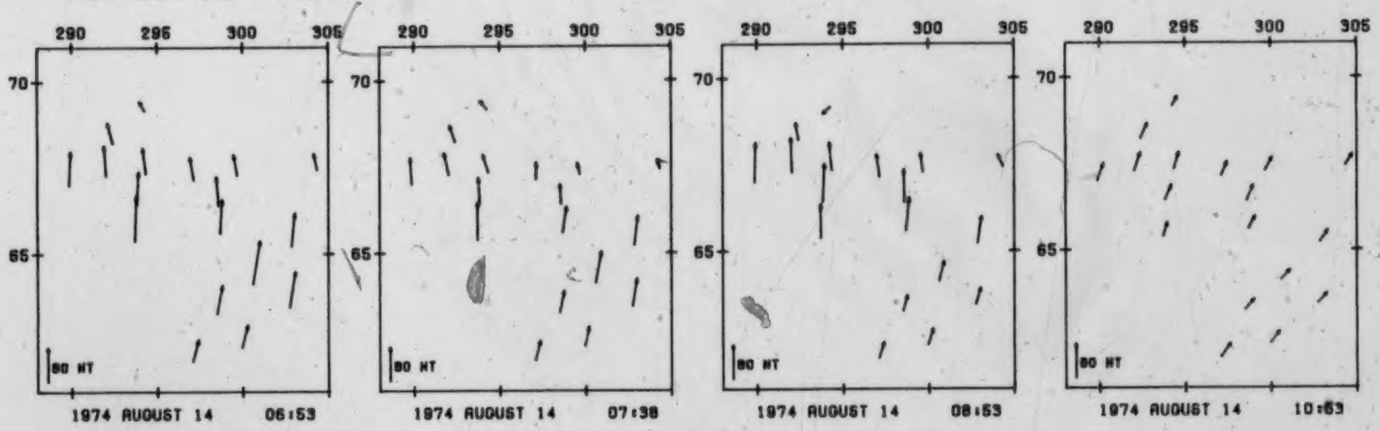

VERTICAL FIELDS

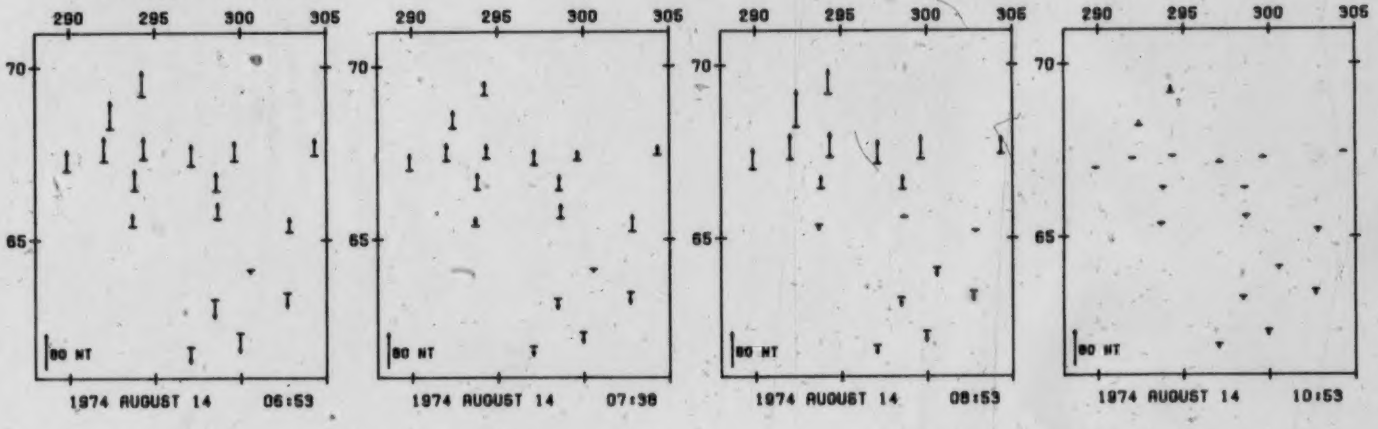

gradual and the small Z components, in the first two epochs and the last, suggest broad sheets of current at those times flowing to the east southeast. The time scale of the substorm can be estimated from Figs. 5.1 and 5.2. These figures depict fields and currents growing over the first hour and declining over the next 5 to 6 hours.

At 04.13 U.T. (Fig 5.2a) the horizontal fields have increased as compared to 03.18 U.T. but the vertical fields do not show any significant change. Quantitative model calculations show that this combination cannot be modelled by an eastward ionospheric current alone, but requires a westward ionospheric current to the north of the main broad eastward current, or some other current system which gives equivalent fields.

In five of the epochs (04.53 U.T., 05.53 U.T., 06.53 U.T., 07.38 U.T. and 08.53 U.T.) (Figs. 5.2a and 5.2b) the prominent counter-clockwise curvature of the horizontal field, convex to the east, is a consequence of the presence near the array of upward field-aligned current at the east end of the eastward ionospheric electrojet. (see also Figs. 5.5 to 5.9)

5.4 Model calculations

The perturbation fields at six epochs of Substorm 4 have been fitted by models of the Boström Type 1 (Boström 1964, Kisabeth 1972, Kisabeth and Rostoker 1977). The general configuration of the current loop is shown in Fig 1.7. This substorm of August 14 could not be modelled by a current of this type with uniform current density across its width. Accordingly a current distribution was estimated by the direct inversion method developed by Oldenburg (1976, 1977) and described in Chapter 4.

The modelling technique used for this substorm allows for independent control of the longitudinal boundaries of both eastward and westward electrojets, and differ in this respect from the modelling technique used for Substorms 2 and 3 (Chapter 4). Following the same procedure as in Chapter 4 the magnetic fields produced at the Earth's surface by the three-dimensional current loop (Fig. 1.7) were calculated from the Biot-Savart law in the manner described by Kisabeth (1972) (Appendix A). Where westward currents appeared, in the ionospheric segments, to the north of the eastward electrojet, two complete loops of current in opposite senses formed the model. Provision was made to introduce a bend in the ionosphere segment to give a change of latitude with a cosine dependence on longitude. By varying certain parameters of the ionospheric current segment, a least-squares fit was obtained between the calculated and observed magnetic perturbation fields. The parameters varied are indicated in Fig. 5.3. The width of the current system was kept constant as obtained with the inversion technique described in Chapter 4, but constant factors (P1, P12; Fig. 5.3) multiplying all current

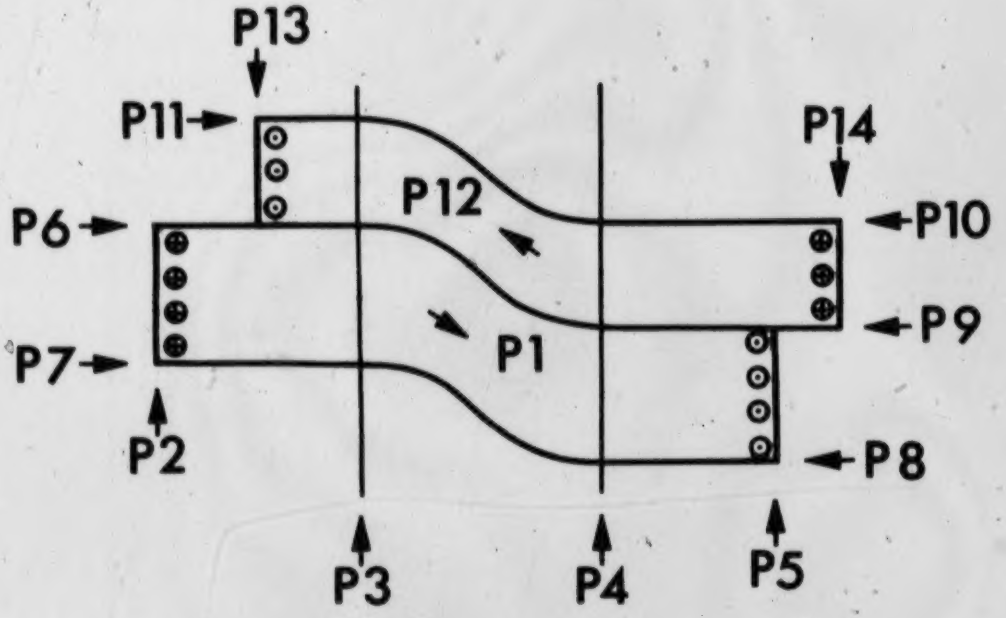
P13
P11
P14
P12
P6
P10
P9
P7
P1
P2
P8
P3
P4
P5

Figure 5.3 Outline of the ionospheric segment of the three-dimensicnal current loop used to model Substorm 4, indicating the different parameters that control the geometry and current. Birkeland field aligned currents are indicated.

densities was allowed to change as a parameter of the least-squares fit. For all cases where a bend was needed, the bounding longitudes (P3 and P4; Fig. 5.3) of the bend where allowed to vary as parameters. The fourth and fifth parameters were the latitudes of the southern edges of the eastern (P8) and western (P7) sections of the current system. For epochs 04.53 U.T. and 05.53 U.T. (See Fig. 5.10) the eastern end of the eastward ionospheric current section (P5) was allowed to move with the eastern limit of the bend (P4). For epoch 04.53 U.T. best fit was obtained when the eastern boundaries of both the eastward and westward electrojet were at the same longitude and so were controlled by the same parameter (P14=P5; Fig. 5.3). For epochs 05.53 U.T., 06.53 U.T., and 08.53 U.T. (see Fig. 5.10) the eastern longitudinal boundary of the westward electrojet (P14, Fig. 5.3) was fixed at 330°E but the boundary of the eastward electrojet (P5, Fig. 5.3) was allowed to change as a parameter. For epoch 07.38 U.T. where the array does not detect a westward electrojet no bend was considered, and only four parameters were allowed to change, namely the total current (P1), the eastern end of the ionospheric current system (P5) and both its northern (P6) and southern (P7) latitudinal limits. Table 5.1 summarizes the parameters that controlled the least square fit for each epoch of Substorm 4; parameters are indicated in Fig. 5.3.

TABLE 5.1

PARAMETERS OF THE IONOSPHERIC SEGMENT VARIED FOR SUBSTORM 4 (referred to Fig. 5.3)

Epoch U.T.	Independent Parameters	Dependent Parameters
04.13	P1,P3,P4,P7,P8	P12=P1,P6,P9,P10,P11
04.53	P1,P3,P4,P7,P8	P12=P1,P5=P4=P14,P6,P9, P10,P11
05.53	P1,P3,P4,P7,P8	P12=P1,P5=P4,P6,P9,P10,P11
06.53	P1,P5	P12=P1
07.38	P1,P5,P6,P7	
08.53	P1,P5	P12=P1

Remote field-aligned currents with very small effects on the observed fields were fixed because there was no point in varying their longitudes. Thus in all cases the western ends of both the eastward and westward electrojets were placed arbitrarily at 255° geomagnetic longitude, and the eastern ends of the westward electrojets at epochs 04.13 U.T., 05.53 U.T., 06.53 U.T. and 08.53 U.T. were arbitrarily placed at geomagnetic longitude 330°.

While the field-aligned currents have been modelled as sheets of negligible thickness, the data could equally well be satisfied by field-aligned currents distributed through several degrees of longitude, as indicated in Chapter 3. In reality the field-aligned currents seem likely to be distributed in longitude.

In all calculations the ionospheric currents were kept at altitude 115 km. Induction in the Earth has been approximated by that in a superconducting sphere at depths chosen empirically to optimize the fits of calculated horizontal and vertical components to those observed. A depth of 250 km was chosen for the superconductor.

As in the previous chapters the least-squares fit was obtained by applying to observed and calculated values, of three magnetic components with equal weights, the iterative subroutine ZXSSQ of the IMSL library.

The models of Substorm 4 approximate observed perturbation fields from the 23.00 U.T. 1974 August 13 baseline. These may be superimposed on some steady-state field corresponding to preexisting currents in the magnetosphere and ionosphere.

5.5 Model currents for six epochs of Substorm 4

Figures 5.4 to 5.9 show observed and calculated fields and residuals (observed-calculated), at six representative epochs of Substorm 4. The northern and southern limits of the ionospheric currents, and the boundary between westward and eastward currents, are indicated. Fig 5.10 shows the complete ionospheric segments of the model currents at six epochs, in Mercator projection of centred dipole geomagnetic coordinates, together with the current density distribution at each epoch found from the Oldenburg inversion. As numerical measures of goodness of fit the following parameters are used:

Figure 5.4 Observed perturbation fields, calculated fields for model currents of best fit, and residuals in the five-minute interval 04.11-04.15 U.T. during Substorm 4. For Z, northward arrows represent upward Z. The full length of the ionospheric segment, and the distribution of current density across the width of the current, are shown in Fig. 5.10.

IONOSPHERIC CURRENT MODEL EASTWARD CURRENT 0.15 MA

WESTWARD CURRENT 0.33 MA

HORIZONTAL PERTURBATION FIELDS

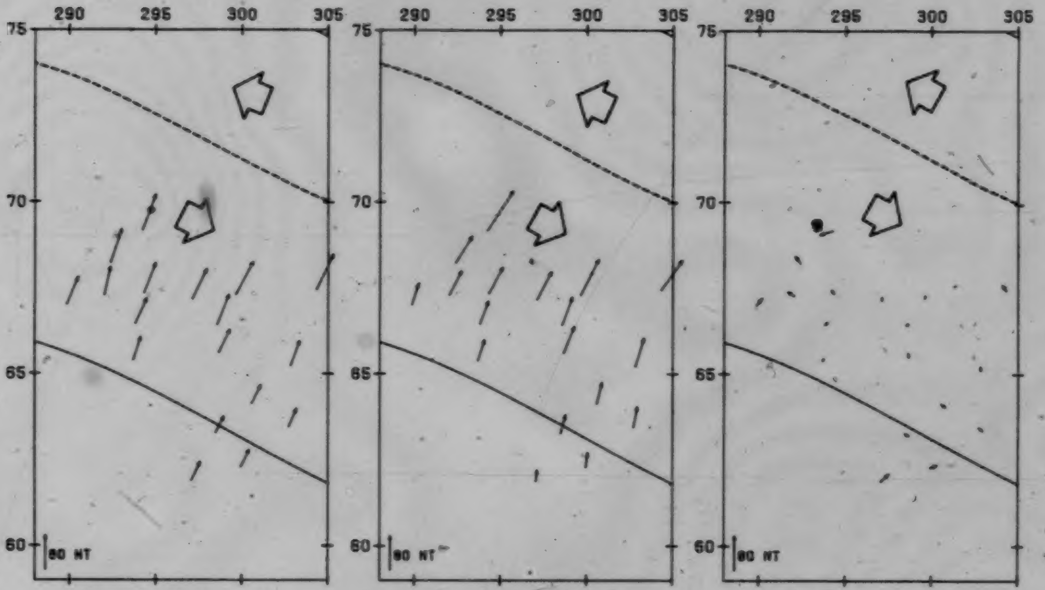

1974 AUGUST 14 04:13
OBSERVED VALUES

1974 AUGUST 14 04:13
CALCULATED VALUES

1974 AUGUST 14 04:13
RESIDUALS

VERTICAL PERTURBATION FIELDS

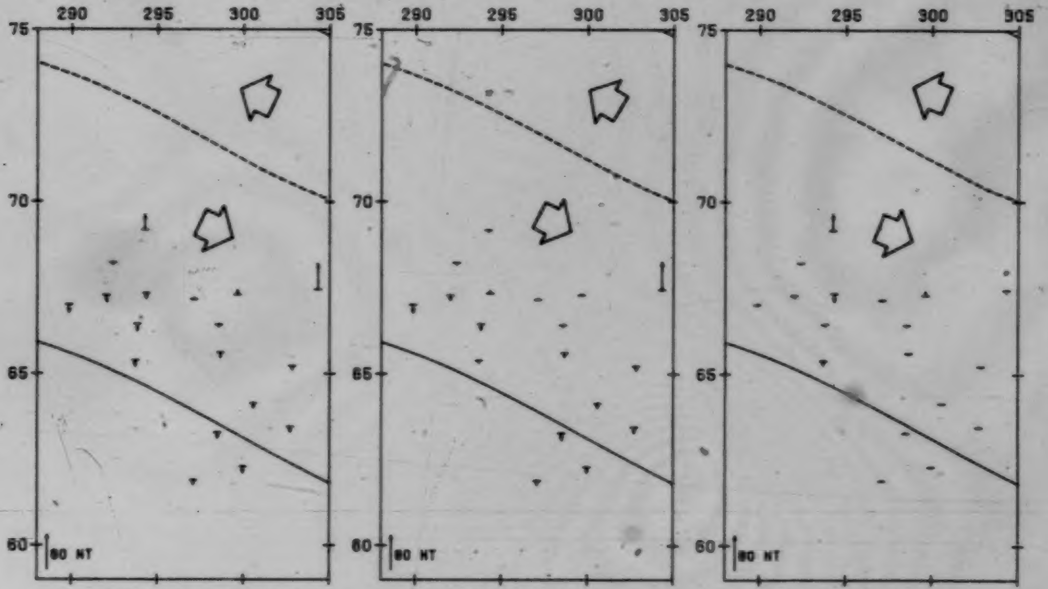

1974 AUGUST 14 04:13
OBSERVED VALUES

1974 AUGUST 14 04:13
CALCULATED VALUES

1974 AUGUST 14 04:13
RESIDUALS

Figure 5.5 Observed perturbation fields, calculated fields for model currents of best fit, and residuals in the five-minute interval 04.51-04.55 U.T. during Substorm 4. For Z, northward arrows represent upward Z. The full length of the ionospheric segment, and the distribution of current density across the width of the current, are shown in Fig. 5.10.

IONOSPHERIC CURRENT MODEL   EASTWARD CURRENT 0.18 MA

WESTWARD CURRENT 0.15 MA

HORIZONTAL PERTURBATION FIELDS

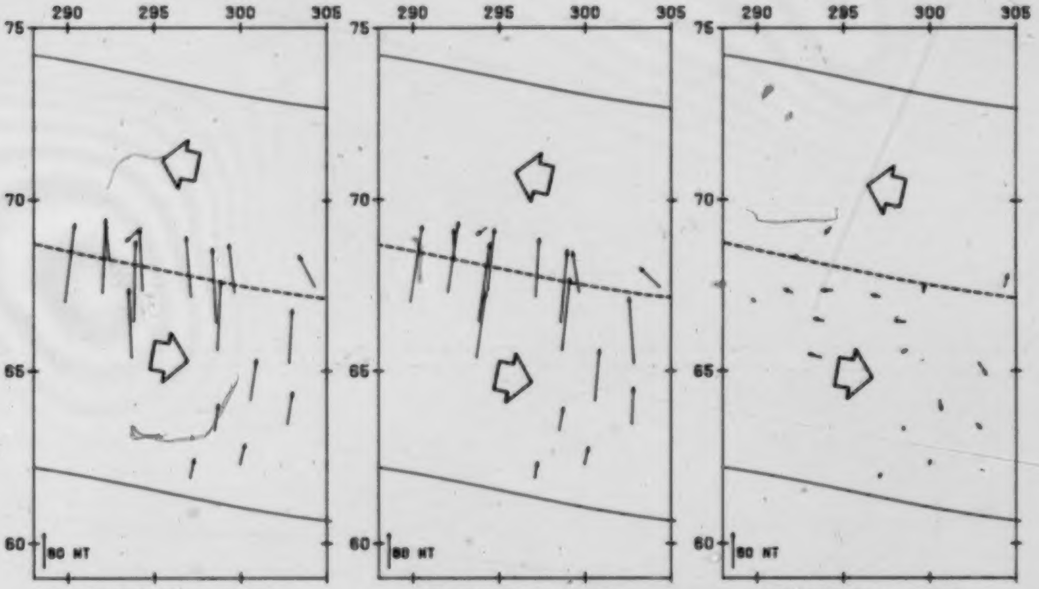

1974 AUGUST 14 04:53 OBSERVED VALUES

1974 AUGUST 14 04:53 CALCULATED VALUES

1974 AUGUST 14 04:53 RESIDUALS

VERTICAL PERTURBATION FIELDS

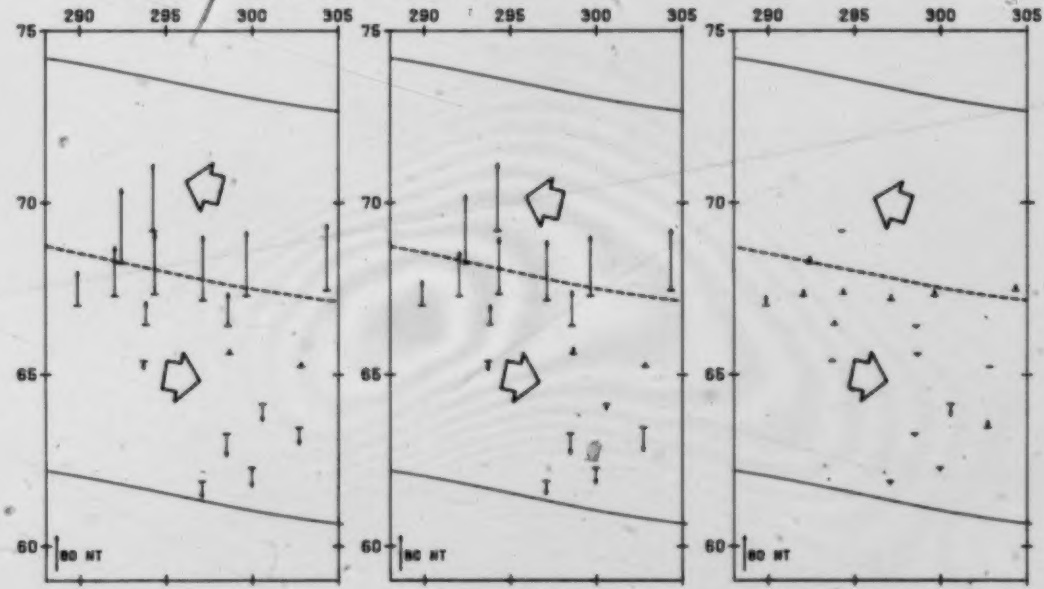

1974 AUGUST 14 04:53 OBSERVED VALUES

1974 AUGUST 14 04:53 CALCULATED VALUES

1974 AUGUST 14 04:53 RESIDUALS

Figure 5.6 Observed perturbation fields, calculated fields for model currents of best fit, and residuals in the five-minute interval 05.51-05.55 U.T. during Substorm 4. For Z, northward arrows represent upward Z. The full length of the ionospheric segment, and the distribution of current density across the width of the current, are shown in Fig. 5.10.

IONOSPHERIC CURRENT MODEL EASTWARD CURRENT 0.19 MA

WESTWARD CURRENT 0.10 MA

HORIZONTAL PERTURBATION FIELDS

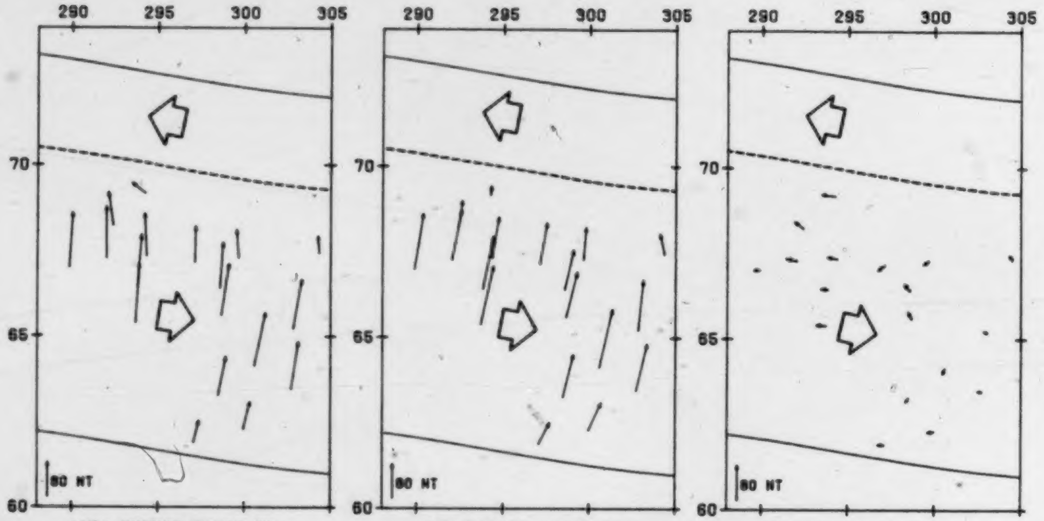

1974 AUGUST 14 05:53 OBSERVED VALUES

1974 AUGUST 14 05:53 CALCULATED VALUES

1974 AUGUST 14 05:53 RESIDUALS

VERTICAL PERTURBATION FIELDS

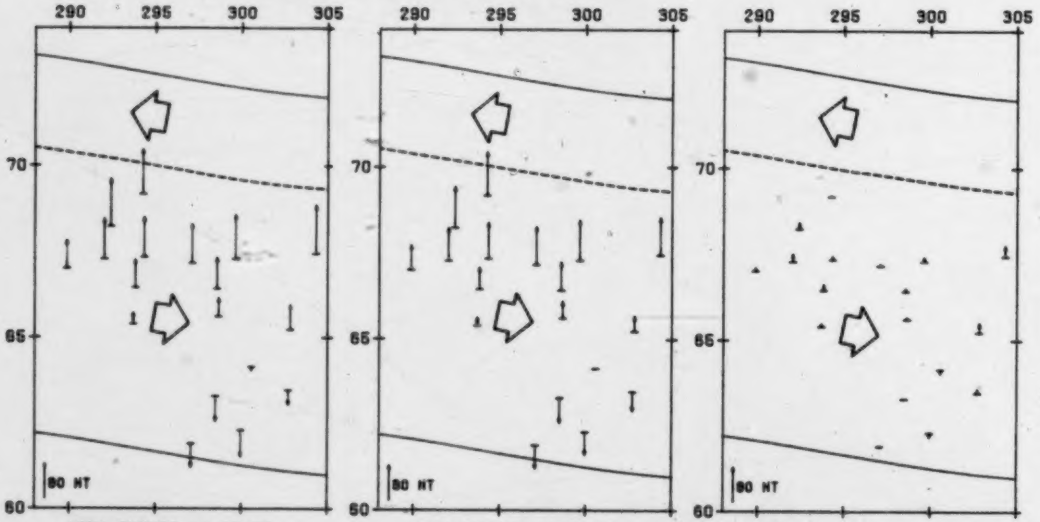

1974 AUGUST 14 05:53 OBSERVED VALUES

1974 AUGUST 14 05:53 CALCULATED VALUES

1974 AUGUST 14 05:53 RESIDUALS

Figure 5.7 Observed perturbation fields, calculated fields for model currents of best fit, and residuals in the five-minute interval 06.51-06.55 U.T. during Substorm 4. For Z, northward arrows represent upward Z. The full length of the ionospheric segment, and the distribution of current density across the width of the current, are shown in Fig. 5.10.

IONOSPHERIC CURRENT MODEL

EASTWARD CURRENT 0.14 MA
WESTWARD CURRENT 0.03 MA

HORIZONTAL PERTURBATION FIELDS

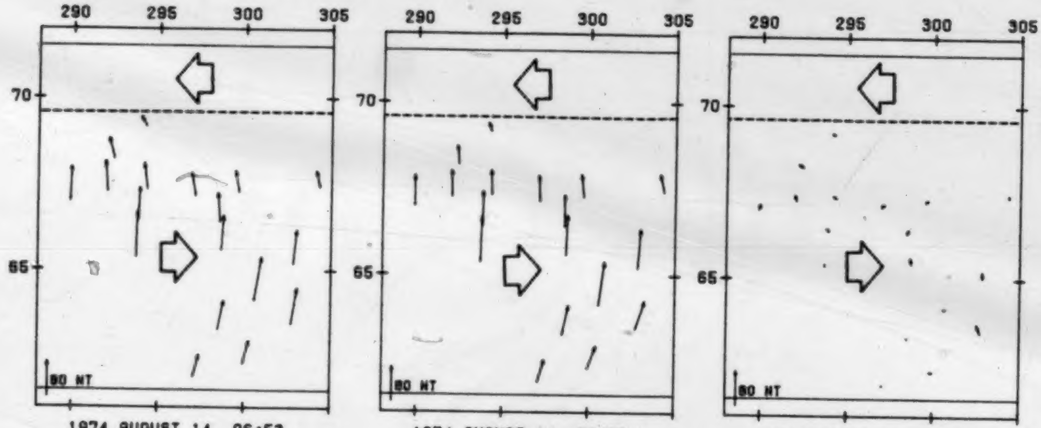

1974 AUGUST 14 06:53
OBSERVED VALUES

1974 AUGUST 14 06:53
CALCULATED VALUES

1974 AUGUST 14 06:53
RESIDUALS

VERTICAL PERTURBATION FIELDS

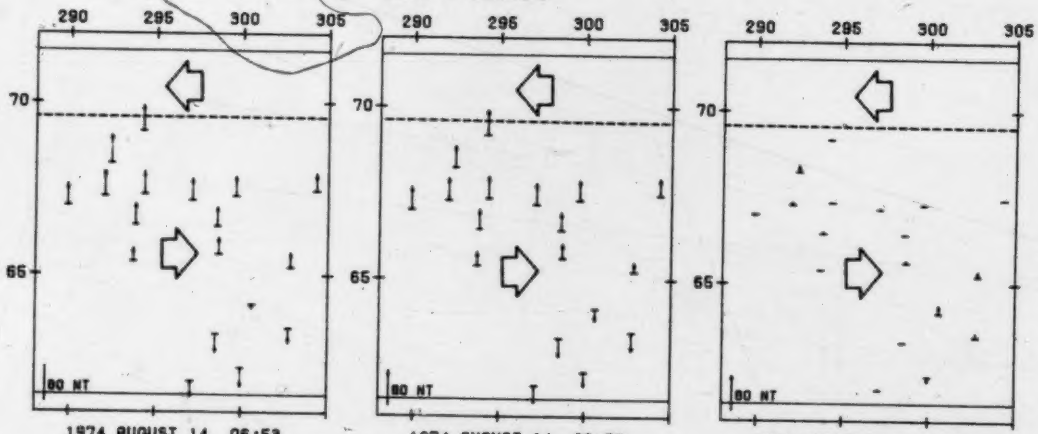

1974 AUGUST 14 06:53
OBSERVED VALUES

1974 AUGUST 14 06:53
CALCULATED VALUES

1974 AUGUST 14 06:53
RESIDUALS

Figure 5.8 Observed perturbation fields, calculated fields for model currents of best fit, and residuals in the five-minute interval 07.36-07.40 U.T. during Substorm 4. For Z, northward arrows represent upward Z. The full length of the ionospheric segment, and the distribution of current density across the width of the current, are shown in Fig. 5.10.

IONOSPHERIC CURRENT MODEL EASTWARD CURRENT 0.12 MA

HORIZONTAL PERTURBATION FIELDS

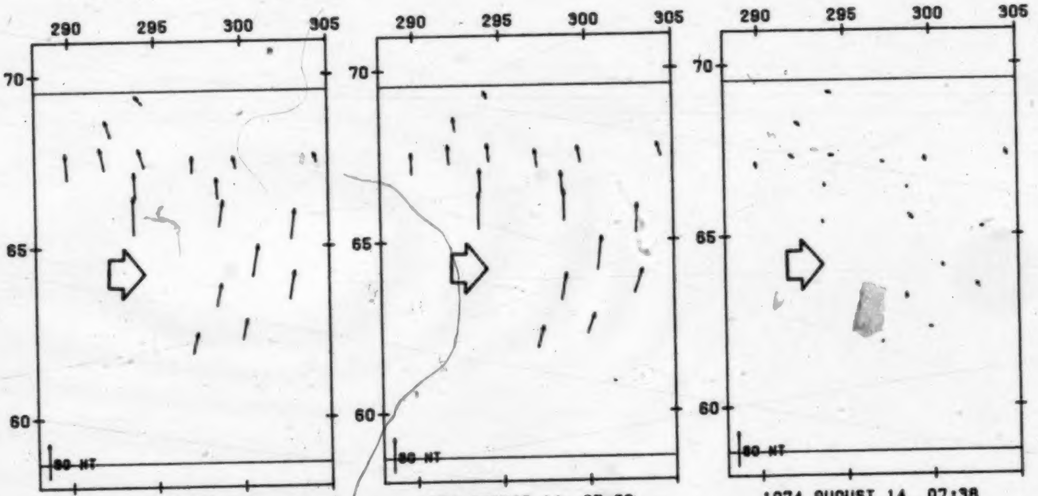

1974 AUGUST 14 07:38
OBSERVED VALUES

1974 AUGUST 14 07:38
CALCULATED VALUES

1974 AUGUST 14 07:38
RESIDUALS

VERTICAL PERTURBATION FIELDS

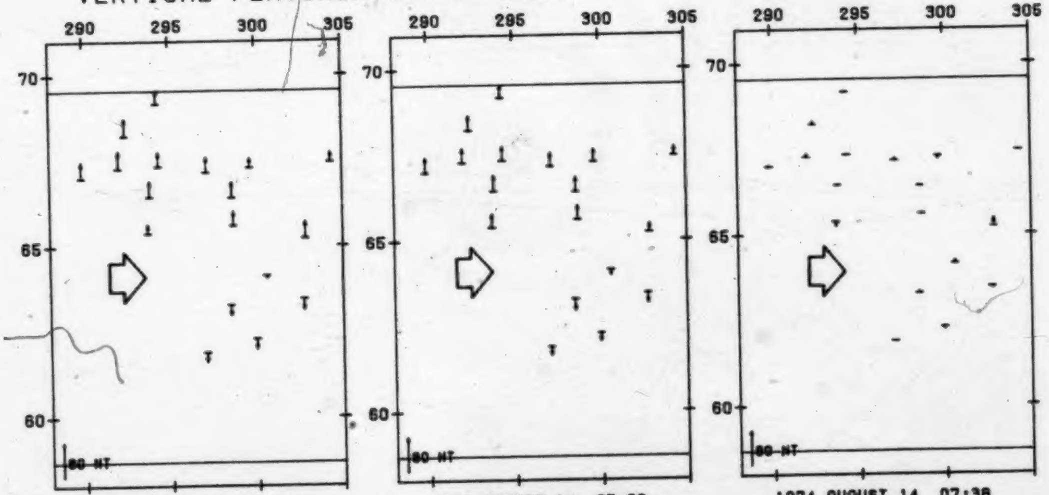

1974 AUGUST 14 07:38
OBSERVED VALUES

1974 AUGUST 14 07:38
CALCULATED VALUES

1974 AUGUST 14 07:38
RESIDUALS

Figure 5.9 Observed perturbation fields, calculated fields for model currents of best fit, and residuals in the five-minute interval 08.51-08.55 U.T. during Substorm 4. For Z, northward arrows represent upward Z. The full length of the ionospheric segment, and the distribution of current density across the width of the current, are shown in Fig. 5.10.

IONOSPHERIC CURRENT MODEL

EASTWARD CURRENT 0.11 MA
WESTWARD CURRENT 0.04 MA

HORIZONTAL PERTURBATION FIELDS

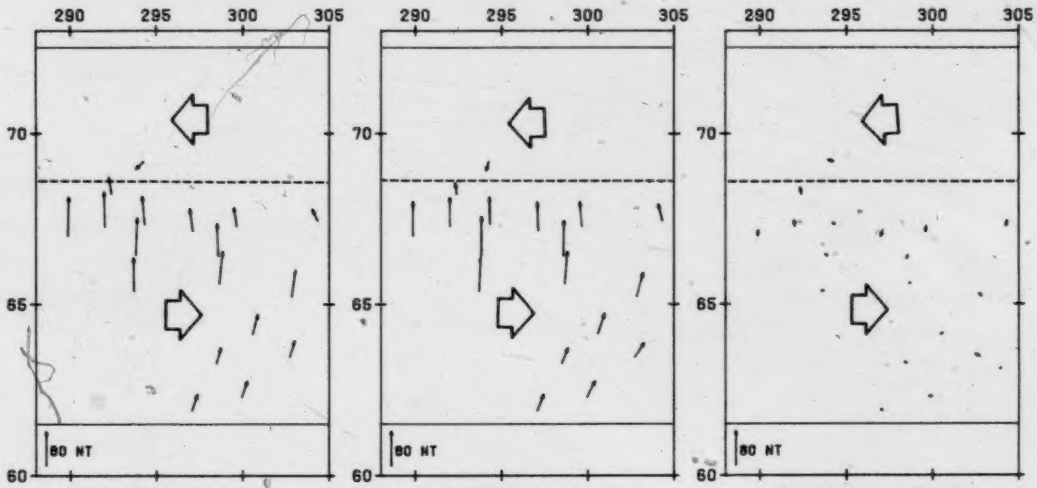

1974 AUGUST 14 08:53
OBSERVED VALUES

1974 AUGUST 14 08:53
CALCULATED VALUES

1974 AUGUST 14 08:53
RESIDUALS

VERTICAL PERTURBATION FIELDS

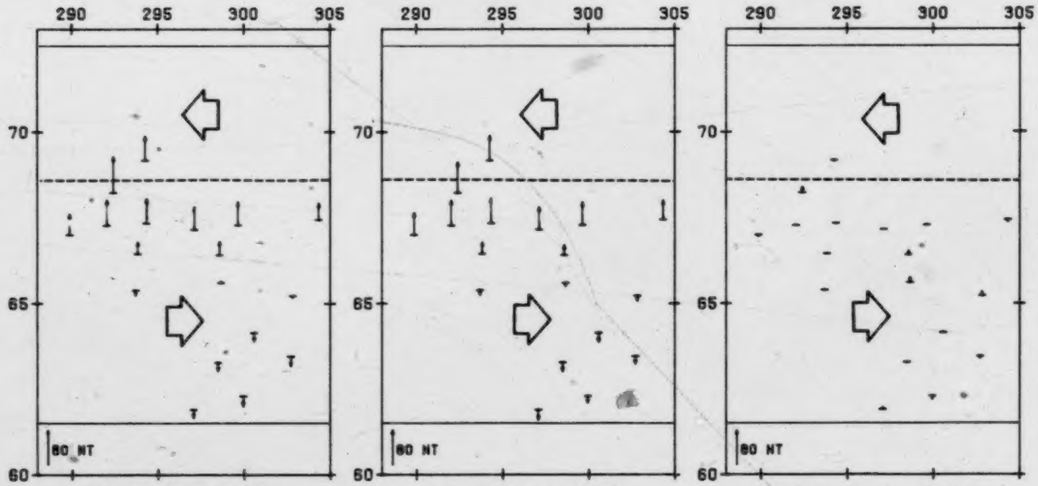

1974 AUGUST 14 08:53
OBSERVED VALUES

1974 AUGUST 14 08:53
CALCULATED VALUES

1974 AUGUST 14 08:53
RESIDUALS

$$\varepsilon = \frac{\Sigma(\text{residual})^2}{\Sigma(\text{observed total field})^2}$$

and

$$\xi = \frac{\Sigma(\text{residual})^2}{\Sigma(\text{observed total field at 03.18 U.T.})^2}$$

and these parameters are listed for the six epochs in Table 5.2.

TABLE 5.2

STATISTICAL PARAMETERS FOR SUBSTORM 4
1974 AUGUST 75

TIME U.T.	SSQ OBSERVED	SSQ RESIDUAL	ε	ξ
03.18	31570	--	--	--
04.13	87677	4701	0.0536	0.149
04.53	467971	9923	0.0212	0.314
05.53	277529	8115	0.0292	0.257
06.53	119852	2445	0.0204	0.077
07.38	67085	2146	0.0320	0.068
08.53	93512	2201	0.0235	0.070
10.53	23857	--	--	--

Note: SSQ denotes sum of squares

This long-lived substorm is characterized by a gradual reduction of the westward current to the north of the array between epochs 04.13 U.T. and 07.38 U.T., (Fig. 5.10) with a small recovery of this westward current in the last epoch (08.53 U.T.). In five of the six epochs presented in Fig. 5.10 the eastern end of the eastward electrojet was placed by the least-squares fit near the eastern stations of the array where in a time space of 4 hours it slowly moved from 309° longitude at 04.53 U.T. to 305° longitude at 08.53 U.T. The main current system and eastward electrojet thus essentially rotate with the Earth over the four-hour decline of the substorm.

At epoch 04.53 U.T. (Figs. 5.5 and 5.10) the current density distribution is calculated with the inversion technique of Oldenburg. This program makes no provision to separate field-aligned currents belonging to the westward and eastward electrojets. The current density distribution was therefore found for field-aligned currents in common longitudes, as shown in Fig. 5.10. If the field-aligned currents are separated in longitude for the least-squares fit, as shown schematically in Fig 5.3, a slightly better fit results at epoch 04.53 U.T.. Extension of the east end of the westward electrojet to 330° longitude causes a slight deterioration of the fit, to $\varepsilon = 0.031$ from $\varepsilon = 0.021$ for the model in Fig. 5.10. This deterioration may reflect only the fact that the Oldenburg inversion was done for the model of Fig. 5.10.

It is worthy of note that at epoch 04.53 U.T. the latitudinal boundary between the eastward and westward

Figure 5.10 Ionospheric segments of current loops, in relation to the magnetometer array, at four epochs, in a Mercator projection of centred-dipole geomagnetic coordinates. GM represents magnetic midnight. The distribution of current density across the width of the current are shown.

IONOSPHERIC CURRENT MODEL

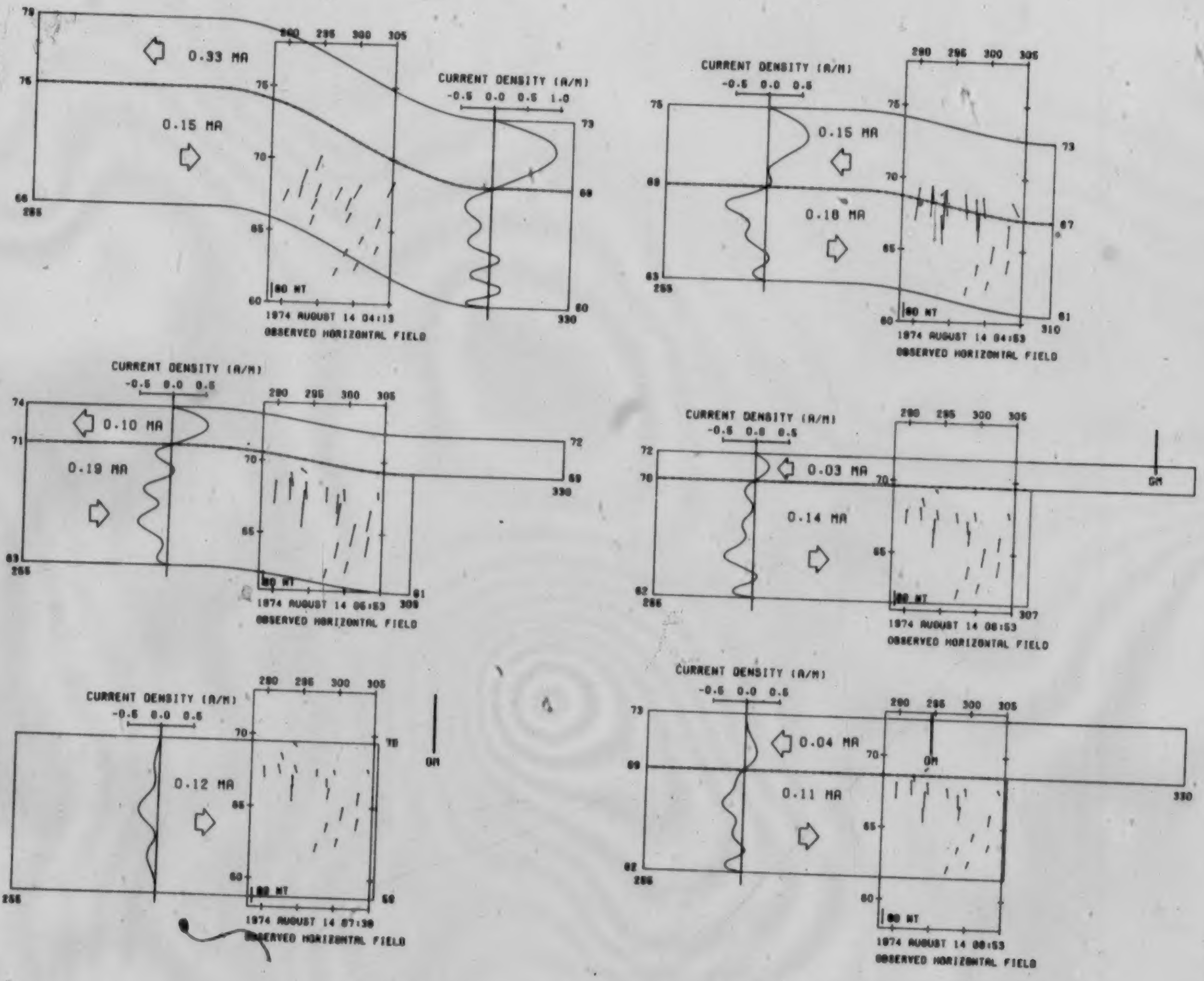

electrojets falls within the array (broken line Figs. 5.5 and 5.10). This indicates that the westward electrojet is somewhat better resolved near its southern limit than the cases discussed in the inversion tests reported in Chapter 4. Perturbation fields calculated from the current models obtained for this substorm (1974, August 14) when compared to the observations (Figs. 5.4 to 5.9) give very small and satisfactory residuals. The largest residuals are at epoch 04.13 U.T. (Table 5.2, Fig. 5.4) where a more sophisticated model appears to be required to produce the uniform horizontal fields and the reduced vertical components observed (Fig. 5.4). Even here the fit is reasonably good considering the simplified model used in the calculations and the rather small fields observed at 04.13 U.T. The prominent counter-clockwise curvature of the horizontal field, convex to the east, observed between 04.53 U.T. and 08.53 U.T. has been well fitted by the current model as can be observed in Figs 5.5 to 5.9.

5.6 Discussion

The ionospheric segments of the three-dimensional current systems (of the type illustrated in Fig. 1.7) are mapped in Fig. 5.11 in azimuthal equidistant projection, centred on the geomagnetic dipole, at the six epochs studied for Substorm 4 (1974 August 14).

The current systems extend to the goemagnetic

Figure 5.11 Ionospheric segments of current loops at six epochs of Substorm 4, 1974 August 14, in azimuthal equidistant projection of centred-dipole geomagnetic coordinates, superimposed on a map of the North American mainland. GM represents geomagnetic midnight.

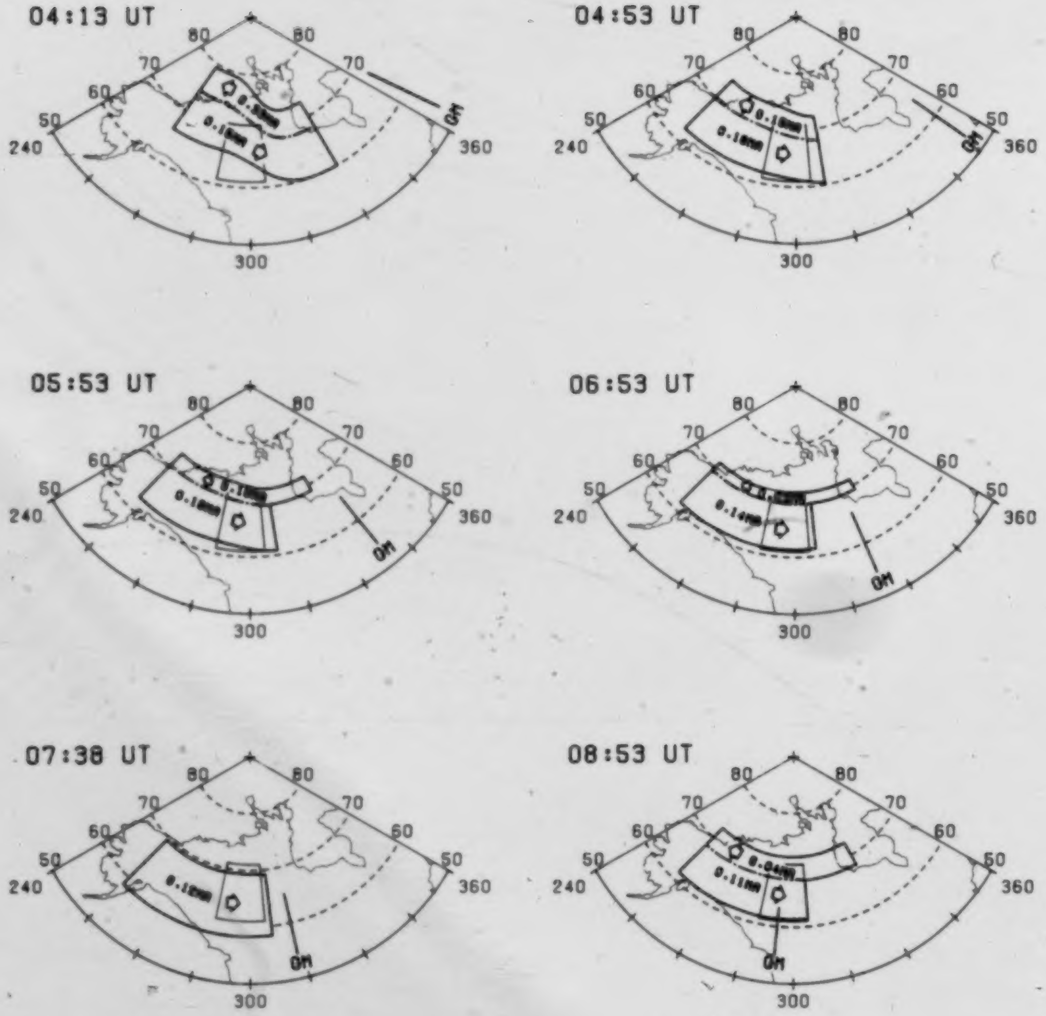
04:13 UT
80
80
70
70
60
50
240
360
300
OM
04:53 UT
80
80
70
70
60
60
50
50
240
360
300
OM
05:53 UT
80
80
70
70
60
60
50
50
240
360
300
OM
06:53 UT
80
80
70
70
60
60
50
50
240
360
300
OM
07:38 UT
80
80
70
70
60
60
50
50
240
360
300
OM
08:53 UT
80
80
70
70
60
60
50
50
240
360
300
OM

longitudes of Canadian and American permanent geomagnetic observatories, and flow above Churchill and Baker Lake at one epoch and above College, Alaska at five epochs. The records of observatories near the current systems have been scaled, with careful attention to baselines, and the perturbation fields at these observatories have been mapped. Perturbation fields at two epochs are shown in Fig. 5.12 and 5.13. In general the perturbation fields at the observatories are consistent with the model currents. The large positive H recorded by BARR at 04.53 U.T. (Fig. 5.12) suggests that the west end of the eastward ionospheric electrojet may have extended to at least 240° longitude. It is possible that the westward electrojet extended as far north as BAKE with the eastern end extending into the morning sector east of WHAL.

Fig. 5.13 depicts the perturbation fields observed by the observatories outside the array at 07.38 U.T. For this epoch the observed fields are consistent with those predicted by the model. The westward electrojet no longer exists near the array. This is indicated by the reduction in the magnitude of the H component at BAKE, CHUR, and WHAL, and the changes observed at MOUL and RSLT as compared to 04.53 U.T. (Fig. 5.12) when this westward electrojet was present. The possibility of a weak westward ionospheric current near BAKE, not detected by the array, must not be discarded.

Figure 5.12 Horizontal perturbation fields recorded by Canadian and U.S. observatories at epoch 04.53 U.T. for Substorm 4 in a azimuthal equidistant projection of centred dipole geomagnetic coordinates. Location of stations is given in table 2.2. GM represents geomagnetic midnight.

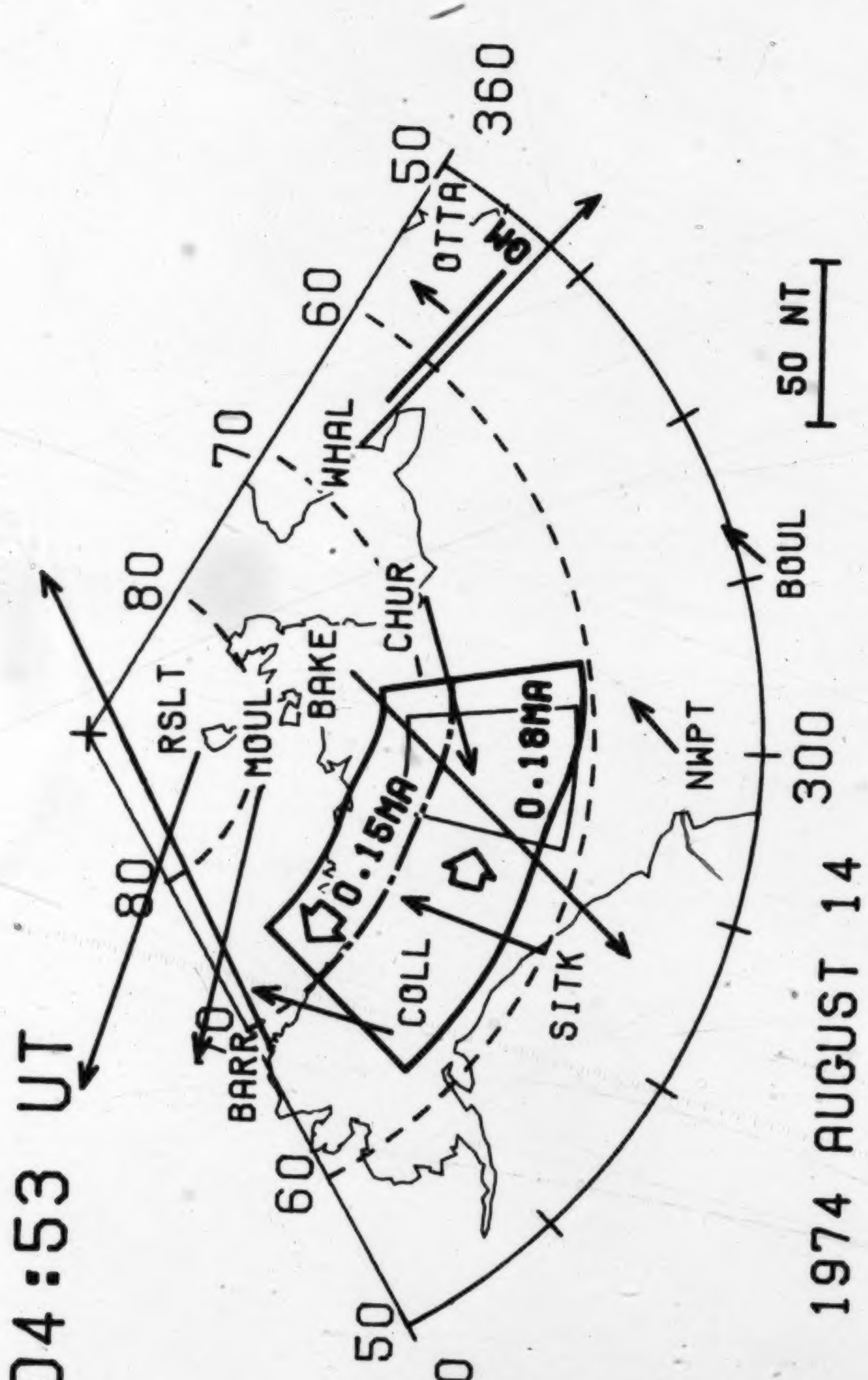
04:53 UT
1974 AUGUST 14
240
300
360
50
60
70
80
80
70
60
50
RSLT
MOUL
BAKE
CHUR
WHAL
OTTA
BARR
COLL
SITK
NWPT
BOUL
0.15MA
0.18MA
5
50 NT

Figure 5.13 Horizontal perturbation fields recorded by Canadian and U.S. observatories at epoch 07.38 U.T. for Substorm 4 in a azimuthal equidistant projection of centred dipole geomagnetic coordinates. Location of stations is given in table 2.2. GM represents geomagnetic midnight.

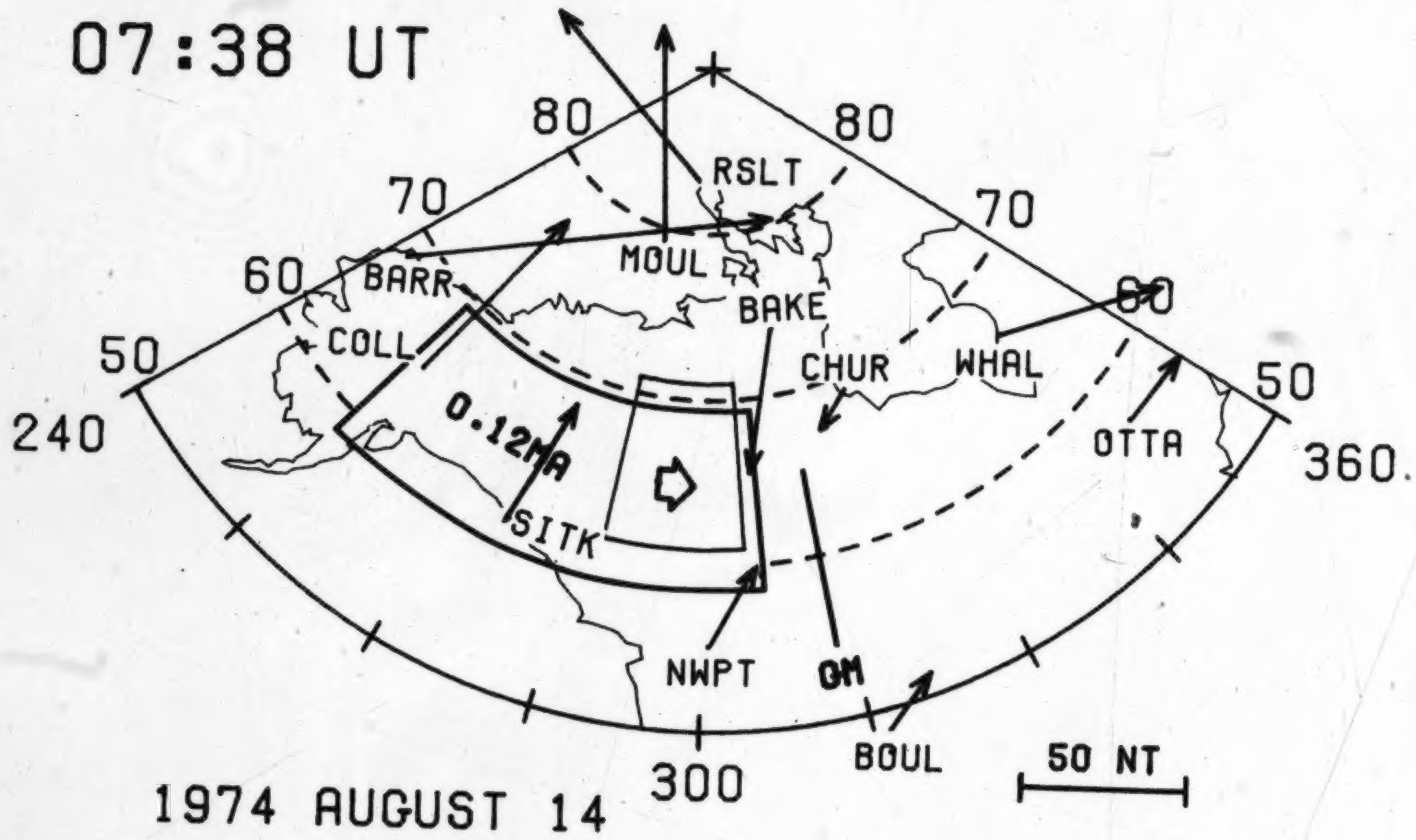
07:38 UT
80
80
70
70
60
60
50
50
240
360.
300
RSLT
MOUL
BARR
COLL
BAKE
CHUR
WHAL
OTTA
0.12MA
SITK
NWPT
OM
BOUL
50 NT
1974 AUGUST 14

At both epochs, 04.53 U.T. and 07.38 U.T. (Figs. 5.12 and 5.13) better agreement with the observatory data could be obtained if the western end of the current system were somewhat north of the position shown. The array does not accurately resolve the latitude and longitude of the far ends of the current systems.

For epoch 04.13 U.T. observatory data (not shown) from stations outside the array indicate that the east end of the eastward electrojet (Fig. 5.10) which was arbitrarily placed at 330° E longitude, would be more realistic if placed about 315°E longitude. The east end of the eastward ionospheric electrojet obtained from the modelling appears to be stationary to the east of the array (within 5° longitude) (Fig. 5.10) in the time period from 04.53 U.T. to 08.53 U.T. In these four hours the array has moved through 60° of longitude with respect to geomagnetic midnight (Montbriand 1967) (Figs. 5.10 and 5.11). Therefore the east end of the eastward electrojet moved about 55° to the east with respect to midnight in this same time interval. In this same period Barrow (BARR) was the observatory that contributed to the AU index (see Appendix B) placing the west end of the eastward electrojet to the west of Barrow. On the other hand, Narssarssuaq (Greenland) contributed to the AL index from 04.00 U.T. to 07.00 U.T. and Great Whale River (WHAL) from 07.00 U.T. to 09.00 U.T. placing the east end of the eastward electrojet to the west of WHAL. This would confirm the results obtained from the modelling where an eastward drift of the eastward ionospheric electrojet has been detected. It is interesting to note, in Fig. 5.10, that the westward electrojet current, between epochs 04.13 U.T. and 07.38 U.T., decreases monotonically while the eastward electrojet becomes more intense reaching a maximum of 190,000 amperes at epoch 05.53 U.T. and then drop to 110,000 amperes at the last epoch (08.53 U.T.).

CHAPTER 6

CONCLUDING REMARKS

Three of the four substorms modelled in this thesis (Substorms 1, 2 and 3) were associated with a main westward ionospheric current flowing in the auroral oval region over the array. The fourth one (Substorm 4) had a main eastward ionospheric current flowing over the array.

Magnetic perturbations associated with these substorms, as observed by the magnetometer array, were successfully fitted to fields produced by a simple three-dimensional model current loop (Boström Type 1) where induction in a superconducting sphere was included. Good control of the parameters that define the boundaries and the path of the ionospheric segment of the current loop was achieved by the use of the two-dimensional magnetometer array. Important contributions related to the development and morphology of substorms have been obtained from a single north-south line of magnetometers (Kisabeth, 1972; Kisabeth and Rostoker, 1971) and in this research I have had the great advantage of the guidance of these and other papers by Rostoker, Kisabeth and others. Nevertheless, the added longitudinal dimension of the 1974 magnetometer array gives the resolving power necessary for accurate location of the nearer longitudinal end of the ionospheric segment of each current loop. The convincing fits obtained when field aligned currents of the model are placed above the array leave little doubt of the reality of these currents.

With data from the two dimensional array it has been possible to observe the longitudinal displacements of the ionospheric segments of the current loop. Substorm 1, a brief event, moved steadily eastward, at least 20° relative to the surface of the Earth and at least 38° relative to geomagnetic midnight (Fig. 3.12). For Substorm 2 (Fig. 4.22), a prolonged event, the ionospheric current system moved slowly westward over the array, and eastward about 18° relative to geomagnetic midnight, between 08.28 and 10.13 U.T. In the next 35 minutes the current system moved about 10° eastward relative to the ground and about 18° eastward relative to geomagnetic midnight, then in its coda moved rapidly westward relative to both. The relatively brief Substorm 3 (Fig. 4.23) has been modelled with ionospheric current segments having the east end always at constant longitude and rapid variations in the longitude of the west end. (The east end was too far from the array to be well fixed for this event, and some variation of its longitude may actually have occurred). At some epochs the current system stretched westward to about 265-270°, simultaneously developing a northwestward bend (see also Fig. 4.21). At other epochs the current system shortened, with its upward field-aligned currents above the array, and simultaneously became 'straight' (i.e. in constant latitude range).

Substorm 4, resulting from a main eastward ionospheric electrojet, maintained a very stable position of the east end with respect to the array. During the four last hours that this substorm was modelled, the current system rotated with the earth, drifting 60° to the east with respect to geomagnetic midnight (Figs. 5.10 and 5.11).

Northwestward bends in the ionospheric currents, taking the western end to higher geomagnetic latitudes, are seen in all four substorms. In Substorms 2 (Fig. 4.13) and 1 (Fig. 3.11) this bend is always within 30° of longitude to the west of geomagnetic midnight. In Substorm 2 the bend occurs both east and west of geomagnetic midnight at different epochs. In all three substorms (1, 2 and 3) the bend disappears once the west end of the ionospheric current lies east of geomagnetic midnight, i.e. in the morning sector. An association between the bend and the Harang discontinuity seems possible (Harang, 1946; Heppner, 1972).

The northwest bend seen in Substorm 4 (Fig. 5.10 and 5.11) was most likely related to the shape of the auroral oval in the evening sector, except at epoch 04.13 (Fig. 5.11) when the bend was more pronounced than required for the oval.

The use of uniform current density distribution in the modelling was only suitable for Substorm 1. All others required a non-uniform current density distribution. Application of the Oldenburg inversion technique to obtain the current density distributions at different epochs in the development of a substorm, has made it possible, by using the three-dimensional current loop model, to observe significant equivalent eastward current to the north of the main westward electrojet. For the three substorms where this technique was used (Substorms 2, 3 and 4, Figs. 4.13, 4.21 and 5.10) it appears that the reverse current north of the main current tends to be large early in the substorm and decays faster than the main electrojet current. In particular, in Substorms 3 and 4 (Figs. 4.21 and 5.10) the reverse current flowing north of the array decays while the main electrojet first grows and later falls in the coda of the event. These two substorms are vastly different; Substorm 3 is a short lived event with a westward main ionospheric current over the array while Substorm 4 is a long lived event with eastward main ionospheric current over the array. Different mechanisms may drive those eastward and westward currents, as the ratio of their magnitudes varies through each event.

An interesting point is made by Figs. 3.12, 4.22 and 4.23 concerning Substorms 1, 2 and 3 respectively. The boundary between westward and eastward ionospheric currents lies close to 70° geomagnetic latitude, especially east of the bend (where there is one), at all epochs of Substorms 2 and 3. The current system of Substorm 1 (Fig. 3.12) lies at latitudes south of 70° geomagnetic (except west of the bend) and no eastward current is required to model the fields. The

70° geomagnetic latitude may have some relation to the existence of eastward current during substorms in which the principal ionospheric current is westward. However, the Oldenberg inversion test described in Chapter 4 (Fig. 4.4) shows that the lack of stations to the north of the array does not allow resolution of the position of the eastward current. The association of the boundary between westward and eastward currents and latitude 70° N may thus be partly an artefact of the location of the magnetometer array. For Substorm 4 (Fig. 5.11) the boundary is also close to 70° latitude, except west of the bend at epoch 04.13 U.T.

Fourier transform maps obtained from data of the array indicate that no significant conductivity anomaly in the earth exists under the array. Future studies will extend this finding to obtain a conductivity distribution with depth and attempt a separation of the perturbation fields into its components of internal and external origin. When obtaining the Fourier transform contour maps in search of conductivity anomalies under the array, it was observed that in general the phases of H and Z at different periods presented a consistent phase lag to the south-west (Figs. 3.2 to 3.4) which may have some significance.

Viewing conditions of the visual auroral for the all sky camera and Auroral Scanning Photometer (ASP) (ISIS-II satellite) over the array were not ideal (Wallis, 1975). In the summer the high sun made viewing poor, making the comparison between visual auroras and ionospheric currents impractical.

At the time of the events presented in this thesis, available TRIAD satellite data came from passes more than 30° west of the array (Kamide, 1976) and are therefore of little use in inferring parameters of field aligned currents above the array. These data could be of interest when the current model predicts field aligned currents near the satellite passes.

In future array studies to extend the results here reported, it is clear that an extension of the two-dimensional array to the north is highly desirable to investigate the fields and currents north of the main electrojets.

The new contributions to the knowledge of polar magnetic substorms recorded in this thesis are the following:

1. Birkeland field aligned currents at the east and west end of the ionospheric current that give rise to the perturbation fields have been firmly established.

2. During substorms there is a general tendency of the current system to drift eastward with respect to geomagnetic midnight.

3. The ionospheric current segment exhibits a bend to

the north-west near or just west of geomagnetic midnight.

4. Eastward electrojet associated with a substorm studied corotates with the earth maintaining the upward field aligned current at the east end near the edge of the array for four hours or more.

5. Eastward ionospheric current (or equivalent current) north of the westward electrojet was observed.

6. Westward ionospheric current north of the eastward electrojet was observed.

REFERENCES

Akasofu, S. I., 1968. Polar and Magnetic Substorms, D. Reidel Publ. Co., Dordrecht, Holland.

Akasofu, S. I., 1972. Magnetospheric substorms: a model. Solar Terrestrial Physics, Leningrad, 1970, part 3 edited by E. R. Dyer and J. G. Roederer, p. 131, D. Reidel Publ. Co., Dordrecht, Netherlands.

Akasofu, S. I. & C. I. Meng, 1969. A study of polar magnetic substorms, J. Geophys. Res., 74, 293.

Alabi, A. O., 1974. A study of the North American central plains conductivity anomaly , Ph.D. thesis, University of Alberta, Edmonton

Alabi, A. O., P. A. Camfield and D. I. Gough, 1975. The North American Central Plains conductivity anomaly, Geophys. J.R. astr. Soc., 43, 815.

Allen, J. H., C. C. Abston and L. D. Morris, 1974. Auroral Electrojet Magnetic Activity Indices AE (11) for 1974. Report UAG - 59, World Data Center A.

Arnoldy, R. L., 1971. Signature in the interplanetary medium for substorm. J. Geophys. Res., 76, 5189.

Axford, W. I., 1962. The interaction between the solar wind and the earth's magnetosphere. J. Geophys. Res., 67, 3791.

Axford, W. I. and C. O. Hines, 1961. A unifying theory of high-latitude geophysical phenomena and geomagnetic storms. Can. J. Phys., 39, 1433.

Backus, G. and F. Gilbert, 1967. Numerical applications of a formalism for geophysical inverse problems. Geophys. J. R. astr. Soc. 13, 247.

Backus, G. and F. Gilbert, 1970. Uniqueness in the inversion of inaccurate gross earth data, Phil. Trans. R. Soc., A266 , 123.

Banks, R. J., 1969. Geomagnetic variations and the electrical conductivity of the upper mantle, Geophys. J. R. astr. Soc., 17, 457.

Biermann, L., 1957. Solar corpuscular radiation and the interplanetary gas. Observatory 77, 109.

Biermann, L., 1951. Komentschwerfe and solare Korpuskularstrallung, Z. Astrophys., 29, 274.

Birkeland, K., 1908. The Norwegian Aurora Polaris Expedition, 1902-03, Vol. 1, Sect. 1, Christiania, Norway.

Birkeland, K., 1913. The Norwegian Aurora Polaris Expedition, 1902-03, Vol. 1, Sect. 2, Christiania, Norway.

Bonnevier, B., R. Boström and G. Rostoker, 1970. A three dimensional model current system for polar magnetic substorms, J. Geophys. Res., 75, 107.

Boström, R., 1964. A model of the auroral electrojets, J. Geophys. Res., 69, 4983.

Burke, M. D., A. O. Alabi and D. I. Gough, 1975. A digital converter and editing system for photographic analog data, J. Geomag. Geoelect., 27, 425.

Camfield, P. A., 1973. Studies with a two-dimensional magnetometer array ai north-western United States and south-western Canada , Ph.D. thesis, University of Alberta, Edmonton.

Chapman, S. and V. C. A. Ferraro, 1931. A new theory of magnetic storms. Terr. Magn. Atmos. Elec., 36, 77.

Chen, A. J. and G. Rostoker, 1974. Auroral-polar currents during periods of moderate magnetospheric activity, Planet. Space Sci., 22, 101.

Dessler, A. J. and R. D. Juday, 1965. Configuration of auroral radiation in space, Planet. Space Sci., 13, 63.

Dungey, J. W., 1953. Conditions for the occurrance of electrical discharges in astrophysical systems, Phil. Mag., 44, 725.

Dungey, J. W., 1961. Interplanetary magnetic field and the auroral zones. Phys. Rev. Letters, 6, 47.

Fairfield, D. H. and L. J. Cahill, 1966. Transition region magnetic field and polar magnetic disturbances. J. Geophys. Res., 71, 155.

Feldstein, Y. I. and G. V. Starkov, 1967. Dynamics of auroral belt polar geomagnetic disturbances, Planet. Space Sci., 15, 209.

Fejer, J. A., 1961. The effects of energetic trapped particles on magnetospheric motions and ionospheric currents, Can. J. Phys., 39, 1409.

Gough, D. I. and J. S. Reitzel, 1967. A portable three-component magnetic variometer, J. Geomag. Geoelect., 19, 203.

Harang, L., 1946. The mean field of disturbance of polar geomagnetic storms, Terr. Mag. Atmos. Elec., 51, 353.

Heikkila, W. J., 1973. Aurora, EOS Trans. AGU, 54, 764.

Heppner, J. P., 1972. The Harang discontinuity in auroral belt ionospheric currents, Geofysiske Publikasjoner, 29, 105.

Hess, W. N., 1968. The radiation belt and magnetosphere, Blaisdell Publishing Co., Mass. U.S.A.

Kamide, Y., 1976. Personal communication.

Kellogg, P. J., 1962. Flow of plasma around the earth. J. Geophys. Res., 67, 3085.

Kern, J. W., 1962. A charge separation mechanism for the production of polar auroras and electrojets, J. Geophys. Res., 67, 2649.

Kisabeth, J. L., 1972. The dynamical development of the polar electrojets, Ph.D. thesis, Univ. of Alberta, Edmonton.

Kisabeth, J. L., 1975. Substorm fields in and near the auroral zone, Phys. Earth Planet. Interiors, 10, 241.

Kisabeth, J. L., 1977. Personal communication.

Kisabeth, J. L. and G. Rostoker, 1971. Development of the polar electrojet during magnetic substorms, J. Geophys. Res., 76, 6815.

Kisabeth, J. L. and G. Rostoker, 1974. The expansive phase of magnetospheric substorms, 1. Development of the auroral electrojets and auroral arc configuration during a substorm, J. Geophys. Res., 79, 972.

Kisabeth, J. L. and G. Rostoker, 1977. Modelling of the three dimensional current system associated with magnetospheric substorms, Geophys. J. R. astr. Soc., 49, in press.

Langel, R. A., 1974. Near-earth magnetic disturbance in total field at high latitudes 2. Interpretation of data from Ogo 2,4, and 6., J. Geophys. Res., 79, 2373.

Mareschal, M., 1976. On the problem of simulating the earth's induction effects in modeling polar magnetic substorms, Rev. Geophys. Space Phys., 14, 403.

McPherron, R. L., C. T. Russell and M. P. Aubry, 1973. Satellite studies of magnetic substorms on August 15, 1968, 9, phenomenological model for substorms, J. Geophys. Res., 78, 3131.

Meng, C. I., B. Tsurutani, K. Kawasaki and S. I. Akasofu, 1973. Cross-correlation analysis of the AE index and the interplanetary magnetic field B(z) components. J. Geophys. Res., 78, 617.

Montbriand, L .E., 1965. A simple method for determining the local time of geomagnetic midnight, Can. J. Phys., 43, 1074 (Erratum, Can. J. Phys., 47, 1888, 1969).

Ness, N .F., 1969. The geomagnetic tail, Rev. Geophys., 7, 97.

Ness, N .F., K. W. Behannon, C. S. Cantaiano and C. S. Scearce, 1967. Observations of the earth's magnetic tail and neutral sheet at 510,000 Kilometers by Explorer 33, J. Geophys, Res., 72, 927.

Oldenburg, D. W., 1976. Ionospheric current structure as determined from ground-based magnetometer data, Geophys. J. R. astr. Soc., 46, 41.

Oldenburg, D. W., 1977. Personal communication.

Parker, E. N., 1958. Dynamics of the interplanetary gas and magnetic fields, Astrophys. J., 128,664

Parker, E. N., 1963. Interplanetary dynamical processes. Interscience Monographs in Physics and Astronomy, Vol. VIII, Interscience Publ.

Reitzel, J. S., D. I. Gough, H. Porath and C. W. Anderson, 1970. Geomagnetic deep sounding and upper mantle structure in western United States, Geophys. J. R. astr. Soc., 19, 213.

Rosenbauer, H., H. Grunwaldt, M. D. Montgomery, T. Paschmann and N. Sckopke, 1975. Heos 2 plasma observations in the distant polar magnetosphere: The plasma mantle., J. Geophys. Res., 80, 2723.

Rostoker, G., 1972. Polar Magnetic Substorms, Rev. Geophys. Space Phys., 10, 157.

Rostoker, G., 1974. Current flow in the magnetosphere during magnetospheric substorms, J. Geophys. Res., 79, 1994.

Rostoker G., 1976. The entry of the solar wind plasma into the magnetosphere and the formation of the plasma sheet. J. Geophys. Res., submitted for publication.

Rostoker, G., J. C. Armstrong and A. J. Zmuda, 1975. Field aligned current flow associated with intrusion of the substorm-intensified westward electrojet into the evening sector, J. Geophys. Res., 80, 3571.

Rostoker, G. and R. Boström, 1976. A mechanism for driving the gross Birkeland current configuration in the aurora oval., J. Geophys. Res., 81 ,235.

Rostoker, G. and C. G. Fälthammar, 1967. Relationship between changes in the interplanetary magnetic field and variations in the magnetic field of the earth's surface. J. Geophys. Res., 72, 5583.

Rostoker, G. and M. Hron, 1975. The eastward electrojet in the dawn sector, Planet. Space Sci., 23, 1377.

Rostoker, G. and J. L. Kisabeth, 1973. The response of the polar electrojets in the evening sector to polar magnetic substorms, J. Geophys. Res. 78, 5559.

Rostoker, G., H. L. Lam and W. D. Hume, 1972. Response time of the magnetosphere to the interplanetary electric field. Can. J. Phys., 50, 544.

Russell, C. T., 1971. Coordinate transformations. Cosmic Electrodynamics, 2,184.

Siscoe, G. L., 1966. A unified treatment of magnetospheric dynamics with applications to magnetic substorms. Planet. Space. Sci., 14,947.

Sckopke, N., G. Paschmann, H. Rosenbauer and D.H. Fairfield, 1976. Influence of the interplanetary magnetic field on the occurrence and thickness of the plasma mantle. J. Geophys. Res., submitted for publication.

Vestine, E. H. and S. Chapman, 1938. The electric current system of geomagnetic disturbance, Terr. Mag. Atmos. Elec., 43, 351.

Wallis, D. D., 1975. Personal communication.

Wiens, R. G. and G. Rostoker, 1975. Characteristics of the development of the westward electrojet during the expansive phase of magnetospheric substorms, J. Geophys. Res., 80, 2109.

Whalen, J. A., 1970. Auroral oval plotter and nomograph for determining corrected geomagnetic local time, latitude and longitude for high latitudes in the northern hemisphere, Air Force Cambridge Research Laboratories, Bedford, Mass.

Wilcox, J. and N. Ness, 1965. Quasi-stationary rotating structure in the interplanetary medium. J. Geophys. Res., 70, 5793.

Zmuda, A. J., F. T. Heuring and J. H. Martin, 1967. Dayside magnetic disturbances at 1100 kilometers in the auroral oval, J. Geophys. Res., 72, 1115.

Zmuda, A. J. and J. C. Armstrong, 1974. The diurnal flow pattern of field-aligned currents, J. Geophys. Res., 79, 4611.

APPENDIX A

THE MAGNETIC FIELD FROM A THREE-DIMENSIONAL LINE CURRENT

This appendix contains a summary of the equations used by Kisabeth (1972) to compute the magnetic field from a three-dimensional current system. These matrix equations are derived from the Biot-Savart's law which not only enables the rapid calculation of any magnetic field due to an arbitrary three-dimensional current system whose paths are known but also contains the necessary terms to represent the Earth's induction effects in the case where these can be simulated by a perfectly conducting sphere.

The magnetic induction B at the observation point (r ,θ_o,ϕ_o) (Fig. A.1) on the surface of the earth (r_o) due to an arbitrary loop C of current intensity J will be evaluated. The coordinate directions at the source $(\hat{r},\hat{\theta},\hat{\phi})$ are different from the coordinate directions $(\hat{r}_o,\hat{\theta}_o,\hat{\phi}_o)$ at the observing position, where both coordinate systems are related by

$$\begin{pmatrix} \hat{r}_o \\ \hat{\theta}_o \\ \hat{\phi}_o \end{pmatrix} = A \begin{pmatrix} \hat{r} \\ \hat{\theta} \\ \hat{\phi} \end{pmatrix}$$

Figure A.1 Diagram defining vectors in spherical coordinates for magnetic field calculations (after Kisabeth, 1972).

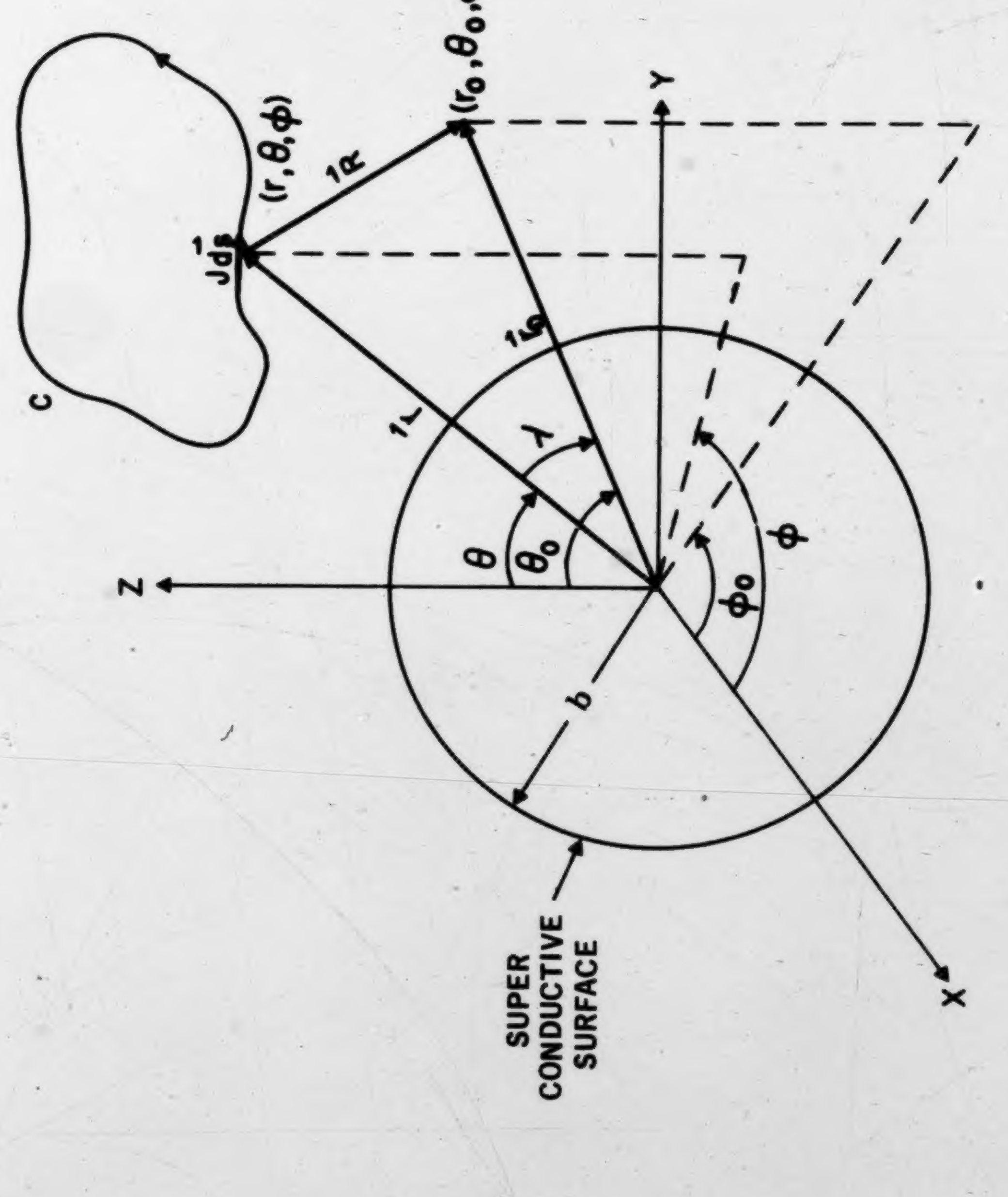
C
$J\bar{ds}$
(r,θ,ϕ)
1_R
(r_0,θ_0,ϕ_0)
1_r
1_{r_0}
Z
Y
X
θ
θ_0
γ
ϕ
ϕ_0
b
SUPER CONDUCTIVE SURFACE

where A is an orthogonal matrix with components:

$$A_{11} = \sin\theta_o \sin\theta \cos(\phi_o - \phi) + \cos\theta_o \cos\theta$$

$$A_{12} = \sin\theta_o \cos\theta \cos(\phi_o - \phi) - \sin\theta \cos\theta_o$$

$$A_{13} = \sin\theta_o \sin(\phi_o - \phi)$$

$$A_{21} = \cos\theta_o \sin\theta \cos(\phi_o - \phi) - \sin\theta_o \cos\theta$$

$$A_{22} = \cos\theta_o \cos\theta \cos(\phi_o - \phi) + \sin\theta_o \sin\theta$$

$$A_{23} = \cos\theta_o \sin(\phi_o - \phi)$$

$$A_{31} = -\sin\theta \sin(\phi_o - \phi)$$

$$A_{32} = -\cos\theta \sin(\phi_o - \phi)$$

$$A_{33} = \cos(\phi_o - \phi).$$

The magnetic field at a location (a, θ_o, ϕ_o) on the surface of the earth $(a = r_o)$ can be expressed as

$$B_j(a, \theta_o, \phi_o) = kJ \int_C \sum_{i=1}^{3} dc_{ij} \tag{A.1}$$

where B_j = Z, H, or D as j assumes values of 1, 2, or 3 respectively. K is the proportionality factor dependent upon the system of units used. The matrix dc has components

$$dc = \begin{bmatrix} 0 & -A_{31}e_2 ds_1 & -A_{21}e_2 ds_1 \\ -rA_{13}e_0 ds_2 & -(rA_{23}e_1 + e_2 A_{32}) ds_2 & (rA_{33}e_1 - A_{22}e_2) ds_2 \\ +rA_{12}e_0 ds_3 & -(A_{33}e_2 - rA_{22}e_1) ds_3 & -(A_{23}e_2 + rA_{32}e_1) ds_3 \end{bmatrix}$$

where

$$e_o = \frac{1}{|R|^3} - \frac{1}{|R'|^3}\left(\frac{b}{a}\right)^3$$

$$e_1 = \frac{1}{|R|^3} + \frac{1}{|R'|^3}\left(\frac{b}{a}\right)^3 - \frac{I_1}{ab}$$

$$e_2 = \frac{r_o}{|R|^3} + \frac{r_o'}{|R'|^3}\left(\frac{b}{a}\right)^3 - \frac{I_2}{ab}$$

and

$$r_o' = b/a$$

$$|R|^2 = r^2 + r_o^2 - 2rr_oA_{11}$$

$$|R'|^2 = r^2 + (r_o')^2 - 2rr_o' A_{11}$$

$$I_1 = \frac{(r_o')^2}{rR'} \frac{1}{R' + r - r_o' A_{11}}$$

$$I_2(A_{11} \leq 0) = rI_1A_{11} - \frac{r_o'}{R'} + \ln\left(\frac{R' + r_o' - r A_{11}}{r(1 - A_{11})}\right)$$

$$I_2(A_{11} > 0) = rI_1A_{11} - \frac{r_o'}{R'} + \ln\left(\frac{r(1 + A_{11})}{R' - r_o' + r A_{11}}\right)$$

where b is the radius of the superconductive sphere (Fig. A.1).

In the ionosphere and ring current

$$ds = ds_2 = 0$$

$$ds_3 = r \sin\theta d\phi$$

and along the field lines

$$ds_1 = 2r \operatorname{ctn}\theta d\theta$$

$$ds_2 = r d\theta$$

$$ds_3 = 0.$$

where ds, ds_2 and ds_3 are the components of the differential current path in the source coordinate system (r,θ,ϕ).

B_1, B_2, and B_3 given by Equation (A.1) are the local Z, X and Y components of the magnetic induction $\vec{B}$ at the observation point. However, it is common practice to use the Z, H and D components in the downward, North and East directions respectively. These are expressed in terms of B_1, B_2, and B_3 as follows:

$$Z = -B_1$$

$$H = -B_2$$

$$D = B_3$$

APPENDIX B

Kp AND AURORAL ELECTROJET MAGNETIC ACTIVITY INDICES

An estimate of the global auroral zone magnetic activity at the time of the substorms discussed in this thesis can be obtained by observing the corresponding Auroral Electrojet index. These are a quantitative measure of the activity produced by enhanced ionospheric currents.

From the report of Allen, Abston and Morris (1976) the hourly averages of amplitude of the upper envelope (AU) and lower envelope (AL) will be listed, with the corresponding station that contributed to that value. The reader is refered to the original report for a complete definition of these indices as for their graphs.

Table B.1 gives a list of the locations of the stations and their code names that contributed to the AE indices at the time of the Substorms 1, 2, 3 and 4. Location of the stations are also shown in Fig. B.1 in a polar azimuthal equidistant projection of centered dipole geomagnetic coordinates.

Kp and Auroral Electrojet indices are given for Substorms 1, 2, 3 and 4 in tables B.2, B.3, B.4 and B.5 respectively.

TABLE B.1

OBSERVATORIES USED FOR THE DERIVATION OF AE INDICES

Observatory	Code	Geographic Coord. N. Lat.	E. Long.	Geomagnetic Coord. N. Lat.	E. Long.
Leirvogur	LR	64.18	338.30	70.22	71.04
Narssarssuaq	NA	61.20	314.16	71.21	36.79
Great Whale River	GW	55.27	282.22	66.58	347.36
Fort Churchill	FC	58.80	265.90	68.70	322.77
College	CO	64.87	212.17	64.63	256.52
Barrow	BW	71.30	203.25	68.54	241.15
Cape Wellen	UE	66.17	190.17	61.79	237.10
Trixie Bay	TI	71.58	129.00	60.44	191.41
Cape Chelyuskin	CC	77.72	104.28	66.26	176.46
Dixon Island	DI	73.55	80.57	63.02	161.57
Abisko	AI	68.36	18.82	66.04	115.08

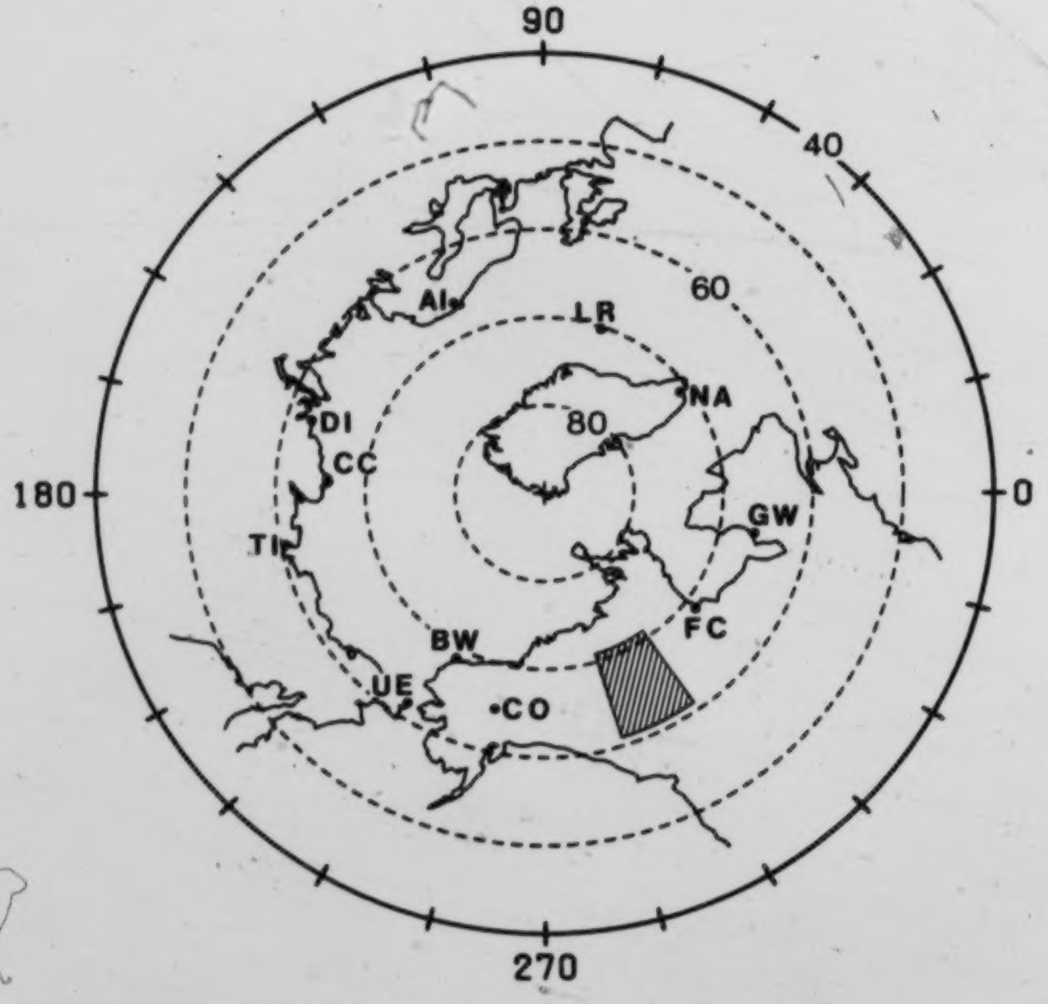
90
40
60
80
180
0
270
AI
LR
NA
DI
CC
GW
TI
FC
BW
UE
CO

GEOMAGNETIC COORDINATES

Figure B.1 Map of observatories used in calculating AE indices, in azimuthal equidistant projection of centred dipole geomagnetic coordinates.

TABLE B.2

AE AND Kp INDICES FOR SUBSTORM 1, 1974 SEPTEMBER 11

U.T.	4	5	6	7	8	9	10	11	12
AE	61	92	76	82	92	110	82	62	54
AL	-018 NA	-061 NA	-038 GW	-026 GW	-024 GW	-063 FC	-027 FC	-017 AI	-014 AI
AU	44 BW	31 BW	38 BW	56 BW	68 BW	46 BW	55 BW	45 BW	40 BW

U.T.	0-3	3-6	6-9	9-12
Kp	2	2-	1+	1-

Units of AE, AL and AU are nanotesla

TABLE B.3

AE AND Kp INDICES FOR SUBSTORM 2, 1974 SEPTEMBER 7

U.T.	1	2	3	4	5	6	7	8	9	10	11	12
AE	83	115	294	228	164	076	123	111	269	377	352	477
AL	-024 UE	-061 NA	-222 LR	-147 NA	-90 NA	-33 NA	-44 FC	-13 AI	-125 GW	-190 GW	-225 GW	-3 CO
AU	58 NA	55 FC	72 BW	80 GW	74 BW	43 BW	79 BW	97 BW	144 CC	187 CC	127 TI	126 DI

U.T.	0-3	3-6	6-9	9-12
Kp	3-	3-	2+	3-

Units of AE, AL and AU are nanotesla

TABLE B.4

AE AND Kp INDICES FOR SUBSTORM 3, 1974 SEPTEMBER 18

U.T.	5	6	7	8	9	10	11	12	13
AE	25	25	30	130	270	143	110	63	102
AL	-020 NA	-019 CO	-021 NA	-062 GW	-180 GW	-085 NA	-077 FC	-047 FC	-060 FC
AU	5 BW	6 BW	9 BW	68 CC	90 CC	58 BW	32 CC	17 CC	42 CC

U.T.	0-3	3-6	6-9	9-12
Kp	0	1-	2+	1-

Units of AE, AL and AU are nanotesla

TABLE B.5

AE AND Kp INDICES FOR SUBSTORM 4, 1974 AUGUST 14

U.T.	21	22	23	24 (1974 August 13)
AE	51	89	111	95
AL	-013 DI	-032 CC	-042 CC	-024 CC
AU	39 NA	53 FC	69 FC	71 NA

U.T.	1	2	3	4	5	6	7	8	9	10	11	12
AE	110	119	74	151	235	349	164	106	93	65	49	37
AL	-035 CC	-049 LR	-034 CC	-094 GW	-131 NA	-186 NA	-063 NA	-021 GW	-028 GW	-029 AI	-028 AI	-022 LR
AU	74 FC	70 FC	40 FC	58 BW	104 BW	163 BW	101 BW	86 BW	65 BW	35 BW	21 TI	15 TI

U.T.	0-3	3-6	6-9	9-12
Kp	2-	2+	1	1-

Units of AE, AL and AU are nanotesla